DISSERTATION

PERFORMANCE MEASUREMENTS AND MODELS FOR VEHICLE-TO-INFRASTRUCTURE COMMUNICATION SYSTEMS

ausgeführt zum Zwecke der Erlangung des akademischen Grades eines
Doktors der technischen Wissenschaften

unter der Leitung von
Univ.Prof. Dipl.-Ing. Dr.-Ing. Christoph F. Mecklenbräuker
Institute of Telecommunications

eingereicht an der Technischen Universität Wien
Fakultät für Elektrotechnik und Informationstechnik

von
Veronika Shivaldova
Landstraßer Gürtel 21/14
1030 Wien

Wien, im April 2015 _____

Die Begutachtung dieser Arbeit erfolgte durch:

1. Univ.Prof. Dipl.-Ing. Dr.-Ing. Christoph F. Mecklenbräuker

   Institute of Telecommunications
   Technische Universität Wien

2. Prof. Dr. Javier Gozálvez

   UWICORE Laboratory
   Miguel Hernández University of Elche

— To Andreas —

Abstract

In this thesis, we provide a comprehensive set of guidelines for roadside unit (RSU) deployment in the context of vehicle-to-infrastructure (V2I) communication systems. Based on an extensive set of real-world measurements, we analyze the effect of various system parameters and components. We first study the impact of packet length and data rate on the performance of transmit power-constrained systems in terms of throughout and communication range. Next, we compare systems using directional and omni-directional RSU antennas. We further analyze performance enhancements achievable using high-gain directional antennas and indicate possible disadvantages. We evaluate to which extent the performance can be improved by the design of vehicular on-board unit (OBU) antennas. We assess the impact of specific highway environments on the communication quality in V2I systems. Finally, we investigate performance advances brought by multi-hop cooperative communication.

We propose a hidden Markov model-based approach to reproduce distance-dependent performance measurements. The packet-error patterns generated by our approach reproduce measured data with high accuracy. Model parameters estimated from real-world measurements are released under a noncommercial academic-use license. This computationally inexpensive model also facilitates the exchange of technical know-how gained through our measurements.

We further extend this model such that V2I communication performance at an arbitrary location can be modeled without need for prior measurements. To this end, we perform a vector quantization of the model parameters. This allows us to find boundaries regarding communication quality and to localize environmental impairments that restrict radio propagation. Furthermore, we introduce a method of modeling signal-to-noise ratio (SNR) patterns that are correlated with the model-generated packet-error patterns. As a proof of concept, we apply this environment-aware modeling approach to a series of V2I measurements taken at 22 carefully selected urban locations. We identify the most significant types of street layouts and impairments, which are typical for urban environments. We provide parameters that are needed to reproduce their influence on communication. With these parameters, V2I performance can be modeled in terms of packet-error and SNR patterns for a multitude of urban locations, based merely on the street layout and topology.

Kurzfassung

In dieser Dissertation werden Leitlinien für die effiziente Anwendung von Straßeneinheiten (RSUs) im Rahmen von Fahrzeug-zu-Infrastruktur (V2I) Kommunikationsystemen ausgearbeitet. Wir analysieren die Auswirkungen von verschiedenen Systemparametern und Komponenten auf Basis von umfangreichen Messkampagnen im echten Straßenverkehr. Zuerst untersuchen wir den Effekt von Paketlänge und Datenrate auf die Leistungsfähigkeit von V2I Kommunikationsystemen, hinsichtlich des Datendurchsatzes und der Reichweite. Zunächst vergleichen wir V2I Systeme mit direktionalen und nicht-direktionalen RSU Antennen. Wir werten die Erhöhung in der Leistungsfähigkeit, die durch direktionale Antennen erzielt werden kann, aus und diskutieren mögliche Nachteile dieser Antennen. Wir bewerten in wie fern die Zuverlässigkeit von V2I Systemen durch die optimierte Konstruktion der Boardeinheit (OBU) Antenne verbessert werden kann. Wir untersuchen die Effekte von besonderen Ausbreitungsbedingungen auf die Qualität von V2I Kommunikationsystemen. Schließlich werden die Vorteile von kooperativen Multi-Hop Kommunikationssystemen evaluiert.

Wir entwerfen ein Hidden-Markov-Modell zur Reproduktion der distanzabhängigen Leistungsfähigkeit von V2I Systemen. Die mit unserem Modellierungsansatz erzeugte Paketfehler-Sequenzen reproduzieren die Messdaten mit hoher Genauigkeit. Die Modellparameter, die auf Basis von umfangreichen Messungen bestimmt wurden, sind unter einer nicht-kommerziellen akademischen Lizenz veröffentlicht. Unter anderem erleichtert dieses recheneffiziente Modell den Austausch von Fachwissen das durch unsere Messkampagnen gewonnen wurde.

Wir erweitern dieses Model so, dass V2I Kommunikation an einem beliebigen Ort modelliert werden kann, ohne Messungen an diesem Ort durchführen zu müssen. Dafür wird eine Vektorquantisierung auf die Modellparameter angewendet. Dies ermöglicht uns eine Einstufung der Kommunikationsqualitäte zu treffen und Beeinträchtigungen der Ausbreitungsbedingungen zu lokalisieren. Weiters entwerfen wir eine Methode zur Modellierung des Signal-zu-Rausch-Verhältnises (SNR). Anschließend wenden wir unser Modellierungsansatz auf die Ergebnisse von 22, an sorgfältig ausgewählten innenstädtischen Standorten durchgeführten, V2I Messungen. Wir identifizieren die wichtigsten Typen von Straßen und Beeinträchtigungen der Ausbreitungsbedingungen, die typisch für innerstädtische Umgebungen sind. Weiters stellen wir die Modellparameter zur Verfügung, die erforderlich sind um den Einfluss besonderer

Ausbreitungsbedingungen zu reproduzieren. Anhand dieser Parameter können realistische V2I Messergebnisse in Form von Paketfehler- und SNR-Sequenzen für eine Vielzahl von innerstädtischen Standorten modelliert werden.

Acknowledgements

Working on my Ph.D. has been a wonderful and often overwhelming experience. It has been a continuous learning process that often challenged me to step out of my comfort zone, to try out something new, to work harder, and to stay focused. Eventually, all these efforts were rewarded by the recognition of my scientific accomplishments and by extensive personal growth. However, none of this would have been possible without the support and company of many individuals, to whom I owe my deepest gratitude.

First of all, I would like to express my sincere gratitude to Christoph Mecklenbräuker for giving me the opportunity to pursue a Ph.D. under his supervision, for believing in me and making me believe in myself, for helping to discover my talents of which I was not aware before, and for teaching me the wisdom of "dancing in the rain". Thanks to Christoph's unique supervision style I learned to work independently, to bravely accept new challenges, and to be more self-confident.

Furthermore, I want to thank Javier Gozálvez whose scientific work has inspired me from the very beginning of my Ph.D. studies. In fact, the results of the Bologna measurement campaign have always been the main reference for my work in the context of performance evaluation. Later on, these measurements entered my own research in the framework of performance modeling. I am therefore particularly happy that Javier agreed to act as my co-examiner.

Over the last several years I have been very privileged to get to know and to collaborate with many great people. First of all, I am very grateful to all participants of the ROADSAFE measurements for spending numerous days on the road and helping me with acquiring the data. I am particularly indebted to Alex Paier, Dieter Smely, and Thomas Paulin for turning this rather exhausting work into a very pleasant experience. Alex, thank you for making the transition from a master student to a Ph.D. candidate so smooth for me, and for giving me the first guidelines for my scientific career. Dieter, I am grateful for your continuous interest in my work, precious feedback, and kind attitude. Thanks go to Thomas for inspiring me with idea of performance modeling and for showing me its importance from an upper-layer perspective. I have greatly enjoyed the opportunity to work with Miguel Sepulcre, who helped me with the Bologna measurement data and became a very supportive co-author. I am indebted to

Erik Ström, Fredrik Tufvesson, and Morten Jakobsen for many insightful discussions in the framework of COST IC1004. Special thanks go to Morten for asking tough questions and persistently bringing up the concept of parsimonious modeling. Enlightening idea exchanges with Thomas Zemen taught me a lot about model performance evaluation and improved my work significantly. I also had the great pleasure of meeting Elisabeth Uhlemann, who became a role model for me in many ways and contributed to my personal growth.

Working towards my Ph.D. would never have been that much fun without my friends at the Institute of Telecommunications who became an important part of my life. I am very grateful to my little "sister" Arrate for sharing her positive and wise attitude towards life and for brining plenty of sun even on the darkest winter day. Furthermore, I want to thank my most frequent travel companion Gregor for all the adventures we went through, for keeping good mood despite cloudy sunrises and scenic sunsets we missed by just few minutes, and for being the undeniable leader of the institute's lunch walks. A very inspiring member of these walks is Günther, who has always been an example of getting things done on time and staying calm, even shortly before his own defense. I am also thankful to Natalie and Andrea, who carefully maintained my daily coffee and sugar intake, and made sure that I do not completely disconnect from reality. Finally, I have always appreciated the cheering attitude of Mona and Jelena who have contributed significantly to the overall warm working atmosphere at the institute.

An dieser Stelle möchte ich mich für die unbegrenzte Unterstützung von Barbara und Helmut bedanken. Danke für Eure offenen Ohren und Eure warmen Herzen, für Eure Hilfe in allen Bereichen meines Lebens und dafür, dass Ihr immer für mich da seid. Ich bin sehr froh, bei Euch meine österreichische Familie gefunden zu haben und schätze Euch sehr.

Я безгранично благодарна своим родителям Наталье и Олегу, а также бабуле Майе за их бесконечную любовь, заботу и поддержку. С самого рождения и по сей день вы окружаете меня теплом и вниманием, вы верите в меня и тем самым не даёте мне опускать руки ни при каких обстоятельствах, вы направляете меня когда я не знаю куда двигаться дальше и помогаете во всем на пути к моим целям. Спасибо вам за то что прошли вместе со мной этот нелегкий путь начиная со вступительных экзаменов в Ташкенте и заканчивая защитой диссертации в Вене. Я очень вас люблю и дорожу вами больше всего на свете!

More than to anybody else I am indebted to my frequent co-author, the most intense collaborator, best friend, and my fiancé Andreas. Thank you for being immensely patient with me, for setting high standards on research work, and for always giving me exactly what I needed the most, ranging from scientific advise to a warm hug and a cup of coffee. Your attention to detail has significantly improved readability of this thesis. I very much appreciate your ability of always seeing the bright side of life and for keeping the sense of humor when I lost mine. You have always been my personal example of extraordinary success, dedication to science, and hard work. I love you!

Contents

1

Introduction

1.1 Overview and Motivation

Our society is now experiencing its fifth and most intense technological revolution. Although we are still living in the era of information, we have already reached an inflection point that will ultimately be followed by transition into the next technological period, referred to as hybrid era. The information era derives its origin from development of the internet in the early 1960s, when it was intended for information exchange, predominantly in scientific and military fields. Since then, the internet has exponentially become cheaper, easier to access, and as consequence ever more ubiquitous. Therefore, we nowadays take connectivity with low latency and high reliability for granted and the enabling technology is no longer a selling point itself. Nevertheless, the matureness and omnipresence of the internet opened the door to an unprecedented era of hybrid connectedness between all kind of devices. This popular today technology, developed to connect devices and to control interactions between them is known as Internet of Things (IoT). It envisions complex, self-configuring, and adaptive networks of sensors and smart objects, including commonplace and industrial objects. The idea is to make things intelligent, programmable, and more capable of interaction with humans. The resulting revolution in the nature of technology will once again drastically change individual's life and society as a whole.

A very significant part of the IoT will be represented by vehicles. This is of no surprise since in 2013 the total number of motorized vehicles on the planet has reached 1.2 billion and continues to grow rapidly [5]. By some estimates, the total number of vehicles worldwide could double by 2050. This ever growing amount of vehicles implies increasing demand on transport efficiency, in order to limit the fuel consumption growth and ensure environmental sustainability. Besides economical and ecological aspects, an increasing number of vehicles would lead to increasing societal disadvantages, expressed in a growing number of deaths and

injuries in road accidents. Nowadays, nearly 1.3 million people die in road crashes each year and an additional 20 to 50 million are injured or disabled worldwide [8]. Unless action is taken, road traffic injuries are predicted to become the fifth leading cause of death by 2030. One attempt to make the driving experience safer and more efficient is to enable communication between the vehicles. In such a system, referred to as intelligent transportation system (ITS), the vehicles act as nodes in a distributed peer-to-peer network and exchange warnings and driver assistance notifications.

Since the early 2000s, car manufacturers as well as road and infrastructure operators are collaborating with the aim of providing reliable, low-latency vehicular connectivity for ITS. The first big step towards harmonized technology enabling wireless access in vehicular environments (WAVE), was made by frequency band allocation. Pioneer in this were the United States which allocated 75 MHz of spectrum at 5.9 GHz, exclusively for vehicular communications. This tendency was followed by Japan, where an 80 MHz band at 5.8 GHz was reserved for the same purpose. Subsequently in August 2008, the European Commission has taken the decision on the harmonized use of radio spectrum in the 5850 MHz to 5925 MHz frequency band for ITS [113]. According to the nominal carrier frequency allocation defined by European Telecommunications Standards Institute (ETSI), the whole frequency band is divided into seven 10 MHz channels [36].

Besides allocation of the protected frequency bands for ITS, important standardization advancements have been made by standardization of the communication protocols. The IEEE 1609 family of standards defines the set of interfaces enabling vehicular communications. In particular, the IEEE 1609.1 standard [58] specifies services and interfaces of the WAVE resource manager applications. Security aspects are addressed in IEEE 1609.2 standard [60] and networking services are defined in IEEE 1609.3 standard [59]. The lower layers of the protocol stack, namely the medium access control (MAC) layer and the physical layer (PHY) are specified in the IEEE 802.11p standard [57], finalized in 2010. According to this standard the packets are transmitted by means of orthogonal frequency-division multiplexing (OFDM) with 64 subcarriers. The IEEE 802.11p communication protocol supports 4 modulation formats and 3 coding rates, resulting in a nominal data rate between 3 Mbit/s and 27 Mbit/s. Two-way, short-to-medium range wireless radio communication is envisioned in two types, namely vehicle-to-vehicle (V2V) and vehicle-to-infrastructure (V2I). Unlike other wireless media, vehicular communication does not require centralized access points and operates purely in ad-hoc peer-to-peer manner. Hence, V2V communications can occur independently of the road infrastructure.

However, the essential prerequisite for reliable operation of such cooperative vehicular networks is large dissemination of communication units. Since the market penetration might take some time, during the early stages of major technology roll-out, vehicles enabled with communication units will often find few to no communication partners. To ensure that the early adopters of ITS benefit from this highly demanded technology right from the start, it is advisable to launch the system by equipping the road infrastructure with communication

units. Such roadside units (RSUs) will be placed at selected locations and provide vehicles with relevant data updates, creating thereby smart roads and facilitating traffic efficiency. The first mover countries in this domain are Austria, Germany, and the Netherlands. These countries are working jointly on the first real-world implementation of an inter-country smart road called the Cooperative ITS Corridor [99]. Starting in 2016, the Cooperative ITS Corridor will guide smart vehicles from Rotterdam through Frankfurt and Munich to Vienna, being the first smart road with harmonized standards among different countries.

The development of such smart mobility initiatives faces many challenges ranging from social acceptance and technological aspects, to standardization and harmonization. One of the main technical challenges is to find optimal RSU deployment strategies, such that reliable connectivity for all network participants is guaranteed. Whereas, much theoretical and simulation-based research has been performed in this regard, the real-world measurements are indispensable in the process of technological design and testing. Despite their absolute necessity, measurements are rarely performed due to prohibitively high costs and severe effort. This is especially true for highway environments, in which access to the road infrastructure need to be granted by road authorities. This yearning research challenges motivate the work presented in the first part of this thesis. We have initiated a collaboration with road authorities and performed a series of extensive measurements on Austrian highways with realistic vehicular traffic. The main goal of these measurements was to develop a set of recommendations for optimal deployment strategies of road infrastructure in the context of ITS.

Although real-world measurements are essential for the development of communication systems, in most cases they need to be supplemented by models. The reasons are manifold, but boil down to two main problems: an exceedingly large number of system components and insufficient reproducibility of measurement results. More precisely, the measurements are usually performed with respect to one or few system aspects. Thus, immensely many measurements would need to be performed to analyze all combinations of system parameters and components. Moreover, unless the measurements are performed in idealized lab conditions, they always are influenced by a multitude of time-varying factors and are therefore hardly reproducible. To overcome these issues, models are often used. They serve to reproduce various aspects of vehicular ad-hoc networks (VANETs), e.g., vehicle mobility, human driver behavior, and radio propagation. To ensure reliability of simulation-based system performance evaluation, all system architecture components need to be represented by realistic models. However, in most cases the cross-layer interaction is largely neglected and simulation toolkits are focusing on either of the protocol stack layers, while performance of the other layers is either fully neglected or overly simplified. In particular, the inevitability of network simulations posing inadequate assumptions on the PHY was timely tackled by the leading research groups in this domain. Such [50] analyzed and quantified the impact of the radio channel on operation of networking and communication techniques for VANETs. The necessity of using accurate MAC and PHY models was further discussed in [34]. Comparing models of

two closely related to IEEE 802.11p network access technologies, the authors concluded that these models are only suitable for modeling of low traffic density scenarios. The influence of radio propagation conditions in urban areas was further studied in [44], where the authors analyzed how individual propagation aspects affect each other and in which situations more detailed propagation models are required. The lack of realistic radio propagation models for packet level simulators motivates the work presented in the second part of this thesis. Our primary objective in this context is to derive a PHY performance model resembling real-world measurements with high accuracy.

1.2 Contributions and Thesis Organization

The core of this thesis is represented by two main parts: characterization and modeling, both with emphasis on PHY performance of IEEE 802.11p-based access networks in V2I scenarios. The performance characterization and model development are built on the real-world measurements.

With respect to **performance characterization** our major contributions are as follows:

- We analyze the influence of transmit parameters, more specifically the packet length and the data rate, on the performance of transmit power-constrained V2I systems. In the course of this analysis we seek for transmit parameters that yield the largest throughput at a constant transmit power.
- We evaluate the system performance in different driving directions for various transmit parameters and mounting positions of the RSU.
- We compare the performance achievable with directional and omnidirectional RSU antennas, and examine advantages and disadvantages of the high-gain directional antennas.
- We investigate performance enhancements achievable with on-board unit (OBU) antennas, featuring different design strategies and gains.
- We study effects of vehicular traffic on the V2I communication with an emphasis on tunnel environments.
- On the basis of two-hop decode-and-forward (DF) relaying experiments, we assess the performance advances achievable by means of cooperative communication in VANETs.

This unique collection of measurement-based results is intended to provide a comprehensive set of guidelines for RSU deployment and thereby set a standard for future V2I systems.

In the framework of **performance modeling** our original contributions can be summarized as follows:

- We introduce a simple and yet accurate approach for reproducing realistic distance-dependent packet-error patterns. This hidden Markov model (HMM)-based approach ensures that on the one hand, the statistical properties of the measured data are maintained and on the other hand, the resulting packet-error patterns are not deterministic.

- We apply the aforementioned modeling approach to our measurement data used for performance characterization in the first part of the thesis. The complete set of model parameters is released under a noncommercial academic use license [7] to ensure reproducibility of our results.

- We propose to apply a vector quantization (VQ) approach for model dimension reduction, by taking into account inherent correlations between the model parameters.

- We show that besides model dimension reduction, the proposed VQ algorithm is able to localize and characterize realistic environmental impairments in terms of model parameters.

- We extend the packet-error model to generate realistic signal-to-noise ratio (SNR) patterns.

- We suggest an environment-aware model that estimates the packet-error and SNR performance for an arbitrary location, based merely on street layout and topology.

- We parametrized our environment-aware model from extensive measurements in an urban environment. With the set of model parameters presented in this thesis, realistic V2I communication performance at nearly any urban location, satisfying certain topological constraints, can be easily modeled.

The models developed in this thesis are meant to facilitate exchange of technical know-how gained through real-world measurements and to provide a computationally inexpensive PHY models, frequently used for higher layer simulations.

The reminder of this thesis is structured in the following four chapters:

- **Chapter 2** presents related work with respect to both, vehicular measurements and models. It further provides the background material that serves as a basis for the subsequent chapters. We present the material in this chapter in such a way that the reader can quickly recall the most important definitions and results without having to browse through the literature.

- In **Chapter 3** we summarize the details of three V2I performance measurement campaigns used for performance characterization and modeling. Next, we define a set of key performance indicators (KPIs) required for comparability of V2I measurements with different parameter settings, equipment, and environments. We present performance analysis with respect to transmit parameters, RSU and OBU antennas, and

quantify the effects of vehicular traffic-induced fading. Finally, we analyze performance improvements achievable by multi-hop cooperative communication.

- **Chapter 4** comprises the aspects of our PHY performance model. We first introduce the range-dependent modified Gilbert model, designed to reproduce measured packet-error performance. Subsequently, we extend this model to allow generation of realistic SNR patterns. Thereafter, we propose the environment-aware performance model and derive the model parameters for urban environments.

- Conclusions are provided in **Chapter 5**. We summarize our main findings and discuss the insights gained in this thesis. Finally, we point out several open problems which may serve as a basis for further research.

2

Preliminaries

This chapter provides an overview of the ongoing research activities is the area of vehicular measurements and models. In particular, we introduce two types of vehicular measurements and elaborate on the most significant outcomes of real-world experiments. Furthermore, we justify the high demand for realistic vehicular models and provide an extensive summary of existing modeling approaches. Finally, we present the background material needed for the development of the vehicular performance model addressed in Chapter 4. Thus the main purpose of this chapter is to set the stage for the research questions addressed in this thesis.

2.1 Vehicular Measurements: State of the Art

Measurements are an integral part of the design and development process of any system. To implement practical and reliable system architectures, the influence of every single system component on the overall performance needs to be carefully evaluated. Some of the components, e.g., antenna type and placement or signal processing aspects are subject to the design. In this case, measurements help to select the components leading to the optimal system performance. The other components cannot be influenced by the design and are given by, e.g., the particular environment or scenario, in which the system will be deployed. In this case, the role of the measurements is to test the system under the most challenging conditions and the system is considered ready for the roll-out, only if the core functionalities remain available in all settings.

Vehicular communication systems are not an exception and their deployment in the scope of public safety puts even higher demand on performance and stress tests. Therefore, vehicular field tests have been ongoing for several years, starting in the early 2000s. Based on the used equipment and evaluated parameters, vehicular measurement campaigns can be divided in two large groups: *channel measurements* and *performance measurements*.

2.1.1 Vehicular Channel Measurements

Channel measurements, frequently referred to as channel sounder measurements, are conducted with the main purpose of understanding the channel behavior. Deep understanding of the channel properties is required for practical system design, since the propagation channel ultimately defines the performance of the whole communication system. To perform channel measurements, a radio channel sounding equipment is required. For real-world field test a channel sounder placed in one of the test vehicles transmits electromagnetic waves to excite the channel. The receiver is placed in the other vehicle and records the channel output. The parameters resulting from channel measurements include, but are not limited to, channel gain, delay and Doppler spread, coherence bandwidth, time- and frequency-selectivity. These parameters are subsequently used either for channel characterization or modeling.

There exist a large number of real-world channel sounding measurements performed in the course of the last decade. Depending on the selected test methodology one may choose between narrow- or wideband channel sounders featuring single-input single-output (SISO) or multiple-input multiple-output (MIMO) capabilities. The early vehicular measurement campaigns often considered narrowband measurements [25, 28, 77, 111]. However, later it was shown that wideband channel sounders are better suited for measurements in doubly-selective vehicular communication environments [84, 86, 89, 90, 96]. Nevertheless, even wideband channel measurements cannot take into account all factors affecting radio propagation. Based on the addressed research questions, the channel measurements can be categorized in two types: (i) measurements with an emphasis on setup and equipment, and (ii) measurements with a focus on the propagation environment.

The majority of channel measurements with an emphasis on the equipment characterize the impact of the number of antennas and their placement. For the measurements presented in [102], omnidirectional monopoles were employed at both link ends and the difference between antenna placement on the vehicle rooftop and inside the vehicle on the dashboard was evaluated. Results have shown that placing the antennas inside the vehicle yields significantly more dispersive channels with larger delay spread. To find the optimal antenna placement on the vehicle rooftop, measurements in [73] evaluated three different positions: absolute center of the car roof, front-right, and back-right. Measurements suggest that the center position provides the best overall performance. Along with the vehicle rooftop position the authors of [10] considered three other possible vehicle antenna placements such as bumper, inside-windscreen, and left-side mirror. The measurement results have shown that a pair of antennas with complementary properties, e.g., a roof-mounted antenna together with a bumper antenna should be used to achieve maximal diversity.

Initially, vehicular channel sounder measurements were performed in settings adopted from the cellular communications domain, such as highway, rural, suburban, and urban environments [12, 25, 75]. However, later the focus shifted towards more specific vehicular scenarios and safety-critical situations. Such radio channels measurements presented in [62] and [9]

were performed at street intersections. Both contributions have shown that scattering objects in and around an intersection contribute a considerable part to the total received power. Additionally, [9] compared channel properties at urban intersections and at merging lanes. The merging lane scenario was found to be more safety critical, due to the lack of significant scatterers such as roadside objects and vehicles. Channel measurements presented in [84] considered safety-critical situations such as overtaking maneuvers in congested traffic and communication in situations when line-of-sight (LOS) is obstructed by a truck. The authors have concluded that in both situations, the majority of multipath contributions are produced by large metallic surfaces, such as traffic signs, trucks, and bridges. The same conclusion was drawn by the authors of [19] in the context of an on-bridge scenario. Channel measurements presented in [18] have shown that the most relevant propagation characteristics for in-tunnel environments are reflections on walls, ceiling, and ventilation system inside the tunnel, as well as reflections on other vehicles and traffic signs.

2.1.2 Vehicular Performance Measurements

Unlike channel measurements, performance measurements are intended to evaluate the whole system, including hardware and signal processing at transmitter and receiver, as well as the wireless radio propagation channel between them. Performance measurements are usually conveyed with a set of at least two standard-compliant devices, one of which is transmitting packets and the other is receiving. The received data is decoded and a cyclic redundancy check (CRC) is performed to identify, whether the packet transmission was successful. In these measurements the only information available for evaluation is the binary identification of packet reception success, the corresponding received signal strength indicator (RSSI) values and positioning information. Based on these informations, typical performance indicators such as throughput and coverage range are evaluated.

Despite the fact that vehicular performance measurements evaluate efficiency of the whole system, they are usually designed to answer a particular question. Based on the targeted investigation area, performance measurements can be classified in three groups:

- Measurements with a focus on environments and scenarios. Typically considered environments are urban, sub-urban, rural, and highway. Vehicular scenarios include, e.g., LOS, non-line-of-sight (NLOS), overtaking and platooning.
- Measurements analyzing transmission parameters, such as data rate, packet length, transmit power, and frequency.
- Measurements with an emphasis on antenna parameters, such as antenna type, gain, and placement.

One of the first vehicular performance measurement campaigns performed in urban, sub-urban and highway environments is presented in [107]. It was conducted with IEEE 802.11b transceiver modules, since the IEEE 802.11p implementation was not yet available. These

measurements were one of the first to prove that a connectivity range of up to 1000 m is potentially achievable. They also concluded that the highest link quality is obtained in sub-urban environments, while highway environment is the most unfavorable for this type of communication. Later it was shown that not the environment itself, but more significantly the LOS conditions between the transmitter and receiver influence the quality of communications. In [22], the connectivity issues under perfect LOS, obstructed LOS, and NLOS conditions were investigated in urban, rural, and highway environments. Analyzing the packet delivery ratios (PDRs) for different LOS conditions, the authors concluded that connectivity is lost almost immediately in absence of LOS. More precisely, high quality communication was achieved in a range of 500 m under LOS conditions, while in NLOS conditions connectivity was lost almost immediately. In the case when LOS was obstructed by vegetation, connectivity was established for 40 to 50 m only.

Effects of vegetation were further addressed by the authors of [112]. They concluded that the density of vegetation has a significant impact on the communication range. The high quality communication is ~10 m for intersections with dense vegetation and may be as large as 200 m for intersections with sparse vegetation. To capture the influence of seasonal variations the measurements at the same location were performed in summer and in winter. The results show that the communication range in winter time, characterized by the absence of foliage is 2 to 7 times larger than in summer. These results were confirmed by the authors of [122]. However, measurements performed in typical urban environments with no vegetation [115], did not show any influence of seasonal variations. This supports the conclusion that the influence of seasonal variations on the performance of intelligent transportation system (ITS), is mainly due to changes in the density of vegetation.

Surprisingly, performance of IEEE 802.11p communication at urban intersections does not depend on LOS conditions as much as on the street width. Results of vehicle-to-vehicle (V2V) measurements presented in [101] show that high quality communication on medium-wide streets is retained 30 m longer than on narrow streets. For intersections of very wide streets however, the range is 10 m shorter than for narrow streets. The authors attribute this reduction in communication range to probabilistic shadowing, which results from the surrounding cars and even more importantly buses. This negative effect of high traffic density and presence of heavy vehicles, was further emphasized by vehicle-to-infrastructure (V2I) measurements in urban [49] and highway [87] environments.

The influence of transmission parameters was studied in [30, 31, 74, 79, 87]. The authors of [31] show a significant dependence of the V2I communication performance in urban intersections on packet transmission intervals, data rates, and packet sizes. The influence of the packet size on V2V communication in different propagation conditions was further analyzed in [74]. In ideal conditions provided by an indoor lab environment, the largest throughput of 2.5 Mbit/s was measured with a packet size of 1500 Bytes and data rate of 3 Mbit/s. For measurements performed in outdoor environments with an inter-vehicle distance of 30 m, the throughput was only slightly lower for all packet sizes, except for the 1500 Bytes, for

which nearly all packets were lost. When the inter-vehicle distance was increased to 150 m, the throughput was significantly reduced. In this case, the largest achievable throughput amounts to 1.9 Mbit/s and was achieved for a packet size of 500 Bytes. Transmission of longer packets resulted in packet error rate close to 1. Similar results were obtained for highway measurements presented in [85], as well as for parking lot, suburban, and urban measurements presented in [79]. In the context of V2I measurements however, packet size does not have a strong negative impact on the throughput. Measurements presented in [87] show that the total throughput (a.k.a. goodput) can be increased from 6 to 10.5 MBytes, when using packet size of 1554 Bytes instead of 200 Bytes. However, the PDR fluctuations are stronger for longer packets.

The influence of vehicle velocity was investigated by the field trials presented in [30], in terms of transmission range and latency. It was shown that the transmission range depends on the vehicle velocity. The largest transmission range of approximately 700 m was obtained when driving 30 km/h, while at 170 km/h the range was limited to 300 m. Interestingly, the latency, defined as the temporal delay between the generation of a packet and its reception, is independent of speed and is always smaller than 4 ms.

The effect of on-board unit (OBU) antennas was addressed in [22, 30, 64]. All authors concluded that imperfect omnidirectionality of the OBU antennas and vehicle's body, have significant impact on the overall performance. In [17] the OBU antenna placement was considered in context of a vehicle platooning application. The platoon consisted of four vehicles: one truck in the lead, followed by three passenger vehicles. The antennas were placed either on the cabin roof or on the rear mirror of the truck. The results show that in these particular settings, the rear view mirror antenna position is superior to the roof antenna position and has more predictable performance.

Along with V2I and V2V measurements, some field measurements considered multi-hop scenarios. For such measurements, [110] considers three equidistant vehicles (a transmitter, a relay, and a receiver) that were driving at the same speed and in the same direction. The measurements show that multi-hop networks have the potential to substantially improve performance in terms of communication range and throughput.

2.2 Vehicular Models: State of the Art

Despite the importance of the real-world measurements for the development of communication systems, measurements alone are rarely sufficient for ultimate comprehension of the entire system. This is mainly due to the fact that even the simplest existing communication system consists of an immensely large number of components, each of significant importance. In the previous section, we have mentioned that measurements are usually designed to answer one particular question. Therefore, to analyze all system dependencies, prohibitively many measurements would be required, resulting in high costs. Furthermore, real-world measurements rarely provide a sufficiently high level of reproducibility. To explain what we mean

by reproducibility in this context, assume that system engineers want to compare performance of two different channel estimation algorithms in realistic vehicular environments. For this purpose, they perform test drives with the same equipment, parameters and location at different times. This, at the first glance insignificant, difference may result in substantial changes of the radio propagation channel. This may, e.g., be due to changes in the density and distribution of scatterers, and different weather conditions. As a result, the testing conditions can become more or less favorable, which might lead to the wrong choice of the channel estimation algorithm. If the two algorithms would have been tested in exactly the same conditions, the comparison would be fair and a more balanced conclusions would be met. However, keeping the propagation channel of realistic vehicular environments constant is impossible.

To overcome the cost and reproducibility issues, simulation tools are frequently used. Depending on the scope of the simulation, some system components can be exchanged and the others are kept the same, ensuring a fair comparison. Coming back to our example with the channel estimation algorithms, in simulations the propagation channel can be kept constant as long as it is required for the testing purposes, which is in contrast to real-world measurements. Such channel representations, also known as (radio) *channel models*, reproduce the evolution of electromagnetic waves emitted by the transmitter and impinged on the receiver. However, the detailedness of the channel models is not necessary for some simulation purposes. In this context so-called *performance models* are often deployed. These models are more general and also include the influence of the complete transceiver chain. The main research challenge in the development of both, channel and performance models, is to reproduce the reality as accurately and efficiently as possible.

2.2.1 Vehicular Channel Models

We next describe the following three types of channel models: deterministic, stochastic and geometry-based stochastic channel models.

Deterministic channel models are intended to reproduce the propagation of electromagnetic waves and their interaction with obstacles in the surrounding environment. In a nutshell, deterministic channel models approximate solutions of Maxwell's equations. The most frequently used types of deterministic channel models are replay and ray-tracing models. The replay models [70,71] use time-variant channel impulse responses (CIRs) obtained by channel sounding experiments (almost) directly for simulation. The only intermediate steps between measurements and simulations are noise floor cancellation and interpolation to the sampling frequency required for simulation (e.g., 10 MHz for IEEE 802.11p). Once the measurements are conducted, the replay models are easy to implement and their accuracy is high. However, they are site-specific and therefore, not sufficiently representative. In contrast, the ray-tracing models [76, 78, 82] encompass all static and mobile objects in the analyzed environment. They evaluate the signal propagation aspects by taking into account direct path, specular reflections and diffuse scattering components. Due to the high level of detailedness,

the deterministic ray-tracing models are computationally demanding. To reduce complexity, some studies suggest to disregard certain details, e.g., to only consider the direct and the reflection paths [121], or only the direct path and the specular components [27]. The authors of [42, 43] propose a complexity reduction method based on a projection of all propagation paths on a subspace, spanned by two-dimensional discrete prolate spheroidal sequences. However, even with recent advances (see, e.g., [95]), these potentially very accurate models require detailed knowledge of the analyzed environment.

Unlike deterministic channel models, stochastic channel models do not require any knowledge of the environment. They describe the physical wave propagation by statistical means only. For this purpose, the probability distribution of the propagation path's parameters are derived from the channel measurements. These parameters usually include path gains, time delays, and frequency offsets. The CIR is then modeled as a sum of all propagations paths. By means of measurement-based calibration of the path parameters, stochastic models can be adjusted to reproduce the radio propagation of desired communication standards in specific environments. For instance statistical channel models for V2V communication in urban, sub-urban, and expressway environments were proposed in [12, 13]. Highway environments are considered in [97]. Another branch of stochastic channel models employ the theory of spatial point processes, to mimic the behavior of time-variant radio channels. In this modeling approach, the appearance and disappearance of multipath components, due to movements of the communicating entities and the surrounding scatterers are modeled as a birth and death process. These models, e.g., [123] are capable of accounting for small- and large-scale fading and polarization aspects. Recent advances of stochastic channel models with temporal birth-death dynamics can be found in [61]. Further stochastic modeling approaches represent the whole propagation environment in terms of a graph, with vertices representing transmitters, receivers, and scatterers, and edges representing propagation conditions between them [52, 93]. The propagation graphs do not only account for scatterer interactions, but are also capable of modeling interference-limited communication [32]. Further they can be applied for analysis of the nearest neighbor network problems as suggested in [53].

A combination of deterministic and stochastic models result in so-called geometry-based stochastic channel models. These models assume the actual physical position of transmitter and receiver, while the position of scatterers and their scattering properties are chosen randomly, according to certain statistical distributions. Depending on the desired model accuracy, there exist more or less realistic models. In the less realistic models, scatterers are randomly placed on two-dimensional rings located around the transmitter and the receiver [26, 119]. In the more realistic models [63, 98], the choice of scatterers' placement is inspired by realistic assumptions. The main advantage of the geometric-stochastic models is their accuracy at reasonable computational cost.

2.2.2 Vehicular Performance Models

Previously in this section we introduced different approaches for modeling the propagation of electromagnetic waves between transmitter and receiver. Depending on the simulation purpose, one can choose the desired level of model abstractness. However, in the context of some specific simulations, e.g., simulations evaluating performance of retransmission mechanisms, scheduling techniques, and similar link or network level algorithms, any of the aforementioned channel modeling techniques would provide too many unnecessary details. Most of the existing packet level simulators, such as ns-2, ns-3, OMNET++, SWAN, OPNET, etc., rely on an indicator of packet reception success and signal power on a packet level. Therefore, having a single channel realization per packet would be sufficient. To meet these requirements, performance models are often deployed. Depending on the produced output, performance models can be divided in two types: propagation and packet error models.

Propagation models generate RSSI patters as a function of the distance. Essentially all these models originate from the free space path loss model [41] that calculates propagation attenuation as a function of distance between transmitter and receiver. With recent advances, this simple model was extended to account for different LOS situations, environments, and even site-specific properties such as street width, geographical shape of intersections, as well as density and position of relevant scattering objects. Based on the model formulation one should differentiate between empirical and analytical propagation models.

Empirical propagation models are derived from real-world measurements with off-the-shelf devices and constitute the best fit of the average measured RSSI performance. The authors of [51] used empirical V2V measurements performed with cooperative vehicle-infrastructure systems (CVIS) communication platforms [1] in urban, rural, and highway environments. They develop a simple channel model for simulation of large-scale vehicular ad-hoc networks (VANETs). In their model, the dual-slope piecewise-linear approach is used for path loss generation, Nakagami fading model for scattering and shadowing is fully neglected. The authors of [109] go one step further in the level of the model detailedness and use real-world measurements to estimate the effect of buildings on the radio communication between the vehicles. The resulting shadowing model for urban environments, takes building geometry and positions of sender and receiver into account. Next, realistic path loss values are generated with the help of 2.5D models of buildings, e.g., OpenStreetMap. As pointed out in Section 2.1, not only buildings but also other scattering objects, for instance vehicles, have severe impact on the signal propagation. To address these issues, the authors of [20] propose a model that incorporates vehicles as obstacles in VANET simulation environments. Based on the concepts of computational geometry, the authors model vehicles as 3D objects and suggest a mechanism for calculating additional attenuation due to vehicles. Obviously, the influence of the vehicles in this regard is growing with increasing vehicle dimension. For instance, a bus driving between the transmitting and the receiving vehicles, might result in additional propagation loss of up to 15 to 20 dB, as shown by the real-world measurements

in [54]. Based on these observations, the authors suggest an empirical propagation model for communication between two passenger cars in LOS conditions obstructed by a bus. V2V communication in NLOS conditions, can be modeled with the empirical propagation model presented in [72]. The proposed model is based on measurement data and allows to account for the influence of inter-building distance.

On the other hand, analytical propagation models provide extensions of well-known theoretical path loss models, such as, e.g., two-ray ground reflection model or knife-edge diffraction model. For example, the two-ray ground reflection model found its continuation in a two-ray interference model, proposed in [108]. This model additionally takes into account the interference of the ground reflection by considering the phase difference between direct and reflected rays, as well as ground reflection coefficient. An example of a model inspired by the knife-edge diffraction model can be found in [47]. This model calculates the path loss as a function of distance between two vehicles and the presence of buildings takes into account. The model can be applied to mimic V2V communication in LOS conditions, in NLOS conditions with one corner of a building along the path, and NLOS conditions with corners of two buildings along the path.

The aforementioned models cover only a small, but representative part of the existing propagation models for packet level simulations. Considering even this subset it becomes evident that the detailedness of the models spans from very abstract models to models taking into account the exact topology and the environment. Regardless of how detailed the propagation models are, they do not (directly) provide information on whether or not a packet was delivered to the dedicated receiver. This fact constitutes the main drawback of the aforementioned models, because eventually every communication system is designed to transfer information (most frequently in form of packets). Therefore, knowledge of RSSI alone is not enough to evaluate system performance. Even though the indicator of packet reception success can be derived from RSSI values, models capable of reproducing realistic packet-error behavior are of great value. Depending on the method of the packet error statistics' aggregation, we classify three types of packet error models:

- RSSI-based packet error models,
- simulation-based packet error models, and
- empirical packet error models.

RSSI-based packet error models determine whether or not a packet was successfully received, based on the corresponding signal to interference plus noise ratio (SINR) at the receiver. Whereas, the SINR is derived from the propagation mode generated RSSI. In general there are two methodologies of mapping the SINR to the indicator of packet reception success. The first one compares the SINR for each packet to certain threshold value and if the threshold value is exceeded, the packet is considered as successfully received. This approach was implemented for the highway propagation model presented in [100]. In [20], packet

reception success was determined based on the threshold values defined in the dedicated short-range communications (DSRC) standard [15]. The second methodology transforms the SINR in to the packet error rate (PER) probabilistically, depending on the used modulation and coding schemes. Such approach was adopted in [120], to design a packet error model for V2V communication in highway scenarios. To develop this model, the authors modeled the radio propagation and calculated the effective SINR for each packet with the WARP2 simulator. Consequently, an upper bound of the PER as a function of the SINR for different IEEE 802.11p modulation and coding parameters, was derived analytically.

Simulation-based packet error models do not require RSSI values, but rather rely on the binary packet reception information generated by simulation tools. In [65], linear least squares curve fitting was used to fit PDR vs. distance curves obtained with ns-2 network simulator. The proposed simulation-based model calculates the probability of packet reception in an IEEE 802.11p network based on four input arguments: distance between transmitter and receiver, transmission power, transmission rate, and vehicular traffic density. Similarly, the authors of [11] developed a packet error model that accounts for signal-to-noise ratio (SNR), data rate, and packet length. As basis the authors used the data generated by an implementation of the IEEE 802.11p physical layer (PHY) model in MATLAB Simulink. The alternative PHY model implementation on the very same MATLAB Simulink platform was used for packet error model proposed in [38]. Here, the authors used the simulated PER traces to develop a Markov model and applied polynomial regression to remove the dependence on SNR and Doppler shift.

In contrast to the previously introduced modeling approaches, empirical packet error models rely on the packet error statistics obtained from the real-world measurements. These models are the most realistic, but unfortunately also the most rare in the vehicular communication domain. An example of empirical packet error model based on measurements in a freeway-like environment can be found in [29]. In essence the modeling approach consists of fitting the measured PER vs. distance curves. Not surprisingly, the results show good agreement between model generated and measured PER traces. As mentioned by the authors, the main disadvantage of this modeling approach is that it does not provide any insights into physical dependencies leading to the obtained PER performance. As a consequence, the model is only representative for the set of measurements used for curve fitting and is thus limited in application. A further example of an empirical packet error model for V2V communications in static and dynamic environments was presented in [118]. The authors analyzed statistics of the consecutively lost/delivered packets and suggested a four state Markov model, to reproduce measured packet error traces. The proposed model is able to accurately reproduce average packet error performance in terms of packet loss statistics, but does not include distance dependencies and is therefore not suitable for realistic simulations of vehicular communications.

Concluding the overview of existing vehicular models, we want to stress that the categorization presented here is by no means intended to serve as an ultimate guide for qualitative

comparison of the models. Neither we want to favor any of the aforementioned modeling approaches. The choice of the model is strictly dependent on simulation purposes and the provided categorization shall merely help to maintain an overview.

2.3 Theoretical Framework

In this section we establish the theoretical framework that serves as a basis for the model development and evaluation in Chapter 4. We first introduce the notion of a discrete-time Markov chain (DTMC). Next, we discuss a special type of Markov models, called hidden Markov models (HMMs) and underline the particularities of both. We further address aspects of state and parameter estimation associated with HMMs. Finally, we outline relevant concepts for evaluation of the model performance.

2.3.1 Discrete-Time Markov Chains

In essence, DTMCs are subclass of stochastic processes and we therefore, begin this section by introducing the concept of stochastic process. In a nutshell, a discrete-time stochastic process $\mathcal{X}$ is a sequence of random variables $\mathbf{x} = (\mathsf{X}_1, \mathsf{X}_2, \ldots)$ and is meant to represent the evolution of not deterministic phenomena over time. The random variable X_t is referred to as the state of the process at time t and it can take different values. The ensemble of all possible values that the random variables in $\mathbf{x}$ can take is called the state space, and is denoted by $\mathcal{S}$. As a very simple example, consider sequential coin tossing. There are only two possible state values and the state space is given as $\mathcal{S} = \{\text{HEADS}, \text{TAILS}\}$. In general, states of stochastic processes can take arbitrary values, for instance natural numbers, integers, or a subset of any of those. If the state space consists of finite or countably infinite number of elements, i.e., $\mathcal{S} = \{-a, \ldots, -2, -1, 0, 1, 2, \ldots, b\}$ with some integers $a, b > 0$, the state space is called finite. A discrete-time stochastic process with finite length is given as:

$$\mathcal{X} = (\mathsf{X}_1, \mathsf{X}_2, \ldots, \mathsf{X}_t, \ldots, \mathsf{X}_T).$$

If in such a process the present state X_t depends on the past only via X_{t-1} it is referred to as DTMC of order 1. Let t be the present time and assume that the past state X_{t-1} is known. If $\mathcal{X}$ is a DTMC, the distribution of the state X_t will only depend on the past state X_{t-1}, i.e., knowledge of X_{t-1} subsumes the information given by the *entire* past. We therefore have:

$$p(X_t \mid X_{t-1}, X_{t-2}, \ldots, X_1) = p(X_t \mid X_{t-1}),\ \forall\ t. \tag{2.1}$$

The relation in (2.1) is called the Markov property. Straightforward use of conditional probabilities shows that any process satisfying the following Markov property satisfies the more general condition:

$$p(X_{t+m}, \ldots, X_t \mid X_{t-1}, \ldots, X_1) = p(X_{t+m}, \ldots, X_t \mid X_{t-1}),\ \forall\ t, m \geq 0.$$

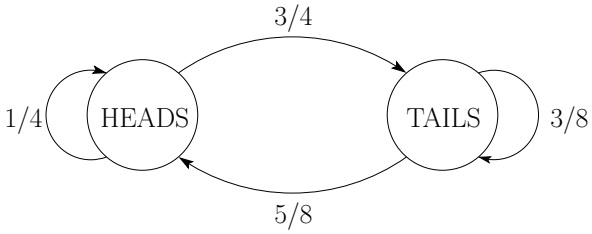

Figure 2.1: State transition diagram for the two-state Markov chain with the state space $\mathcal{S} = \{\text{HEADS}, \text{TAILS}\}$. The edges are labeled with the corresponding state transition probabilities.

The probability that the Markov chain at the next time instant is in state j, given that it is currently in state i, is called state transition probability and is denoted as:

$$a_{ij}(t) = \mathbb{P}\{\mathsf{X}_{t+1} = j \mid \mathsf{X}_t = i\}. \tag{2.2}$$

Clearly, the transition probabilities are $0 \leq a_{ij} \leq 1$. If the transition probabilities are independent of t, then the processes is said to be *homogeneous*. For homogeneous processes we use the notation a_{ij} to denote the probability that the Markov chain moves into state j, whenever it is in state i. The transition probabilities between all states of the state space $\mathcal{S} = \{1, 2, \ldots, N\}$ are given by the following N x N transition matrix $\boldsymbol{A}$:

$$\boldsymbol{A} = \begin{pmatrix} a_{11} & a_{12} & \ldots & a_{1N} \\ a_{21} & a_{22} & \ldots & a_{2N} \\ \vdots & \vdots & \ddots & \vdots \\ a_{N1} & a_{N2} & \ldots & a_{NN} \end{pmatrix}. \tag{2.3}$$

From the definition of conditional probabilities it is straightforward to see that the sum of every row of the transition matrix must be equal to one, i.e., $\sum_{j \in \mathcal{S}} a_{ij} = 1, \ \forall \ i \ \in \mathcal{S}$.

A Markov chain can be represented graphically by a state transition diagram, a signal flow graph, in which the vertices represent the states and the edges the transition probabilities. Recall the coin tossing example described by the two-state Markov chain with the state space $\mathcal{S} = \{\text{HEADS}, \text{TAILS}\}$. Assume that the coin is "unfair" and has memory, meaning that the transition probabilities are not equally likely and are given by the following transition matrix:

$$\boldsymbol{A} = \begin{pmatrix} 1/4 & 3/4 \\ 5/8 & 3/8 \end{pmatrix}.$$

The state transition diagram for this two-state Markov chain is shown in Figure 2.1.

2.3.2 Hidden Markov Models

In the broadest sense, a HMM is a DTMC split into two components: an observable component and an unobservable or "hidden" component. Let us assume that $\mathcal{X}$ is a DTMC with

finite number of states $\mathcal{S} = \{s_1, s_2, \ldots, s_N\}$ and it is not observable. However, there exists another DTMC $\mathcal{Y}$ with finite number of states $\mathcal{V} = \{v_1, v_2, \ldots, v_M\}$, which depends probabilistically on $\mathcal{X}$ and is observable. Then $(\mathcal{X}, \mathcal{Y})$ is a HMM with N states and M observation symbols. Adopting terminology from signal processing, we will refer to the unobserved component $\mathcal{X}$ as the signal process and $\mathcal{S}$ as the signal state space, while the observed component $\mathcal{Y}$ is called the observation process and $\mathcal{V}$ is the observation state space. To understand the origin of the signal/observation process terminology one could think of a communication system, in which a random signal $\mathcal{X}$ is transmitted through a noisy communication channel. The receiver then observes a corrupted signal $\mathcal{Y}$, from which the original signal need to be reconstructed.

Just as in the case of DTMCs, the probability that the state i of $\mathcal{S}$ will be followed by the state j is given by the transition probability a_{ij}. The set of all transition probabilities is given by N x N transition matrix $\boldsymbol{A}$ (see Equations (2.2) and (2.3)). The probability of an observation k in state j at time instance t is called emission probability and is denoted as:

$$b_j^k(t) = \mathbb{P}\{\mathsf{Y}_t = k \mid \mathsf{X}_t = j\}. \tag{2.4}$$

The emission probabilities must satisfy $0 \leq b_j^k \leq 1$ and can be written in form of an N x M emission matrix $\boldsymbol{B}$:

$$\boldsymbol{B} = \begin{pmatrix} b_1^1 & b_1^2 & \ldots & b_1^M \\ b_2^1 & b_2^2 & \ldots & b_2^M \\ \vdots & \vdots & \ddots & \vdots \\ b_N^1 & b_N^2 & \ldots & b_N^M \end{pmatrix}. \tag{2.5}$$

The sum of every row of the emission matrix must be equal to one, i.e., $\sum_{k \in \mathcal{V}} b_j^k = 1, \ \forall \ j \ \in \mathcal{S}$. The HMM is called homogeneous, if both the transition matrix $\boldsymbol{A}$ and the emission matrix $\boldsymbol{B}$.

For the complete description of a HMM we only need to introduce the initial state distribution, which shows how large is the probability that the HMM will start in any of the states from the signal state space and is denoted as:

$$\boldsymbol{\pi}_1 = (\pi_1(1), \pi_1(2), \ldots, \pi_1(N)), \tag{2.6}$$

where $\pi_1(i) = \mathbb{P}\{\mathsf{X}_1 = i\} \ \forall \ i \ \in \mathcal{S}$. The set of model parameters $\Theta = (\boldsymbol{\pi}_1, \boldsymbol{A}, \boldsymbol{B})$, including the initial state distribution, the transition and the emission matrices, is sufficient to describe any HMM.

In the context of communications, HMMs can be effectively applied for modeling the signal transmission over burst-noise channels. The burstiness of a channel implies that once an error occurs at time t, the chance of having errors in subsequent time instances tends to be high. To model burst-noise channels, Gilbert [46] has suggested a simple HMM with two states "good" and "bad" and two observation symbols "0" (no error) and "1" (error).

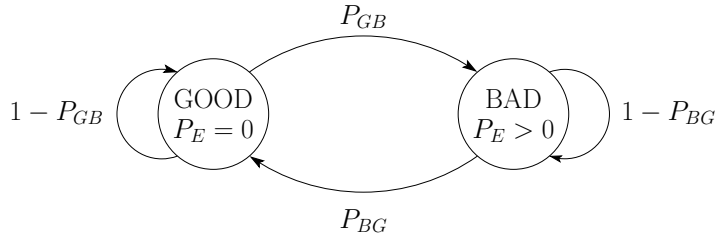

Figure 2.2: State transition diagram for Gilbert's model.

That is, the signal state space is given as $\mathcal{S} = \{\text{GOOD}, \text{BAD}\}$ and the observation space as $\mathcal{V} = \{0, 1\}$. In Gilbert's model the good state is always error-free, and in the bad state an error occurs with some probability P_E. The transition matrix of the Gilbert's model is given as:

$$\boldsymbol{A} = \begin{pmatrix} 1 - P_{GB} & P_{GB} \\ P_{BG} & 1 - P_{BG} \end{pmatrix}, \tag{2.7}$$

where $P_{GB} = \mathbb{P}\{\mathsf{X}_{t+1} = \text{BAD} \mid \mathsf{X}_t = \text{GOOD}\}$ denotes probability of changing from the good state to the bad state, and $P_{BG} = \mathbb{P}\{\mathsf{X}_{t+1} = \text{GOOD} \mid \mathsf{X}_t = \text{BAD}\}$ denotes probability of changing from the bad state to the good. The emission matrix of the Gilbert's model is given as:

$$\boldsymbol{B} = \begin{pmatrix} 0 & 1 \\ P_E & 1 - P_E \end{pmatrix}. \tag{2.8}$$

The corresponding state transition diagram is shown in Figure 2.2.

Thus, the set of model parameters is given by the four probabilities $\Theta = (\pi_1(\text{GOOD}), P_{GB}, P_{BG}, P_E)$[1]. Given the model parameters Θ, error patterns featuring a realistic bursty structure can be generated with a simple two-phase algorithm (cf. Algorithm 2.1). In the first phase of the algorithm the state of the model is selected and in the second phase a binary error pattern digit is produced.

2.3.3 Model Parameter Estimation

HMMs and Gilbert's model in particular, are widely used for reproducing various realistic phenomena, for instance error-prone transmission over a noisy channel with memory. To ensure that the model reproduces the actual behavior of a real system, the model parameters $\Theta = (\boldsymbol{\pi}_1, \boldsymbol{A}, \boldsymbol{B})$ need to be carefully selected. Therefore an initial guess of the parameters is made in some manner and then observations (training data) are used to find better suiting parameters. This process is referred to as parameter estimation and is intended to update the parameters such that the model is more likely to generate the training samples. There exist no known way to analytically find an expression for a maximum likelihood estimate of model parameters. However, by using an iterative procedure as, e.g., the Baum-Welch algorithm [16], one could choose Θ such, that the probability to obtain the training data given the model parameters is locally maximized.

[1] Here the initial state distribution is fully described by $\pi_1(\text{GOOD})$, since $\pi_1(\text{BAD}) = 1 - \pi_1(\text{GOOD})$.

Algorithm 2.1 *Error pattern generation algorithm with Gilbert's model.*

Input:
T - number of observations to be generated
$\Theta = (\pi_1(\text{GOOD}), P_{GB}, P_{BG}, P_E)$ - model parameters

for $t = 1$ to T **do**

Phase 1 - State selection

if $t = 1$ **then**
select state $X_t \in \mathcal{S} = \{GOOD, BAD\}$ according to $\pi_1(\text{GOOD})$
else
select state $X_t \in \mathcal{S} = \{GOOD, BAD\}$ according to (P_{GB}, P_{BG})
end if

Phase 2 - Observation generation

if X_t =GOOD **then**
generate observation $Y_t \leftarrow 0 \Rightarrow$ no error
else
generate observation $Y_t \in \mathcal{V} = \{0, 1\}$ according to P_E
end if
end for

Output:
$\boldsymbol{y} = (Y_1, Y_2, \ldots, Y_T)$ - vector of observations (binary error pattern) of length T

To understand the Baum-Welch algorithm for parameter estimation we first need to introduce the concept of forward and backward probabilities. The forward probability $\alpha_t(i)$ is defined as the probability of being in state i at time instance t and observing the training sequence $(Y_1, Y_2, \ldots Y_t)$ until time instance t, given the model parameters Θ:

$$\alpha_t(i) = \mathbb{P}\{\mathsf{Y}_1 = Y_1, \mathsf{Y}_2 = Y_2, \ldots, \mathsf{Y}_t = Y_t, \mathsf{X}_t = i; \Theta\}. \tag{2.9}$$

The backward probability $\beta_t(i)$ is defined as the probability of observing the training sequence $(Y_{t+1}, Y_{t+2}, \ldots, Y_T)$ starting at time instance $t + 1$ till the end, given that the model is in state i at time instance t and the model parameters Θ:

$$\mathbb{P}\{\mathsf{Y}_1 = Y_1, \mathsf{Y}_2 = Y_2, \ldots, \mathsf{Y}_T = Y_T \mid X_t = i; \Theta\}. \tag{2.10}$$

Since the forward probability $\alpha_t(i)$ accounts for the part of the observation sequence up to time t and the backward probability $\beta_t(i)$ accounts for the remaining observations, we can calculate the probability of being in state i at time instance t, given the sequence of observations $\boldsymbol{y} = (Y_1, Y_2, \ldots, Y_T)$ and the model parameters Θ as:

$$\gamma_t(i) = \mathbb{P}\{\mathsf{X}_t = i \mid \boldsymbol{y}; \Theta\} = \frac{\alpha_t(i)\beta_t(i)}{\mathbb{P}\{\boldsymbol{y}; \Theta\}} = \frac{\alpha_t(i)\beta_t(i)}{\sum_{i=1}^{N} \alpha_t(i)\beta_t(i)}, \tag{2.11}$$

here $\mathbb{P}\{\boldsymbol{y};\Theta\} = \sum_{i=1}^{N} \alpha_t(i)\beta_t(i)$ is a normalization factor, which ensures that $\gamma_t(i)$ is a probability measure with $\sum_{i=1}^{N} \gamma_t(i) = 1$. Summing $\gamma_t(i)$ over time would provide the expected number of times that the state i is visited, or equivalently, the number of transitions made from the state i:

$$\sum_{t=1}^{T} \gamma_t(i) = \text{expected number of transitions from state } i. \tag{2.12}$$

Similarly, we can calculate $\xi_t(i,j)$, the probability of being in state i at time instance t and in state j at time instance $t+1$, given the sequence of observations $\boldsymbol{y} = (Y_1, Y_2, \ldots, Y_T)$ and the model parameters Θ denoted as:

$$\xi_t(i,j) = \mathbb{P}\{\mathsf{X}_t = i, \mathsf{X}_{t+1} = j \mid \boldsymbol{y};\Theta\} = \frac{\mathbb{P}\{\mathsf{X}_t = i, \mathsf{X}_{t+1} = j, \boldsymbol{y};\Theta\}}{\mathbb{P}\{\boldsymbol{y};\Theta\}}, \tag{2.13}$$

where $\mathbb{P}\{\boldsymbol{y};\Theta\}$ is again a normalization factor. Applying forward and backward probabilities, we obtain the following expression for $\xi_t(i,j)$:

$$\xi_t(i,j) = \frac{\alpha_t(i) a_{ij} b_j^{Y_{k+1}} \beta_{t+1}(j)}{\sum_{i=1}^{N}\sum_{j=1}^{N} \alpha_t(i) a_{ij} b_j^{Y_{k+1}} \beta_{t+1}(j)}, \tag{2.14}$$

where a_{ij} is the transition probability as defined in (2.2) and $b_j^{Y_{k+1}}$ is the probability of emitting observation $Y_{k+1} \in \mathcal{V}$ in state j as defined in (2.4). The total expected number of transitions from state i to state j can be calculated as the sum over all $\xi_t(i,j)$:

$$\sum_{t=1}^{T} \xi_t(i,j) = \text{expected number of transitions from state } i \text{ to state } j. \tag{2.15}$$

Applying the concept of counting event occurrences on the aforementioned quantities $\sum_{t=1}^{T} \gamma_t(i)$ and $\sum_{t=1}^{T} \xi_t(i,j)$, Baum proposed the following way of model parameter reestimation:

$$\begin{aligned}
&\overline{\pi}_0(i) = \gamma_1(i) \implies \text{expected number of times in state } i \text{ at time instance } t = 1,\\
&\overline{a_{i,j}} = \frac{\sum_{t=1}^{T} \xi_t(i,j)}{\sum_{t=1}^{T} \gamma_t(i)} \implies \frac{\text{expected number of transitions from state } i \text{ to state } j}{\text{expected number of transitions from state } i},\\
&\overline{b_j^k} = \frac{\sum_{t=1,\ \text{s. t. } Y_t = k}^{T} \gamma_t(i)}{\sum_{t=1}^{T} \gamma_t(i)} \implies \frac{\text{expected number of times emitting observation } k \text{ in state } j}{\text{expected number of times in state } j}.
\end{aligned} \tag{2.16}$$

It has been proven by Baum that either the observation sequence is more likely to be produced by the model with reestimated parameters $\overline{\Theta} = (\overline{\boldsymbol{\pi}_1}, \overline{\boldsymbol{A}}, \overline{\boldsymbol{B}})$, or the initial model parameters define the critical point of the likelihood function, in which case $\overline{\Theta} = \Theta$ and no better estimate can be found. The reestimation algorithm is terminated when either $\overline{\Theta} = \Theta$ or the maximum number of iterations have been reached. Thus iteratively using $\overline{\Theta}$ instead of Θ and reestimating model parameters will eventually lead to a higher probability $\mathbb{P}\{\boldsymbol{y}; \overline{\Theta}\}$ of observing $\boldsymbol{y}$ from the model with parameters $\overline{\Theta}$.

The main drawback of this iterative parameter estimation algorithm is that it only finds local maxima. Therefore, parameters selected by the iterative Baum-Welch algorithm for the same training data may differ. To overcome this issue in the development stage of the packet-error models presented in this thesis, we repeatedly estimated the model parameters with the Baum-Welch algorithm 10^4 times and the choose parameters resulting in the largest probability $\mathbb{P}\{\boldsymbol{y}; \Theta\}$.

2.3.4 Model Performance Evaluation

The challenge of finding a model that represents training data in the most accurate way does not only emerge in the context of parameter estimation, but is essential for modeling per se. Since the main purpose of any model is to represent realistic phenomena with application-defined accuracy, the decision about its quality is usually made by comparison of model generated data with measured data. Therefore, the definition of meaningful and comprehensive measures to assess the agreement between modeled and measured results, comprises the main focus of model performance evaluation. There exist a large number of metrics for model performance evaluation. These metrics can be classified in two classes: statistical and distance-dependent measures. The main difference between the two, is that the statistical measures are intended to compare the structure of data sets, while the distance-dependent measures evaluate the similarity of data sets as such.

Statistical measures can be broken in two parts: descriptive and inferential. Descriptive statistical measures are used to quantitatively describe the data and to summarize them in a way that facilitates visualization and interpretation. Interpretation of raw data and consequently comparison between data sets is often quite challenging, due to the large amount of information. To overcome this challenge the whole data set is often characterized by a single value or measure. A variety of such numerical measures have been suggested, however the proportion, or percentage, of data values in each category is still one of the most significant descriptive statistical measures. In the context of packet-error modeling we suggest to quantitatively describe the data in terms of **percentage of erroneous packets**, denoted as $\hat{P}_e$. The percentage of erroneous packets is defined as the ratio between the number of lost (N_{lost}) and transmitted (N_{trans}) packets and is directly related to total throughput as follows:

$$\text{total throughput} = (100 - \hat{P}_e) \cdot N_{\text{trans}} \cdot \text{packet length}. \tag{2.17}$$

As the relation between the two measures is straightforward, we will only provide the values for $\hat{P}_e$ in this thesis.

Although descriptive statistical measures are broadly used and well suited for characterizing the features of data samples, their outcomes cannot be used to characterize the population as a whole. For instance if one particular measurement resulted in $\hat{P}_e$ of 20 %, we cannot claim that all other measurements in the same settings will have exactly the same percentage of erroneous packets. In contrast, inferential statistical measures use data from a sample to draw conclusions about the whole population. A broadly used inferential statistical measure is hypothesis testing. For hypothesis testing, first a tentative assumption about certain parameter or distribution is made. Next, sample data is used to determine whether or not the initial assumption is valid. One of the most practical and general approaches for comparing two data samples in this way is the so-called two-sample Kolmogorov-Smirnov test. It is a nonparametric method[2] used to test, whether two samples come from the same distribution.

Suppose that we want to test, whether the two samples $\boldsymbol{x} = (X_1, X_2, \ldots, X_m)$ of size m and $\boldsymbol{y} = (Y_1, Y_2, \ldots Y_n)$ of size n come from the same distribution. We therefor calculate empirical cumulative distribution functions (CDFs) of the two samples, denoted as $F_m(x)$ and $G_n(x)$. Next, we make the initial assumption, also called null hypothesis and denoted by H_0, that the two samples come from the same distribution, i.e., $H_0 : F_m(x) = G_n(x)$. The alternative hypothesis is that two samples come from different distributions, i.e., $H_1 : F_m(x) \neq G_n(x)$. The **Kolmogorov-Smirnov statistic** is defined as:

$$D_{KS} = \sup_x |F_m(x) - G_n(x)|, \tag{2.18}$$

which is simply the largest vertical distance between the two empirical CDFs. The null hypothesis H_0 is rejected at significance level α if:

$$D_{KS} \cdot \sqrt{l} > \lambda_0. \tag{2.19}$$

Whereas in the contrary case the test does not lead to the rejection of H_0. In (2.19) $l = \frac{n \cdot m}{n+m}$ is simply a normalization factor, taking into account the length of both samples. While λ_0 is a value, such that the CDF $Q(\lambda_0)$, defined as $Q(\lambda_0) = P\{D_{KS} \cdot \sqrt{l} \leq \lambda_0\}$, satisfies $Q(\lambda_0) = 1 - \alpha$. For the most frequently used significance levels α, the values of λ_0 can be found in the form of tables (see, e.g., [40]). For $\alpha = 0.05$ the threshold value equals $\lambda_0 = 1.36$. Hence if $D_{KS} \cdot \sqrt{l} > 1.36$ the null hypothesis is rejected, leading to the conclusion that two samples come from different distributions. If however, the null hypothesis is accepted it is interesting to evaluate the value of $Q(\lambda)$ at $\lambda = D_{KS} \cdot \sqrt{l}$. The relationship between λ and

[2] In this context nonparametric method means that it does not assume data to be sampled from any particular distribution.

$Q(\lambda)$ is given by the Kolmorogov's theorem [66], which shows that for sufficiently large l:

$$Q(\lambda) = \begin{cases} \sum_{i=-\infty}^{l} (-1)^i \exp(-2i^2\lambda^2) & \text{for } \lambda > 0, \\ 0 & \text{for } \lambda \leq 0 \end{cases} . \tag{2.20}$$

Thus, the closer $Q(\lambda)$ is to 1, the more similar are the distributions of the two samples $\boldsymbol{x}$ and $\boldsymbol{y}$. In this sense $Q(\lambda)$, also referred to as **p-value** can be seen as a bounded measure of similarity in distribution of two samples.

Although statistical measures can be successfully employed for quantitative comparison of average performance, they are well suited for evaluation of the difference between the samples that change their properties over time or distance. To clarify this statement let's consider a packet-error trace resulting from a V2I measurement as an example. It is obvious that the PDR, defined as the ratio between the number of received and transmitted packets, is decreasing with increasing distance between the transmitter and the receiver. Therefore, in the context of this example the PDR is the a property that changes over the distance. A good packet-error model will not only reproduce the percentage of erroneous packets, but will also mimic the realistic dependence of PDR on the distance. Therefore we would like to evaluate the difference between the measured and modeled PDR samples at every distance point. For that reason we introduce the following distance-dependent measures used for model performance evaluation in this thesis:

- **Kullback-Leibler divergence (KLD)** between two vectors $\boldsymbol{x}$ and $\boldsymbol{y}$ is a measure of deviation between the vectors and is defined as:

$$\mathbf{D}_{\mathrm{KL}}(\boldsymbol{x}, \boldsymbol{y}) = \sum_{i=1}^{N} \left(X_i \log \left(\frac{X_i}{Y_i} \right) - X_i + Y_i \right). \tag{2.21}$$

  It is a non-negative measure, meaning that $\mathbf{D}_{\mathrm{KL}}(\boldsymbol{x}, \boldsymbol{y}) \geq 0$, for any $\boldsymbol{x}$ and $\boldsymbol{y}$. We have $\mathbf{D}_{\mathrm{KL}}(\boldsymbol{x}, \boldsymbol{y}) = 0$ if and only if $\boldsymbol{x} = \boldsymbol{y}$. The larger the incongruity of the vectors $\boldsymbol{x}$ and $\boldsymbol{y}$, the greater is the value of $\mathbf{D}_{\mathrm{KL}}(\boldsymbol{x}, \boldsymbol{y})$. To avoid numerical problems when calculating KLD, we assign a value of 10^{-10} for all elements $Y_i \in \boldsymbol{y}$ such that $Y_i = 0$. If $\boldsymbol{x}$ and $\boldsymbol{y}$ are probability vectors, which implies that $\sum_{i=1}^{n} X_i = 1$ and $\sum_{i=1}^{m} Y_i = 1$, KLD is the same as relative entropy and is given as $\mathbf{D}_{\mathrm{KL}}(\boldsymbol{x}, \boldsymbol{y}) = \sum_{i=1}^{N} X_i \log \left(\frac{X_i}{Y_i} \right)$.

- **Mean squared error (MSE)** is defined as the elementwise average of the squared difference between two vectors $\boldsymbol{x}$ and $\boldsymbol{y}$ and is calculated as follows:

$$\mathbf{MSE}(\boldsymbol{x}, \boldsymbol{y}) = \frac{1}{N} \sum_{i=1}^{N} (X_i - Y_i)^2. \tag{2.22}$$

  Similarly to the KLD, the MSE is a non-negative measure and we have $\mathbf{MSE}(\boldsymbol{x}, \boldsymbol{y}) = 0$, if and only if $\boldsymbol{x} = \boldsymbol{y}$.

Both the KLD and the MSE are not upper bounded. Therefore they are better suited for relative comparison rather then for quantitative. In other words, if $\mathbf{D}_{\mathrm{KL}}(\boldsymbol{x}, \boldsymbol{y}) > \mathbf{D}_{\mathrm{KL}}(\boldsymbol{x}, \boldsymbol{z})$, or alternatively $\mathbf{MSE}(\boldsymbol{x}, \boldsymbol{y}) > \mathbf{MSE}(\boldsymbol{x}, \boldsymbol{z})$, we can conclude that vector $\boldsymbol{z}$ is certainly more similar to vector $\boldsymbol{x}$ as $\boldsymbol{y}$ (in KLD or MSE, sense). However, neither the KLD nor the MSE value will answer the question, to what extent vector $\boldsymbol{x}$ is more similar to $\boldsymbol{z}$ than to $\boldsymbol{y}$.

- To allow a quantitative comparison we introduce the **collinearity** as an upper bounded distance-dependent measure. According to the definition in [55], the collinearity between two vectors $\boldsymbol{x}$ and $\boldsymbol{y}$ is given as:

$$\boldsymbol{\gamma}(\boldsymbol{x}, \boldsymbol{y}) = \frac{\langle \boldsymbol{x}, \boldsymbol{y} \rangle}{\|\boldsymbol{x}\| \|\boldsymbol{y}\|} = \frac{\sum\limits_{i=1}^{N} X_i \cdot Y_i}{\sum\limits_{i=1}^{N} |X_i| \cdot \sum\limits_{i=1}^{N} |Y_i|}. \tag{2.23}$$

  The collinearity becomes 1 if and only if $\boldsymbol{x} = \boldsymbol{y}$, and 0 if the two vectors are orthogonal. In this sense based on the measure of collinearity, we can perform not only relative but also quantitative comparison.

In Equations (2.21)–(2.23), N is the number of elements in the vectors $\boldsymbol{x}$ and $\boldsymbol{y}$. If the number of elements in both vectors is not the same, $N = \max(n, m)$ is the number of elements in the longest vectors among $\boldsymbol{x}$ and $\boldsymbol{y}$. We perform zero-padding to ensure that both vectors have the same length N.

Despite the versatility of the aforementioned measures, none of them is capable to provide a comprehensive statement about the similarity of two observation samples. Therefore, neither statistical nor distance-dependent measures, bounded or unbounded, should be used as a sole criterion for model performance evaluation. Instead we suggest to use a combination of different measures, to assess model performance as conclusive and well-founded as possible.

3

Vehicle-to-Infrastructure Performance Measurements

3.1 Vehicular Performance Measurement Campaigns

In this section we summarize the details of three measurement campaigns: ROADSAFE2010, ROADSAFE2011, and iTETRIS. The first two measurement campaigns were performed in highway environments in Austria. They serve as a basis for the performance evaluation of vehicle-to-infrastructure (V2I) communications presented in this chapter. The iTETRIS measurement campaign was performed in urban environments in Italy. The data gained from this measurement campaign is used to parametrize the environment-aware performance model introduced in Chapter 4.

All these measurements are focused on evaluation of the performance of V2I communications under various settings and conditions. For this purpose, in each experiment the roadside unit (RSU) equipment was installed at preselected locations. The RSU equipment consists of an IEEE 802.11p-compliant transmitter that is connected to the transmit antenna. The transmit antenna is mounted above the vehicle level. The RSU transmits packets of a predefined format in broadcast mode. The payload of each transmitted packet includes a unique packet identifier. In each experiment, there was only one active RSU at a time. Therefore, all results presented in this thesis correspond to interference-free communication.

For packet reception, on-board unit (OBU) equipment was placed inside a test vehicle. The OBU equipment consists of an IEEE 802.11p-compliant receiver that is connected to the receive antenna and to a global positioning system (GPS) module. The test vehicle was driving by the RSU and recording the received signal. There was no uplink signaling of any kind and communication was performed outside the context of a basic service set mode (avoiding latency caused by channel scanning, authentication and association phases).

Table 3.1: RSU locations for the ROADSAFE2010 measurement campaign.

	Latitude	**Longitude**
Position 1	48.1264	16.3934
Position 2	48.1515	16.4870

(a) RSU at position 1.

(b) RSU at position 2.

Figure 3.1: Environment at RSU locations for the ROADSAFE2010 measurement campaign. The red circles indicate position of the RSU.

For each detection event, the OBU recorded time and location (provided by the GPS receiver) along with the corresponding received signal strength indicator (RSSI). For the purpose of accurate RSSI estimation, the equipment was carefully calibrated through laboratory measurements. All detection events underwent a cyclic redundancy check (CRC) to determine whether the detected packet was decoded correctly or not. If the packet was decoded correctly, the unique packet identifier was extracted from the payload. The packet identifiers were used in the post processing stage to create a binary packet-error pattern containing information about all detection events. This error pattern together with the GPS data and the RSSI values were used for performance evaluation and modeling.

In the following, we provide a detailed description of the equipment and settings used in each of the measurement campaigns.

3.1.1 ROADSAFE2010

The ROADSAFE2010 measurements were conducted in September 2010 in the framework of project ROADSAFE [6]. In these measurements we investigated the influence of the transmit parameters, RSU antenna type, and antenna gain on the performance of V2I communications. Furthermore, we analyzed the impact of tunnel environments on the signal propagation.

The measurements were performed at two different locations on highways S1 and A4, hereafter denoted as position 1 and position 2, respectively. The exact RSUs positions are provided in Table 3.1. The surrounding environment is illustrated in Figure 3.1. Here, the RSU positions are indicated by red circles. The highway stretch near the RSU position 1 consists of two driving lanes in each direction. The highway is bordered by grass-covered embankments from both sides, creating a kind of a canyon (cf. Figure 3.2c). As shown in Figure 3.1a, the environment at position 1 is rural, with no significant impairments in the

Table 3.2: RSU antenna parameters for the ROADSAFE2010 measurement campaign.

Parameter	**Value**			
	Antenna 1	Antenna 2	Antenna 3	Antenna 4
Type	omni-directional	directional	directional	directional
Gain [dBi]	9	6	10	13
EIRP [dBm]	20.3	12.8	16.8	19.8
3 dB BW hor./ver. [°]	360 / 14	60 / 60	35 / 35	42 / 23
Polarization	vertical	RHCP	RHCP	RHCP
Height [m]	9.1	7.1	7.1	7.1

(a) RSU antenna 1. (b) RSU antennas 2-4. (c) RSU antenna mounting.

Figure 3.2: RSU antennas for the ROADSAFE2010 measurement campaign.

direct vicinity of the RSU, apart from a tunnel and an overpass. The 300 m long tunnel ends 150 m before the position of the RSU and the overpass is located 140 m behind the RSU. The RSU position 2 is located on a two-lane highway, next to a junction. This highway connects the city of Vienna with the international airport of Vienna. This implies dense traffic and a significant amount of road signs. Apart from that the environment can be categorized as semi-rural with vegetation along the roadside, as shown in Figure 3.1b. At either RSU position, the measurements were performed in both driving directions.

As transmitters we used two nodes of the so-called cooperative vehicle-infrastructure systems (CVIS) platform [1], equipped with a radio module implementing the IEEE 802.11p protocol. We placed the transmitter platforms inside a weather protected cabinet next to a highway gantry, where it was connected to the mains and a local area network (LAN). The LAN connection was used for remote control of the transmitters. The radio frequency (RF) front end of the CVIS platform was connected with a low-loss cable to the RSU antenna under test. For measurements at position 1, a set of two directional RSU antennas was used. One of the antennas was radiating in the direction of the tunnel exit and the other in the opposite direction along the highway (cf. Figure 3.2b). Both directional antennas were mounted directly on the metallic constructions of the highway gantry, at a height of 7.1 m above ground. The directional antennas were connected to the transmitter platform via a 3 dB power splitter followed by a 17 m long low-loss cable. To analyze the effect of the

(a) OBU antenna 1. (b) OBU antenna 2.

Figure 3.3: OBU antennas for the ROADSAFE2010 measurement campaign.

transmit antenna gain, we have used three sets of directional antennas, subsequently denoted as RSU antenna 2, RSU antenna 3, and RSU antenna 4. All three antennas were placed in the same antenna housing. At RSU position 2, an omni-directional antenna manufactured by "SMARTEQ" was used. We refer to this antennas as RSU antenna 1. Similarly to the RSU antennas 2 to 4, this antenna was mounted on a highway gantry. On top of a 1 m long metallic mast. We used the mast to ensure that the metallic gantry construction does not affect the radiation pattern of the antenna and homogeneous coverage is obtained in all directions. To connect antenna 1 to the RF front end of the CVIS transmitter a cable of the same length and type as for antennas 2 to 4 was used. At both RSU positions, the RSU antennas were mounted on the right side of the highway gantry in direction of driving, closer to the roadside. The detailed characteristics of the transmit antennas are summarized in Table 3.2.

As receiver we used another node of the CVIS platform. The receiving node was placed inside the test vehicle, where it was connected to a power supply and a laptop. The laptop was used to control the recording process. The RF front end of the receiver was connected to the OBU antenna under test. The CVIS platform has an internal GPS receiver and therefore it requires a GPS antenna in addition to the OBU antenna. In these experiments two types of OBU antennas were used: (i) a CVIS vehicle rooftop antenna unit (cf. Figure 3.3a) and (ii) a windshield antenna (cf. Figure 3.3b). We denote the CVIS vehicle rooftop antenna unit as OBU antenna 1. It contains five individual antennas including antennas for communications access for land mobiles (CALM) M5, CALM 2G/3G, dedicated short-range communications (DSRC), wireless local area network (WLAN), and GPS. In our measurements only the CALM M5 and GPS antennas were utilized for signal reception and positioning, respectively. The CVIS antenna for CALM M5 communication is a vertically polarized double-fed printed monopole and has a radiation pattern close to isotropic. The nominal antenna gain is 6.5 dBi. The OBU antenna 1 was mounted using magnets in the center of the rooftop of the test vehicle (cf. Figure 3.3a). The windshield antenna is a circularly polarized directional antenna with a

Table 3.3: Measurement parameters for the ROADSAFE2010 measurement campaign.

Parameter	**Value**		
	Setting 1	Setting 2	Setting 3
Data rate [Mbit/s]	6	6	12
Packet length [Bytes]	200	1554	200
Transmit rate [packets/s]	1600	400	2100
Transmit power [dBm]	16		
Center frequency [MHz]	5880		
Average speed [km/h]	100		

nominal antenna gain of 6 dBi. The antenna was mounted on the inner side of the windshield next to the front passenger seat, as shown in Figure 3.3b. We denote this antenna as OBU antenna 2.

To test the influence of the transmit parameters on the performance of V2I communications we have performed experiments with three different settings. In setting 1, we transmitted 200 Bytes long packets at a data rate of 6 Mbit/s. This corresponds a QPSK modulation with code rate 1/2. In setting 2, we transmitted 1554 Bytes long packets at the same data rate of 6 Mbit/s. This packet length corresponds to the maximum allowed packet size of the CVIS transmitter. Finally, in setting 3, 200 Bytes long packets were transmitted at a data rate of 12 Mbit/s, corresponding to 16-QAM modulation with code rate 1/2. The packets were sent at the maximum rate achievable by the CVIS transmitter. This rate was varying depending on the chosen parameter setting. In particular, the transmit rate amounts to 1600 packets/s, 400 packets/s, and 2100 packets/s for settings 1, 2, and 3, respectively. The transmit power was set to 16 dBm. The resulting equivalent isotropically radiated power (EIRP) values for the different RSU antennas are provided in Table 3.2.

The measurements were performed at a center frequency of 5880 MHz with real vehicular traffic. The average test vehicle velocity was 100 km/h (27.8 m/s) with marginal deviations due to traffic. The parameters of the ROADSAFE2010 campaign are summarized in Table 3.3.

3.1.2 ROADSAFE2011

The ROADSAFE2011 measurements were conducted in August 2011 in the framework of project ROADSAFE [6]. The emphasis of this measurement campaign was on the influence of realistic highway impairments as well as the impact of OBU antenna gain and type on the quality of V2I communications. For this purpose, four RSU positions were selected along highway A4. The exact positions of the RSUs are provided in Table 3.4. The surrounding environment is illustrated in Figure 3.4. Here, the RSU positions are indicated by red circles. The highway A4 connects the city of Vienna with the international airport of Vienna. This implies dense traffic and a significant amount of road signs. As shown in Figure 3.4a, the

Table 3.4: RSU locations for the ROADSAFE2011 measurement campaign.

	Latitude	**Longitude**
Position 1	48.1540	16.4801
Position 2	48.1474	16.4994
Position 3	48.1423	16.5177
Position 4	48.1402	16.5221

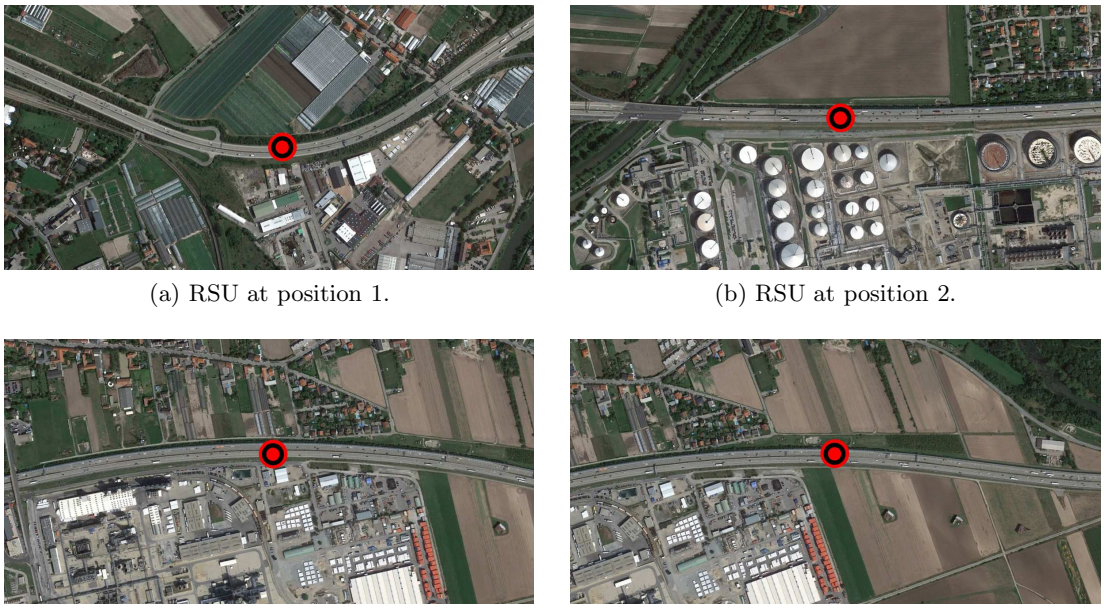

(a) RSU at position 1.

(b) RSU at position 2.

(c) RSU at position 3.

(d) RSU at position 4.

Figure 3.4: Environment at RSU locations for the ROADSAFE2011 measurement campaign. The red circles indicate the positions of the RSUs.

environment in the vicinity of RSU position 1 is semi-rural, with vegetation on the roadside. The RSU positions 2 to 4 were selected in an industrial area, next to a refinery, as shown in Figures 3.4b to 3.4d. There is a noise protection wall on one side of the highway, starting exactly at RSU position 2 and ending 120 m after RSU position 4. On the other side of the highway there is almost no vegetation. Except for RSU position 1, all highway segments selected for the measurements are straight, with three lanes in both directions. The measurements were performed in both driving directions at all RSU positions.

For these measurements, an IEEE 802.11p-compliant transmitter (provided by Kapsch TrafficCom)was used. It consists of an embedded personal computer (PC) with ethernet connection and protection units, e.g., for overvoltage protection. The PC is needed for remote control of the transmitter. Additionally, a GPS receiver is installed in order to deliver sync pulses to the transmitter. The RF front end of the transmitter was connected to two directional antennas by a low-loss cable followed by a 3 dB power splitter. One of these antennas is shown in Figure 3.5a. The antennas were mounted directly on the metallic

Table 3.5: RSU antenna parameters for the ROADSAFE2011 measurement campaign.

Parameter	**Value**
Type	directional
Gain [dBi]	14
EIRP [dBm]	12.2
3 dB BW hor./ver. [°]	40 / 30
Polarization	vertical
Height [m]	7.1

(a) RSU antenna 5. (b) OBU antenna 3. (c) OBU antenna 4.

Figure 3.5: RSU and OBU antennas for the ROADSAFE2011 measurement campaign.

constructions of the highway gantry in a height of 7.1 m and were pointing in both directions of the highway. We denote this antenna as RSU antenna 5. The detailed characteristics of RSU antenna 5 are given in Table 3.5.

As receiver we used the same CVIS platform as in the ROADSAFE2010 measurement campaign. The receiving node was placed inside of the test vehicle, where it was connected to a power supply and a laptop. The laptop was used to control the recording process. The RF front end of the receiver was connected to the OBU antenna under test. During the ROADSAFE2011 experiments, we used three different OBU antennas. One of them was the same CVIS vehicle rooftop antenna as in the ROADSAFE2010 measurement campaign. The detailed characteristics of this antenna can be found in Section 3.1.1. Furthermore, we used the planar OBU antenna shown in Figure 3.5b. This antenna consists of a single planar element with patterns for CALM M5 and GPS. The patch itself forms the GPS antenna which is tuned by the location of the feed posts and the corner cuts. The CALM M5 antenna is formed by a ring slot structure etched into the substrate above the GPS patch. This results in an omni-directional vertically polarized CALM M5 antenna with a gain of 4 dBi. The antenna is packaged into a molded plastic housing with integrated magnets. We denote this antenna as OBU antenna 3. We also used the surface mount antenna shown in Figure 3.5c. This is a wideband (1.7 - 6.0 GHz) antenna with an omni-directional radiation pattern, manufactured

Table 3.6: Measurement parameters for the ROADSAFE2011 measurement campaign.

Parameter	**Value**
Data rate [Mbit/s]	6
Packet length [Bytes]	500
Transmit rate [packets/s]	150
Transmit power [dBm]	17
Center frequency [MHz]	5880
Average speed [km/h]	100

by "Mobile Mark". It has a ground plane independent omni-directional configuration and a gain of 5 dBi. The antenna radome consists of plastic with a heavy metal base and a threaded feed-thru. The bottom mounting plate is outfitted with a gasket for a watertight seal. We denote this antenna as OBU antenna 4. All OBU antennas were mounted using magnets in the center of the rooftop of the test vehicle.

The measurements were performed at the center frequency of 5880 MHz with real vehicular traffic. The average test vehicle velocity was 100 km/h (27.8 m/s) with marginal deviations due to traffic. As transmit parameters we used 500 Bytes long packets at a data rate of 6 Mbit/s, corresponding to QPSK modulation with code rate 1/2. However, the transmit rate was restricted to 150 packets/s only, which is significantly lower than for the ROADSAFE2010 measurements. Therefore, a quantitative comparison of the throughput obtained in these measurement campaigns is not possible. The transmit power was set to 17 dBm and the resulting EIRP with RSU antenna 5 is 12.2 dBm (cf. Table 3.5). The complete set of measurement parameters is given in Table 3.6.

3.1.3 iTETRIS

The iTETRIS measurement campaign was conducted in the city of Bologna, Italy as part of the European FP7 project iTETRIS [2]. The main focus of this extensive field testing campaign was to analyze the impact of urban characteristics on the quality of V2I communications. The results of the campaign were presented in [49] and the measurement traces were openly released to the research community [3].

To analyze the impact of urban characteristics, 22 RSU locations were carefully selected on 20 km of urban road network. Analyzing the street topology at the measurement locations, we identified four types of urban street layouts. The identified street layouts are as follows:

Layout 1 - street surrounded by buildings from both sides.

Layout 2 - street surrounded by buildings from one side and by vegetation from the other side.

Layout 3 - street surrounded by vegetation from both sides.

Table 3.7: RSU locations for the iTETRIS measurement campaign.

	Latitude	**Longitude**	**Street name**	**Driving direction**
Street layout 1				
Primary	44.4946	11.3143	A. Costa	East
Secondary	44.4947	11.3284	A. Costa	East
Street layout 2				
Primary	44.4844	11.3559	G. Gozzadini	West
Secondary	44.5021	11.3530	A. Massini	North-East
Street layout 3				
Primary	44.4863	11.3397	E. Panzacchi	East
Secondary	44.5012	11.3310	S. Porrettana	South-East
Street layout 4				
Primary	44.5024	11.3179	A. Saffi	North-West
Secondary	44.4986	11.3096	M. Gandhi	West

Layout 4 - open area street.

The detailed topological parameters of each street layout are provided in Section 4.4. For each street layout, we selected two representative RSU locations, the exact positions of which are given in Table 3.7. Figure 3.6 illustrates the environment at the selected locations. Here, the RSU positions are indicated by red circles. Figure 3.6 only shows the environment to one side of the RSU, which is in contrast to Figures 3.1 and 3.4. This is due to the fact that in iTETRIS, the measurements were performed only to one side of the RSU. The performance was evaluated for both driving directions.

As transmitter, an IEEE 802.11p DENSO wireless safety unit (WSU) prototype controlled by a standard laptop was used. The RF front end of the transmitter was connected using an LMR400 antenna cable to RSU antenna. The cable was 14 m long, resulting in a cable loss of approximately 5 dB cable loss. As RSU antenna, an ECO12-5800 omni-directional antenna was used, detailed characteristics of which are given in Table 3.8. The antenna was placed on top of a portable pneumatic telescope mast with a maximum height of 11 m. To emulate possible RSU deployments, three different antenna heights were tested. In this thesis, we focus on measurements with an antenna height of 6.5 m.

As receiver another unit of the IEEE 802.11p DENSO WSU prototype was used. The RF front end of the receiving platform was connected using a 3 m long LMR240 antenna cable to the OBU antenna. The resulting cable loss amounts to approximately 3 dB. As OBU antenna, a Nippon omni-directional antenna with 0 dBi gain was used. Additionally, two Novatel SMART-V1-2US-PVT GPS receivers were employed at the receiver side. All these antennas were placed on the roof of the test vehicle.

(a) Street layout 1 primary measurement.

(b) Street layout 1 secondary measurement.

(c) Street layout 2 primary measurement.

(d) Street layout 2 secondary measurement.

(e) Street layout 3 primary measurement.

(f) Street layout 3 secondary measurement.

(g) Street layout 4 primary measurement.

(h) Street layout 4 secondary measurement.

Figure 3.6: Environment at RSU locations for the iTETRIS measurement campaign.

Table 3.8: RSU antenna parameters for the iTETRIS measurement campaign.

Parameter	**Value**
Type	omni-directional
Gain [dBi]	12
EIRP [dBm]	27
3 dB BW hor./ver. [°]	360 / 7
Height [m]	6.5

Table 3.9: Measurement parameters for the iTETRIS measurement campaign.

Parameter	**Value**
Data rate [Mbit/s]	6
Packet length [Bytes]	126
Transmit rate [packets/s]	10
Transmit power [dBm]	20
Center frequency [MHz]	5890
Average speed [km/h]	40

The measurements were performed at a center frequency of 5890 MHz with real vehicular traffic. The average test vehicle velocity was 40 km/h (11.1 m/s) with marginal deviations due to traffic. Packets of 126 Bytes length were transmitted using a data rate of 6 Mbit/s, corresponding to a QPSK modulation with code rate 1/2. The transmit rate was set to 10 packets/s. The transmit power was set to 20 dBm, resulting in an EIRP of 27 dBm (cf. Table 3.8). The parameters of the iTETRIS measurement campaign are summarized in Table 3.9.

3.2 Definition of Key Performance Indicators

To enable comparability of the V2I measurements performed with different parameter settings, equipment, and in different environments, we define a set of key performance indicators (KPIs) in this section.

The measured data used for communication performance evaluation is in the form of binary packet-error patterns, in which "1" indicates a lost packet and "0" indicates a successfully decoded packet. These binary packet-error pattern as a function of the distance between RSU and OBU are the basis for our performance evaluation. However, packet-error patterns are not well suited for quantitative assessment and comparison. To avoid the visual representation of the packet-error pattern, we introduce the packet delivery ratio (PDR). The PDR is defined as the number of packets that were successfully decoded in the distance interval Δd divided by the number of packets transmitted during this interval. Thus, we have PDR $\in [0, 1]$, where PDR $= 0$ means that all transmitted packets were lost and PDR $= 1$ means that all transmitted packets were successfully decoded. To calculate the PDR as a function of the relative distance from the RSU, we first need to define the length of the sliding window Δd. Once Δd is defined, we place the sliding window at the position of the first detection event d_1, such that it starts at distance $d_1 - \frac{\Delta d}{2}$ and ends at $d_1 + \frac{\Delta d}{2}$. Next, we calculate the PDR based on the part of the packet-error pattern inside the sliding window and place the resulting value at position d_1. Finally, we shift the sliding window by 1 m in the driving direction and calculate the next PDR value. We repeat this procedure until the

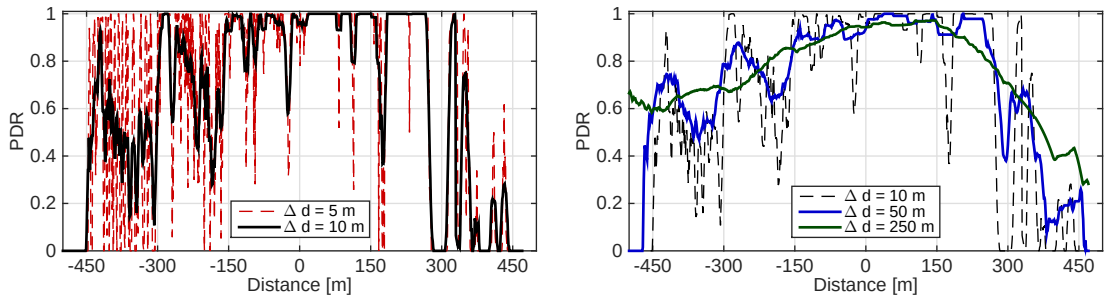

Figure 3.7: Influence of the sliding window size Δd on the PDR as a function of the relative distance.

position of the last detection event in the measurement is reached. In this manner, we obtain one PDR value for each meter.

Figure 3.7 illustrates PDR curves vs. relative distance calculated with different sliding window sizes. Here, the origin of the abscissa (0 m) corresponds to the position of RSU. Negative values on the abscissa indicate positions of the vehicle approaching the RSU. The positive distances represent positions after passing by the RSU. These results underline the importance of the choice of Δd. If the length of the sliding window is too short, there will be not enough observations for calculation of the PDR. As a consequence, the PDR values tend to be close to 0 or 1 and the curve won't be smooth (cf. red dashed line in Figure 3.7). On the other hand, a too long sliding window averages out important environmental effects, as shown by solid green and blue lines in Figure 3.7 for $\Delta d = 50\,\text{m}$ and $\Delta d = 250\,\text{m}$, respectively. Therefore, the sliding window should not be longer then the distance, within which the channel remains approximately constant. According to results in [83], this stationarity distance for vehicle-to-vehicle (V2V) channels is different in urban and highway environments. It depends on the relative vehicle velocity and on the number of scatterers, and it is time-variant. For urban environments the mean stationarity distance is approximately $11,7\,\text{m}$, while for highway environments it amounts to approximately 37 m. The stationarity distance for V2I measurements should be even larger, since the influence of the scatterers is not as strong as in V2V measurements. However, the exact values of the stationarity distance in V2I scenarios are not known. Therefore, we take stationarity distance for V2V scenarios as a guideline and suggest to use $\Delta d = 10\,\text{m}$ for the PDR calculation.

As can be seen from Figure 3.8a, the PDR is strongly distance dependent and is not symmetric around the position of RSU. However, for reasons of simplicity, the PDR performance is often assumed to be symmetric and is given as a function of the absolute distance. Figure 3.8b illustrates the PDR vs. absolute distance derived from the PDR vs. relative distance curve shown in Figure 3.8a. Here, the PDR at absolute distance $|d|$ is given by arithmetic mean of PDRs at relative distances $-d$ and d.

Based on the definition of the PDR as a function of the absolute distance, we now define the following KPIs:

- The *Reliable communication range (RCR)*, introduced in [49], is the range over which

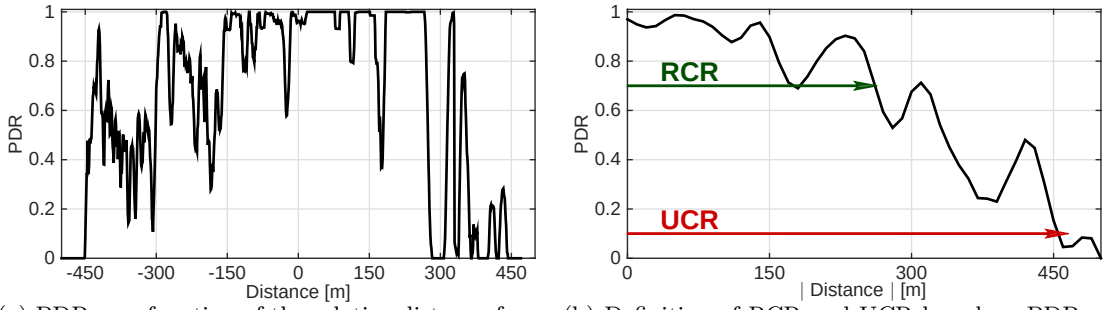

(a) PDR as a function of the relative distance from the RSU.

(b) Definition of RCR and UCR based on PDR as a function of the absolute distance from the RSU.

Figure 3.8: Example of the PDR as a function of the relative and absolute distance.

high quality communications can be established. It is defined as the absolute distance from the RSU, within which the PDR values are greater than 0.7, as shown by the green arrow in Figure 3.8b. As can be seen from this example, the PDR drops below the threshold of 0.7 several times (e.g., at 180 m and at 260 m). For these cases, we define a subthreshold of 0.5 and define the RCR as the distance at which the PDR is larger than 0.7 for the last time, before dropping below 0.5. We also note that for certain operation modes, the PDR values in the close vicinity to (or directly under) RSU are below the threshold of 0.7. These PDR values are excluded from the RCR calculation.

- The *Unreliable communication range (UCR)*, introduced in [49], is the distance at which the PDR drops below 0.1 for the first time, as shown by the red arrow in Figure 3.8b. Therefore, for RCR$\leq |d| \leq$UCR, we cannot guarantee reliable communication. The communication quality achievable in this range is nevertheless sufficient for some vehicular applications.

- The *throughput* is the number of packets decoded during one measurement multiplied by the packet length. It is directly related to the percentage of erroneous packets $\hat{P}_e$ by (2.17). Therefore, we restrict to throughput values for most of the measurement evaluations presented in this chapter. However, in some cases as, e.g., in Section 3.5, it is useful to analyze the percentage of erroneous packets in addition to the throughput. The percentage of erroneous packets facilitates a quantitative comparison of measurements with different transmit parameters.

3.3 Data Rate and Packet Length

In this section, we analyze the influence of the transmit parameters on the performance of V2I systems. In particular, we seek for a set of transmit parameters yielding the largest throughput at a constant transmit power. Parts of the material presented in this section have been published in [104].

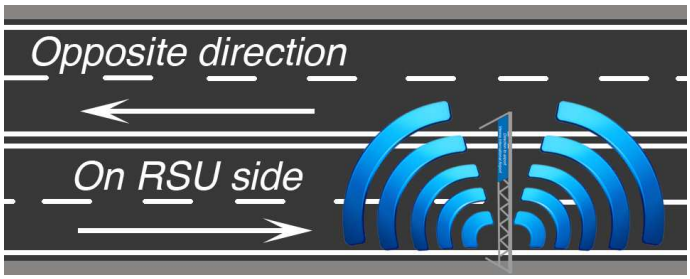

Figure 3.9: Schematic illustration of driving direction with RSU antenna on highway side.

One possible approach to achieve larger throughput is to increase the packet length, thereby decreasing the overhead. The main disadvantage of this approach is the deterioration of the preamble-based channel estimates due to the increased transmission time. This is especially true in the highly time-variant vehicular propagation environments. Furthermore, for a given bit error probability, it is more likely to observe a bit error, and thus a packet-error, in a longer packet. Therefore, we expect that the error fraction will grow with increasing packet length. Another possibility to achieve higher throughput is to use higher data rates. In this case, the time required to transmit a packet will be reduced, resulting in higher quality of channel estimates.

To check these claims, we compare the results of experiments performed with three different settings, details of which are given in Table 3.3. The measurements were performed in the framework of ROADSAFE2010 at RSU position 1. The coordinates of the RSU are provided in Table 3.1 and the respective environment is shown in Figure 3.1a. As transmit antenna, we used RSU antenna 3, detailed characteristics of which are given in Table 3.2. As receive antenna, OBU antenna 1 was used, characteristics of which can be found in Section 3.1.1. Measurements were performed in both driving directions. The part of the measurements in which the test vehicle was driving directly under the RSU antenna is referred to as *on RSU side*. The measurements performed in the other driving direction are referred to as *opposite direction*. This difference in driving direction is schematically illustrated in Figure 3.9. All results presented in this section are calculated as an average over 10 repetitions of the same measurement.

We first consider the measurements performed on RSU side. Figure 3.10a shows the average PDR vs. absolute distance performance for different system parameters. Here, the result for setting 1 (6 Mbit/s, 200 Bytes) is shown by the blue curve, the performance for setting 2 (6 Mbit/s, 1554 Bytes) is demonstrated by the red curve, while the green curve represents the measurements with setting 3 (12 Mbit/s, 200 Bytes). From these results, we conclude that both, higher data rate and larger packet size lead to a significant performance degradation in terms of the PDR. Besides the PDR degradation we also obtain a considerable decrease of the communication range. The results presented in Table 3.10 show that in measurements with longer packets (setting 2) the RCR is reduced by 40 % and the UCR is reduced by 12 %. For higher data rate (setting 3) we obtain up to 55 % and 30 % decrease in the RCR and

Table 3.10: Comparison of system performance achievable for different transmit parameters in different driving directions.

Parameter settings	**Mean throughput [Mbit]**	**Mean RCR [m]**	**Mean UCR [m]**
On RSU side			
Setting 1	67	250	430
Setting 2	116	150	380
Setting 3	61	115	300
Opposite direction			
Setting 1	56	220	490
Setting 2	97	150	440
Setting 3	48	80	300

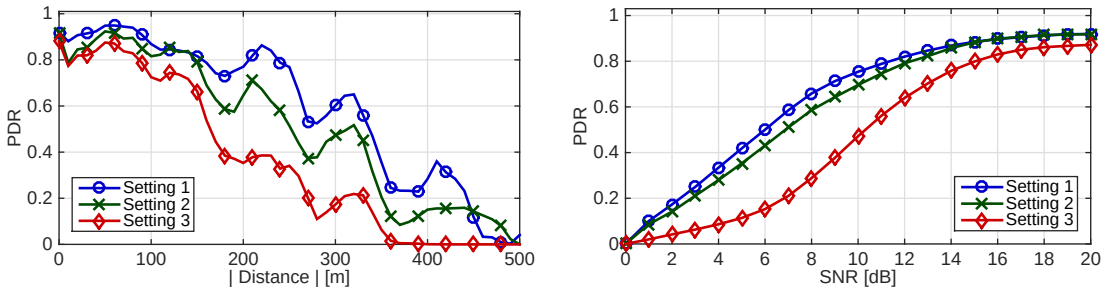

(a) PDR as a function of the absolute distance.

(b) PDR as a function of the SNR.

Figure 3.10: Performance comparison for different transmit parameters.

UCR, respectively. However, when using longer packets the throughput is increased by more than 70%. On the other hand doubling the data rate resulted in a throughput decrease of up to 10%. We thus conclude that in contrast to our initial expectations, shortening the packet duration by using a higher-order modulation scheme yields a performance degradation. This can be explained as follows:

1. In the considered measurement setup, the RSU antenna was mounted high above the road. Consequently, there was always a strong line-of-sight (LOS) component between transmitter and receiver. Therefore, the underlying channel is less time-variant compared to V2V channels and the aforementioned dependence between the packet length and the channel estimation accuracy is less pronounced.

2. On the other hand, higher data rates impose increased signal-to-noise ratio (SNR) requirements. More precisely, for the same transmit power, the constellation symbols of higher-order modulation schemes are spaced more densely. Consequently, for higher data rates, the same SNR results in a lower PDR.

To support the latter statement Figure 3.10b shows the PDR vs. SNR performance for measurements with different parameters settings. Here, the PDR vs. SNR for settings 1 and 2 are fairly close to each other and essentially coincide for SNR$>$ 14 dB. This confirms our assumption that the difference in SNR requirements for measurements with larger packet size

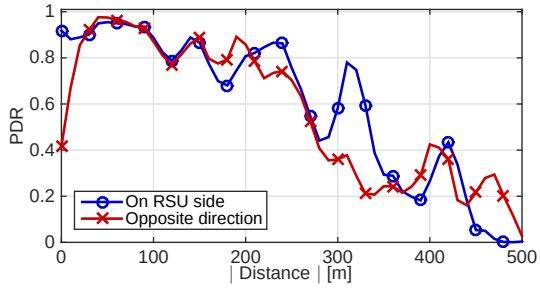

(a) Setting 1: 6 Mbit/s, 200 Bytes.

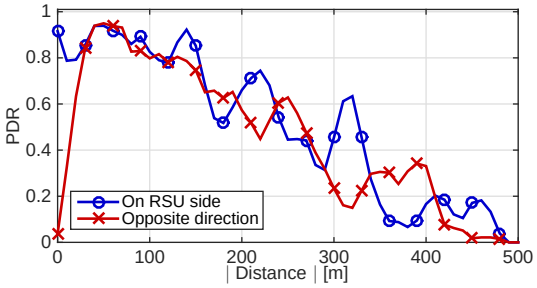

(b) Setting 2: 6 Mbit/s, 1554 Bytes.

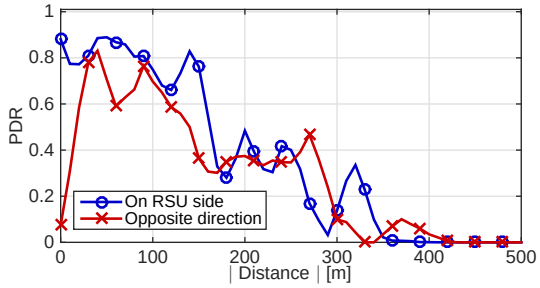

(c) Setting 3: 12 Mbit/s, 200 Bytes.

Figure 3.11: Influence of driving direction on the PDR performance for different transmit parameters.

is nearly negligible. However, for higher data rate (cf. red curve in Figure 3.10b) the SNR needs to be higher to achieve a certain PDR is always higher. In particular, an up to 4 dB higher SNR is required to obtain the same PDR value, when doubling the data rate.

Next, we extend our investigation of the performance dependance on the transmit parameters by comparing the PDR vs. distance curves for different driving directions. In Figure 3.9 the PDR performance on RSU side is shown with blue lines, while the performance in opposite direction is indicated with red lines. Comparing the measurements with different parameter settings, we observe that the influence of the driving direction is more pronounced for the measurements with higher data rates (cf. Figure 3.11c). In particular, for the same distance separation the PDR obtained in opposite direction is up to 20 % lower, than the PDR obtained on RSU side. Based on the KPIs summarized in Table 3.10, we conclude that the throughput and communication range for measurements in opposite direction are always less than for measurements on RSU side. However, the throughput reduction due to change of the driving direction amounts to 16.5 % for settings 1 and 2, and to 21.5 % for setting 3. The same holds for the RCR that is reduced by 12 % for settings 1 and 2, and by 31 % for setting 3.

A further remarkable difference between the driving directions is the distinctive notch of the PDR values around $0 \leq |d| \leq 30$ m for the opposite direction (irrespective of the transmit parameters). Our observations suggest that this drop of the PDR in close vicinity of RSU is due to the combination of the RSU antenna type and the antenna mounting position. We verify this claim in Section 3.4.

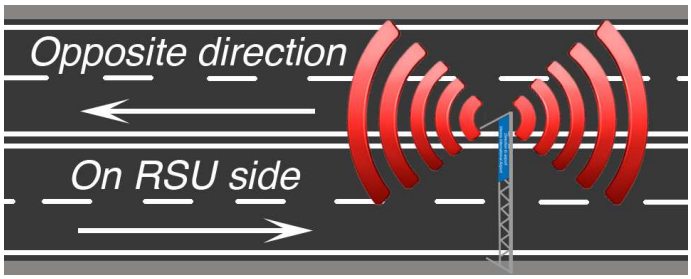

Figure 3.12: Schematic illustration of driving direction with RSU antenna in the middle of the highway.

The measurement results presented in this section show that both, higher data rates and the longer packets lead to performance degradation in terms of the reliability and communication range. Moreover, our results reveal a strong influence of the driving direction, in particular for measurements with higher data rates. Therefore, to achieve higher throughput in transmit-power constrained V2I communications systems, we suggest to transmit longer packets instead of increasing the data rate.

3.4 Roadside Unit Antenna Types and Placement

In this section, we present a performance evaluation of V2I measurements with different RSU antenna placements, gains, and types. More specifically, we analyze if deliberate RSU antenna placement can help to reduce the influence of the driving direction on the PDR performance. We furthermore investigate the performance increase in terms of the communication range and throughput, achievable with high-gain directional antennas. The material presented in this section has been published in part in [105].

The measurement results presented in Section 3.3 indicate a strong influence of the driving direction on the performance of V2I systems, in terms of the reliability and communication range. We have shown that the PDR performance in measurements conducted on RSU side is significantly better than in measurements performed in other direction, regardless of the transmit parameters. We concluded that this performance decrease is due to the specific antenna mounting, schematically illustrated in Figure 3.9. As suggested by this schematic illustration, the RSU antennas is mounted on the outer side of highway, closer to the service lane and the road shoulder. We denote this RSU antenna mounting position as *on side*. We anticipate that this mounting position results in inhomogeneous coverage for different driving directions, which is most notable in the close vicinity of RSU.

To check these claims, we performed measurements with different RSU antenna mounting positions in the framework of ROADSAFE2011. In these measurements, we used OBU antenna 1, characteristics of which can be found in Section 3.1.1. As transmit antenna the directional RSU antenna 5 was used, detailed characteristics of which are given in Table 3.5. The directional RSU antennas were mounted on a highway gantry closer to the inner side

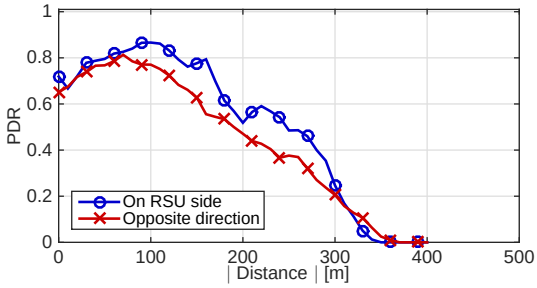

Figure 3.13: Influence of driving direction on the PDR performance for measurements with RSU antenna mounted in the middle of the highway.

of highway, as schematically shown in Figure 3.12. We refer to this mounting position as *in the middle*. The measurements were performed in both driving directions at RSU position 1, coordinates of which are provided in Table 3.4. The surrounding environment is shown in Figure 3.4a. The transmit parameters are summarized in Table 3.6. All results presented in this section are calculated as an average over 10 repetitions of the same measurement.

Figure 3.13 highlights the influence of the driving direction in systems with RSU antennas mounted in the middle. Comparing the performance on RSU side (cf. blue curve) and in opposite driving direction (cf. red curve), we notice that the notch around the origin of the abscissa is not present anymore (cf. Figure 3.11). Analyzing the achievable communication range and the throughput, we observe that the RCR for measurements in opposite direction is on average only 10 m shorter than on RSU side and the UCR is equal for both driving directions. The throughput in opposite driving direction is reduced by 5 % compared to the throughput obtained on RSU side[1]. Our observations suggest that this marginal performance loss obtained for measurements in opposite driving direction is due to a minor inaccuracy of the RSU antenna alignment. We also note that in the considered settings, the communication between RSU and OBU is not fully reliable, i.e., even in the close vicinity of the we have RSU PDR $(d) < 0.9$. This is due to the OBU antenna, as we show in Section 3.5. We therefore suggest to mount RSU antennas in the middle rather than on the side, to avoid inhomogeneous coverage and undesirable performance degradation for one of the driving directions.

We next discuss how the RSU antenna gain influences the performance of V2I communications. To this end, we compare the results of the experiments performed with directional RSU antennas 2, 3, and 4, detailed characteristics of which are given in Table 3.2. The experiments were conducted in the framework of ROADSAFE2010 at RSU position 1. The RSU coordinates are provided in Table 3.1 and the surrounding environment is shown in Figure 3.1a. As transmit parameters we used setting 1, details of which are given in Table 3.3. In the following we present the results of the measurements conducted on RSU side.

Figure 3.14 shows the PDR as a function of the absolute distance for RSU antennas 2, 3, and 4. Here, the measurements with RSU antenna 2 (6 dBi gain) are shown by the

[1] We note that quantitative comparison between the throughput values presented here and those summarized in Table 3.10 is not possible, since the transmit parameters of the corresponding experiments differ significantly.

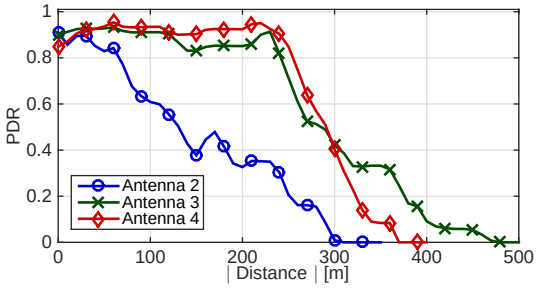

Figure 3.14: Comparison of PDR performance achievable with directional RSU antennas having different antenna gains.

Table 3.11: Comparison of system performance achievable for different RSU antenna types and gains.

Parameter settings	**Mean throughput [Mbit]**	**Mean RCR [m]**	**Mean UCR [m]**
Antenna 1	44	85	380
Antenna 2	28	45	290
Antenna 3	63	250	430
Antenna 4	56	280	370

blue line, the performance achieved with RSU antenna 3 (10 dBi gain) is indicated by the green line, and the results attained with RSU antenna 3 (13 dBi gain) are shown by the red line. Comparing these results, we first conclude that the UCR is almost doubled when using antenna 3 instead of antenna 2 (4 dBi higher antenna gain). Even more important is the increase of the RCR by a factor of five. A further 3 dBi increase of the antenna gain (cf. red line in Figure 3.14) did not yield a proportional communication range extension. Although the RCR was extended by 12 % compared to antenna 3, the average UCR was reduced by 15 %. Table 3.11 compares the communication range and throughput performance achievable with RSU antennas 2, 3, and 4. From these results in follows that RSU antenna 3 has the best performance. Particularly, the throughput obtained with this antennas is on average 125 % larger than with antenna 2 and 12 % larger than with antenna 4.

We anticipate that the overall performance of systems with directional RSU antennas can be increased considerably by using high-gain directional antennas. However, the performance growth is not proportional to the antenna gain increase, since with increasing antenna gain the importance of precise antenna positioning is increasing as well. To verify these observations, we performed a sequence of experiments with identically equipped RSUs in the framework of ROADSAFE201. As RSU antenna we used directional antennas 5, characteristics of which are given in Table 3.5. The RSUs were placed at four different positions along the highway (cf. Table 3.4). These measurements allow us to analyze the influence of the road geometry and the environment on the performance of V2I communication systems. The environment at the selected RSU positions is shown in Figure 3.4. We recall, that there is a noise protection wall on one side of the highway, starting exactly at RSU position 2 and ending 120 m after RSU position 4.

Table 3.12: Comparison of system performance achievable with the same RSU equipment in different locations.

Parameter settings	**Mean throughput [Mbit]**	**Mean RCR [m]**	**Mean UCR [m]**
Position 1	11	140	300
Position 2	14	140	400
Position 3	14	140	520
Position 4	16	145	720

The average throughput and communication range results for all RSU positions are summarized in Table 3.12[2]. Although the RSUs were identically equipped and operated, the measured performance was varying significantly for different locations. Comparing the performance of the RSUs at positions 1 and 4, we obtain a difference of up to 50 % in the throughput and nearly 250 % difference in the UCR. The RCR is almost equal for all measurements.

To highlight the difference in V2I performance, we show the SNR as a function of the absolute distance from the RSU in Figure 3.15a. Although the SNR curves seem to be quite different, they in fact have a common tendency within the first 200 m from the RSU. Based on the SNR values obtained from all RSUs within this range, we calculate a mean SNR vs. distance. This SNR vs. distance performance is shown by the black dashed line in Figure 3.15a. The corresponding 95 % confidence interval is shown by the green shaded area. We note that the only measured curve that falls in to the 95 % confidence interval is the curve of RSU at position 1, which is the only RSU not located in the vicinity of a noise protection wall. The SNR vs. distance curves of the other RSUs overlap with the green area only within the first 200 m. Later all curves flatten and the SNR remains nearly constant until it eventually drops rapidly.

Based on these observations, the SNR behavior is influenced by the noise protection wall and can be divided into three regions, each having a different slope and being caused by different propagation phenomena. These regions are shown in Figure 3.15b. Here, the SNR vs. distance curve for the RSU at position 3 on a logarithmic scale. Within *region 1*, the receiver has a direct LOS link to the transmitter and the SNR performance is mainly influenced by the antenna characteristics, e.g., antenna height, pattern and the EIRP. Starting at around 200 m after the RSU, the environment, e.g., the noise protection wall becomes essential for the signal propagation. We conjecture that the flattening of the SNR in *region 2* is due to constructive interference, introduced by the reflections from the metallic surface of the noise protection wall. With increasing distance between the transmitter and the receiver not only the phase of the reflections changes, but also the number of the multipath components is increased. Therefore, we obtain an instantaneous drop of the SNR in *region 3*. In this region,

[2]We note that a quantitative comparison of the throughput reported in Tables 3.11 and 3.12 is not possible, since the transmit parameters of the corresponding experiments differ significantly.

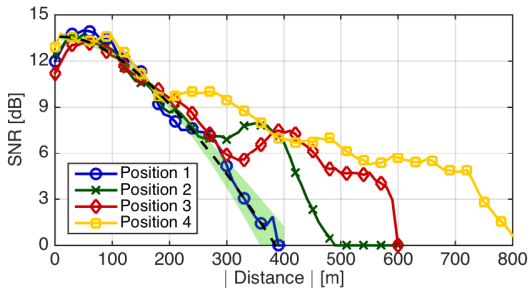

(a) SNR as a function of the absolute distance.

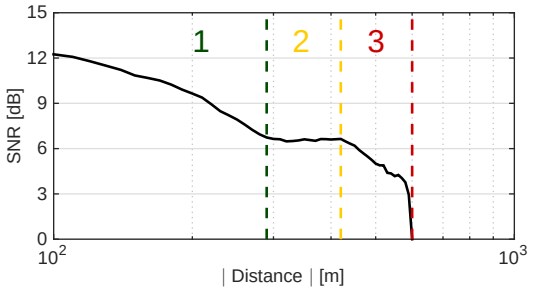

(b) Illustration of SNR ranges on basis of SNR vs. absolute distance performance for position 3.

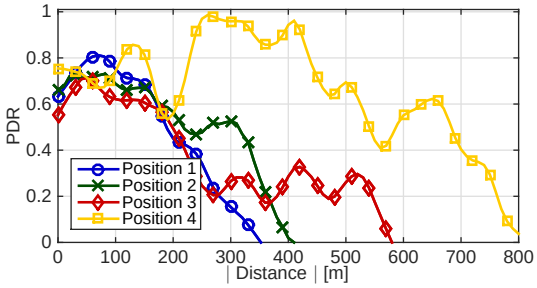

(c) PDR as a function of the absolute distance.

Figure 3.15: Performance comparison achievable with the same RSU equipment in different locations.

the receiver is no longer able to resolve the multipath components. These effects are also applicable for RSUs at positions 2 and 4.

Interestingly, the noise protection wall does not only influence the mean SNR, but more importantly it has a strong impact on the PDR, as shown in Figure 3.15c. Within the first 200 m all curves are similar, whereas the behavior changes drastically within region 2. Here, we obtain an increase of the PDR measured at RSU position 4. Our observations emphasize the influence of environmental propagation impairments on the performance of V2I systems with high-gain directional RSU antennas.

Along with the gain and the mounting position of the RSU antenna, the type of antenna itself plays a fundamental role for the performance of V2I systems. Therefore, in the following we compare the performance achieved with the directional RSU antenna 3 to that of the omni-directional RSU antenna 1. Both measurements were performed in the framework of ROADSAFE2010 with transmit parameters corresponding to setting 1 (cf. Table 3.3). The directional antenna was placed at position RSU 1 and the omni-directional antenna was placed at RSU position 2. The exact positions are given in Table 3.1 and the surrounding environment is shown in Figures 3.1a and 3.1b.

We compare the PDR performance of antennas 1 and 3 in Figure 3.16a. With RSU antenna 1, we observe clear (up to factor of three) reduction of the range in which reliable high quality communication is possible. From the distinct gap between the two curves we note that the packet loss probability in measurements with omni-directional antenna is on

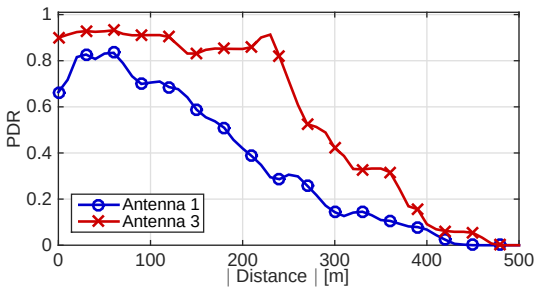

(a) PDR as a function of the absolute distance.

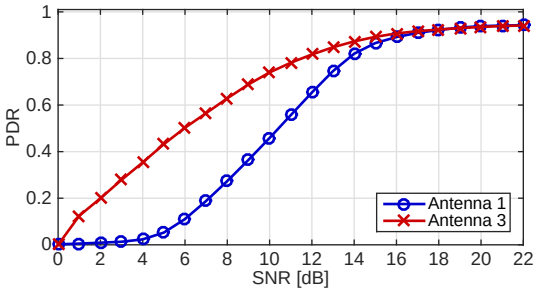

(b) PDR as a function of the SNR.

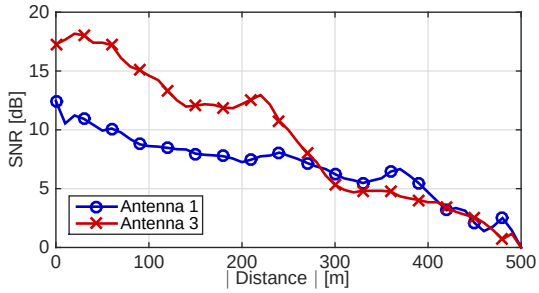

(c) SNR as a function of the absolute distance.

Figure 3.16: Performance comparison of directional and omni-directional RSU antennas.

average 20 % higher, for the same distance between the RSU and the test vehicle. In fact the two curves never converge, meaning that even under the best conditions, communication in systems with omni-directional RSU antennas is 5 % to 10 % less reliable, than in systems with directional antennas.

To further investigate the PDR performance for directional and omni-directional antennas, we show the PDR as a function of the SNR for both RSU antennas in Figure 3.16b. The PDR achievable for SNR $\geq$ 15 dB is the same for both antennas. However, in the range 0 dB $\leq$ SNR $<$ 15 dB the PDR achievable with the directional antenna is significantly higher. We further note the difference in the slopes of these curves. The PDR in measurements with RSU antenna 3 is monotonically increasing over the whole SNR range. While the PDR achievable with antenna 1 is close to zero for SNR $<$ 6 dB and for 6 dB $\leq$ SNR $\leq$ 15 dB the slope of the PDR curve is much steeper. One possible reason for this dissimilarity is the difference in the field distribution of directional and omni-directional antennas. The most straightforward illustration for this difference is shown in Figure 3.16c. Here, the averaged SNR values are plotted vs. absolute distance from RSU. The SNR at distance d is computed by averaging the SNR values in the intervals $[-d-\Delta/2, -d+\Delta/2]$ and $[d-\Delta/2, d+\Delta/2]$. These results show that the average SNR achieved with directional antennas is considerably higher than with omni-directional antennas. Furthermore, we observe an abrupt drop of the SNR curve for antenna 1 at $d = 410$ m. This implies that the average SNR of the measurements with the omni-directional antenna is varying in the range 5 dB $\leq$ SNR $\leq$ 12 dB and SNRs below 5 dB occur only rarely. This clarifies the fact that the PDR of the omni-directional antenna for 0 dB $\leq$ SNR $\leq$ 5 dB is close to 0 in Figure 3.16b. It also confirms that for

$d \geq 410\,\text{m}$, communication with the RSU equipped with omni-directional antenna is no longer possible (cf. blue curve in Figure 3.16a). Finally, we note that even in close vicinity of the RSU, the SNR in the measurements with the omni-directional antenna is varying between 10 dB and 12 dB. According to Figure 3.16b, these SNR values result in a maximum achievable PDR of 0.5 to 0.8.

A quantitative comparison of directional and omni-directional RSU antennas is provided in Table 3.11. We observe that the RCR in measurements with directional antennas is up to a factor of three larger than with omni-directional antennas. The deployment of directional RSU antennas allows us to expand the UCR by 12 % and to increase the throughput by 30 %. We therefore conclude that directional RSU antennas are more suitable for V2I communications than omni-directional antennas.

3.5 On-board Unit Antenna Types and Placement

In this section, we discuss the performance achievable with different OBU antennas in the context of the V2I communications. First, we compare the performance of OBU antennas 1 and 2 in terms of throughput and communication range. Next, we perform a similar comparison using the OBU antennas 1, 3, and 4. This separation in the evaluation process is necessary to ensure a fair benchmarking of the OBU antennas deployed in measurements with different transmit parameters and RSU equipment. To facilitate comparability between the two groups of experiments, we evaluate the percentage or erroneous packets (denoted as $\hat{P}_e$) in addition to the throughput and the communication range.

To compare the performance of OBU antennas 1 and 2, we performed a series of measurements in the framework of ROADSAFE2010. The RSU was located at position 1, coordinates of which are provided in Table 3.1 and the respective environment is shown in Figure 3.1a. As transmit antenna we used the directional RSU antenna 3 that has the best performance according to the results in Section 3.4. The IEEE 802.11p packets were transmitted by the RSU with the transmit parameters corresponding to setting 1 (cf. Table 3.3). The measurements were performed in both driving directions. However, as shown in Section 3.4, the specific antenna mounting illustrated in Figure 3.9 results in inhomogeneous signal propagation along different driving directions. We therefore restrict to evaluating of the measurements performed on RSU side. All results presented in this section are calculated as an average over 10 repetitions of the same measurement.

Figure 3.17 presents the PDR as a function of the relative and the absolute distance for OBU antennas 1 (blue line) and 2 (red line), respectively. This relative comparison shows that OBU antenna 2 performs inferior to antenna 1 in the context of V2I communications. As shown in Figure 3.17a, the communication range achievable with OBU antenna 1 is one-sided. Furthermore, when approaching the RSU, the packet reception with OBU antenna 2 starts about 200 m later than with OBU antenna 1. We also note that in measurements with both antennas, the PDR drops at roughly $-150\,\text{m}$. However, the notch in the PDR

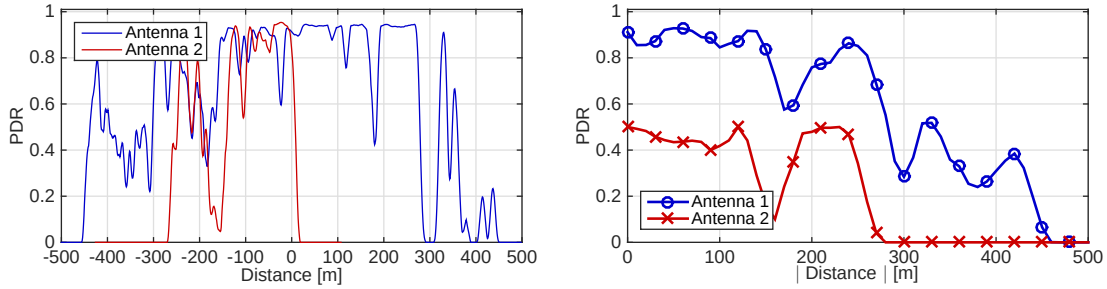

(a) PDR as a function of the relative distance.

(b) PDR as a function of the absolute distance.

Figure 3.17: Performance comparison for OBU antennas 1 and 2.

Table 3.13: Comparison of system performance achievable with different OBU antennas at RSU position 1 of ROADSAFE2010 measurements.

OBU antenna	**Mean throughput [Mbit]**	**Mean $\%_{\mathbf{pe}}$ [%]**	**Mean RCR [m]**	**Mean UCR [m]**
Antenna 1	71.14	19.8	160	440
Antenna 2	19.18	47.5	0	260

is significantly deeper in measurements with OBU antenna 2. In Section 3.6, we show that this performance degradation at the tunnel exit is caused by a significant change in the propagation environment, as well as an increased number of multipath components that cannot be resolved by the receiver hardware. Apart from this environment-induced notch, the PDR obtained in the range $-250\,\mathrm{m} < d < 0\,\mathrm{m}$ is nearly the same with both OBU antennas.

A quantitative comparison of OBU antennas 1 and 2 in terms of the communication range and throughput is given in Table 3.13. The throughput achieved with OBU antenna 1 is by a factor of four larger than with OBU antenna 2. This considerable difference is partially due to the reduced communication range of measurements with OBU antenna 2. Additionally, in measurements with this antenna, up to 47.5 % of all transmitted packets were lost. In contrast, the percentage of erroneous packets in measurements with OBU antenna 1 is less than 20 %. The mean RCR of measurements with OBU antenna 1 is 0 m. However this, does not imply that for V2I measurements with this OBU antenna no reliable communication can be achieved at all. This result is due to our definition of RCR, which is not applicable for evaluation of the antennas with one-sided communication range. We recall, that the PDR at the absolute distance $|d|$ is given as arithmetic mean of the PDRs at relative distances $-d$ and d. The definition of the UCR is nevertheless valid even for measurements with one-sided communication range. We thus conclude that the communication range achievable with OBU antenna 1 is on average 70 % larger than the communication range achievable with OBU antenna 2.

We next compare the performance of OBU antennas 1, 3, and 4 based on the measurements performed in the framework of ROADSAFE2011. In this case, the RSU was located at position 1, coordinates of which are provided in Table 3.4 and the respective environ-

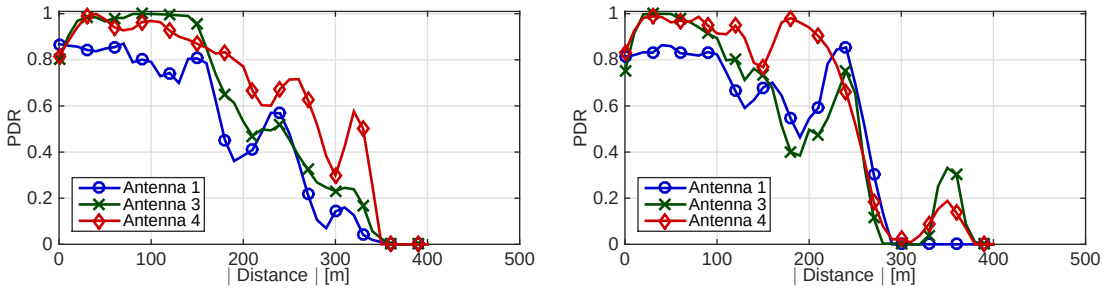

(a) PDR as a function of the absolute distance for measurements on RSU side.

(b) PDR as a function of the absolute distance for measurements in opposite direction.

Figure 3.18: Performance comparison for OBU antennas 1, 3, and 4.

ment is shown in Figure 3.4a. As transmit antenna we used the directional RSU antenna 5, details of which are given in Table 3.5. The transmit parameters for these measurements are summarized in Table 3.6. Measurements were performed in both driving directions. All results presented in this section are calculated as an average over 10 repetitions of the same measurement.

The performance of OBU antennas 1, 2, and 3 in terms of the PDR as a function of the absolute distance is shown in Figure 3.18 with blue, green, and red lines, respectively. We first note that the performance achievable in different driving directions is nearly the same for all three OBU antennas. However, the best performance in terms of reliability and coverage is achieved with OBU antenna 4. According to the results summarized in Table 3.14, the RCR obtained with OBU antenna 4 amounts to 210 m. This is 60 % more than for measurements with OBU antenna 1 and 30 % more than with OBU antenna 3. However, within the first 150 m, OBU antenna 3 results in more reliable performance. The RCR for measurements with OBU antenna 4 in opposite driving direction is even wider and equals 230 m. This is by 100 % and 60 % more than for OBU antennas 1 and 3, respectively. The difference in UCR is not that significant. For measurements on RSU side, the largest UCR of 350 m is achieved with OBU antenna 4. The UCR for measurements with antennas 1 and 3 are 20 % and 6 % less, respectively. In the opposite driving direction, the UCR is nearly the same for all OBU antennas and amounts to 280 m.

In terms of the throughput, the best performance was also achieved with OBU antenna 4. The throughput obtained with this antenna on RSU side amounts to 16 Mbit, which is 30 % more than with OBU antennas 1 and 3. The same percentage ratio is true for the measurements in opposite driving direction, for which the throughput achieved with OBU antenna 4 equals 14.3 Mbit.

We note that a quantitative comparison between the throughput presented in Tables 3.13 and 3.14 is not possible, since the transmit parameters of the corresponding experiments differ significantly. However, the percentage of erroneous packets can be used for comparison instead. The validity of this performance comparison criterion is verified by comparing the percentage of erroneous packets for measurements with OBU antenna 1 in Table 3.13 and

Table 3.14: Comparison of the system performance achievable with different OBU antennas at RSU position 1 of ROADSAFE2011 measurements.

OBU antenna	**Mean throughput [Mbit]**	**Mean $\hat{P}_e$ [%]**	**Mean RCR [m]**	**Mean UCR [m]**
On RSU side				
Antenna 1	12.3	20	130	290
Antenna 3	12.7	22.7	160	330
Antenna 4	16	16	210	350
Opposite direction				
Antenna 1	11	33.5	115	280
Antenna 3	11.3	23.8	140	280
Antenna 4	14.3	21.2	230	280

for measurements with the same antenna in Table 3.14 (on RSU side). The percentage of erroneous packets is about 20 % in both cases. We therefore conclude that $\hat{P}_e$ is a valid performance indicator for comparison of OBU antennas deployed in measurements with different settings. For measurements performed on RSU side, the smallest percentage of erroneous packets is obtained with OBU antenna 4. The percentage of erroneous packets for measurements with OBU antennas 1 and 3 is only 4 % and 6 % more, respectively. This difference in $\hat{P}_e$ is however more pronounced in measurements in opposite direction. Here, the worst performance was achieved with OBU antenna 1.

We conclude that careful design of OBU antennas is essential for the reliability of V2I communication systems. The best performance in terms of the throughput, communication range and percentage of erroneous packets is obtained with OBU antenna 4. A careful choice of the OBU antenna resulted in 30 % higher throughput and up to 100 % larger communication range. Although the performance of OBU antenna 2 is inferior to all other OBU antennas, it still can be successfully deployed for other applications, e.g., tolling systems.

3.6 Vehicular Traffic-induced Fading

In this section, we analyze the effects of vehicular traffic on the performance of the V2I communications with an emphasis on tunnel environments. The effects of vehicular traffic in more general urban environments are elaborately evaluated in [49]. The material presented in this section has been partially published in [103].

To analyze the effects of vehicular traffic on the performance of V2I systems, real-world experiments were performed in the framework of ROADSAFE2010. The RSU equipment was located at position 1, coordinates of which are given in Table 3.1. The respective environment is shown in Figure 3.1a. We recall that this location is characterized by a 300 m long tunnel that ends 150 m before the RSU position. As transmit antennas we used the directional RSU antenna 2, detailed characteristics of which are provided in Table 3.2. As receive

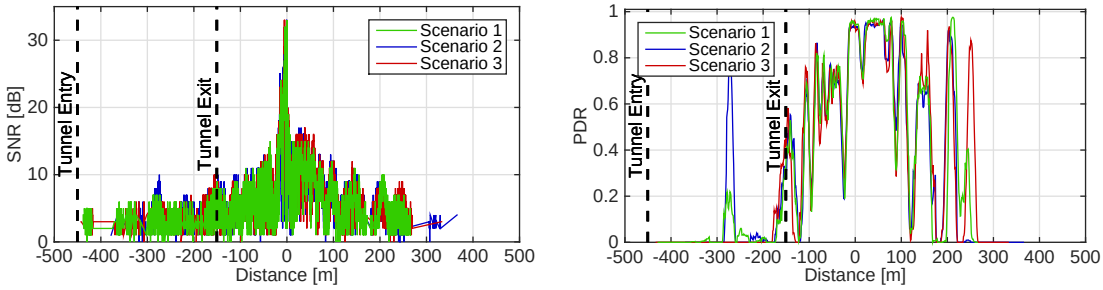

(a) SNR as a function of the distance.

(b) PDR as a function of the distance.

Figure 3.19: PDR and SNR as functions of the distance. Different colors represent the performance under different vehicular traffic scenarios. Dashed black lines respectively mark the tunnel entry and exit.

antenna, OBU antenna 1 was used, characteristics of which can be found in Section 3.1.1. The measurements were performed with transmit parameters corresponding to setting 1 (cf. Table 3.3).

Figure 3.19 shows the PDR and SNR performance obtained in measurements with different vehicular traffic conditions. We note that for all measurement repetitions the SNR at positive distances exhibits typical large and small scale fading behavior (cf. Figure 3.19a). However, the envelope of the SNR curve at negative distances lacks the large scale fading behavior. Particularly interesting is the SNR behavior in the tunnel, where we observe only minor fluctuations around the median SNR value, which remains constant at roughly 10 dB. As shown in Figure 3.19b, the PDR experiences a distinct performance drop immediately after the tunnel exit. We conjecture that this drop is caused by a significant change in the propagation environment and an increased number of multipath components, which our receiver cannot resolve.

Furthermore, Figure 3.19b demonstrates the impact of the vehicular traffic on the performance of V2I systems, most significantly in tunnels. The PDR curves outside of the tunnel are very similar for different measurement repetitions. However, the PDR inside the tunnel varies in the range from 0 to 0.8, depending on the vehicular traffic scenario. This observation can be explained by the absence of a LOS between OBU and RSU. As a direct consequence thereof, the signal propagating inside the tunnel is strongly dependent on the traffic situation.

To identify different traffic scenarios, we used video documentation and thoroughly analyzed the traffic density, the type of vehicles, and the distance between the test vehicle and the next vehicle inside the tunnel. Based on this analysis we identify the following traffic scenarios:

- *Traffic scenario 1* (low traffic density) is shown in Figure 3.20a. This figure is an extracted frame of the video that corresponds to the measurement represented by the green curve in Figure 3.19. This scenario is characterized by a low traffic density inside the tunnel and distances of $\geq$ 100 m between the test vehicle and the next vehicle. Based on the PDR and SNR performance shown in Figure 3.19, we conclude that such propagation conditions are not favorable for the signal propagation in tunnels.

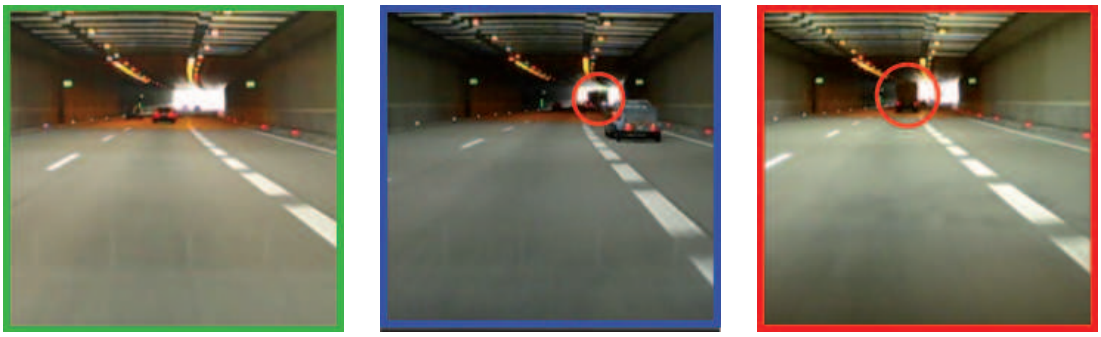

(a) Scenario 1: low traffic density. (b) Scenario 2: large vehicle ahead. (c) Scenario 3: blocked LOS.

Figure 3.20: Definition of vehicular traffic scenarios in tunnel environments.

- *Traffic scenario 2* (large vehicle ahead) is shown in Figure 3.20b. In this case, the traffic density is higher than in scenario 1. Moreover, there are two trucks driving approximately 200 m ahead of the test vehicle. While these trucks were approaching the exit of the tunnel they acted as reflectors. Therefore, the signal was penetrated deeper into the tunnel. The performance of this scenario is shown by the blue line in Figure 3.19. Despite the increased traffic density and the presence of large vehicles, this scenario yields the best performance in terms of the PDR inside the tunnel.

- *Traffic scenario 3* (blocked LOS) is shown in Figure 3.20c. This scenario is characterized by the highest vehicle density and the presence of a truck approximately 80 m ahead of the test vehicle. In contrast to scenario 2, here the truck has negative influence on the signal propagation. It is not only blocking the LOS, but also attenuates the dominant multipath components inside the tunnel. The performance in this scenario is shown by the red line in Figure 3.19. We identify scenario 3 as the most disadvantageous traffic situation for V2I communications in tunnel environments.

To further investigate the influence of the identified vehicular traffic scenarios on the performance of the V2I systems in tunnels, we show the PDR as a function of the SNR in Figure 3.21. Similarly to Figure 3.19, the green line represents the traffic scenario 1, the blue line corresponds to the scenario 2, and the red line depicts the performance in scenario 3. These results illustrate the performance inside the tunnel, i.e., for distances d such that $-450\,\mathrm{m} < d < -150\,\mathrm{m}$. The black line in Figure 3.21 shows the performance outside the tunnel at the same distance, i.e., $150\,\mathrm{m} < d < 450\,\mathrm{m}$. For the sake of clarity, we show the PDR vs. SNR performance of only one measurement outside the tunnel. Recall that the measurement results in the open area are very similar (cf. Figure 3.19).

Figure 3.21 shows that outside of the tunnel the PDR saturates at a value close to 1 for an SNR of roughly 9 dB. Furthermore, in the medium SNR regime (5 to 8 dB), the slope of the PDR curve is steeper than for the measurements inside the tunnel. This implies that the same increase in SNR causes larger PDR increase in the open area environments than in tunnels. The PDR inside the tunnel saturates at a slightly larger SNR of about 9 dB. However, the

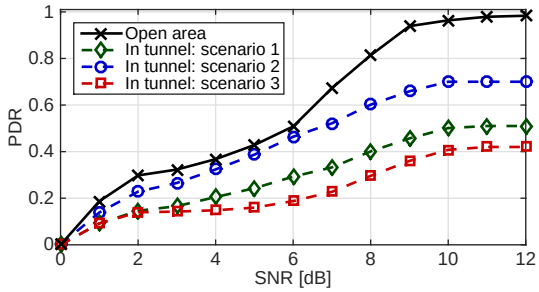

Figure 3.21: PDR as function of the SNR for different vehicular traffic scenarios inside the tunnel.

maximum achievable PDR is significantly lower than for the open area. Furthermore, the PDR vs. SNR performance depends on the vehicular traffic scenario. The largest PDR of roughly 0.7 is achieved in scenario 2, in scenario 1 PDR saturates at approximately 0.5. However, the worst performance is obtained in scenario 3, where PDR saturates at roughly 0.4.

We thus conclude that the instantaneous traffic situation inside the tunnel severely impacts the signal propagation. Furthermore, we have shown that the position and the size of the vehicles between the OBU and the RSU are of great significance.

3.7 Multi-Hop Measurements

The results of Sections 3.3 to 3.6 have shown that the connectivity in V2I communications systems is strongly dependent on the existence of a LOS path between transmitting RSU and receiving OBU. One straightforward way to overcome this performance limiting dependence is to deploy cooperative inter-vehicle networks. In such networks, data generated by the RSU is retransmitted by the vehicles in its communication range if necessary. The key idea behind cooperative communication networks is to exploit the diversity inherent in multiple spatially distributed wireless links. A number of relay-based cooperative schemes have been proposed in the literature. However, the most notable forwarding-based concepts are amplify-and-forward (AF) and decode-and-forward (DF). In AF-based transmission schemes, the relay transmits an amplified version of the noisy received signal without performing data detection. In DF-based relaying schemes, the relay decodes the received signal and, if the decoding was successful, transmits a re-encoded version of the source data. While AF is easy to implement, it performs inferior to DF at least when the relay is relatively close to the source node. The performance benefit of DF comes at the price of higher computational complexity and increased delay due to the decoding.

In this section, we present results of a two-hop DF-based relaying experiment with off-the-shelf IEEE 802.11p devices. This results were partially published in [106]. The experiments were performed in the framework of ROADSAFE2011. As source we used the RSU located at position 1, coordinates of which are given in Table 3.4 and the respective environment is

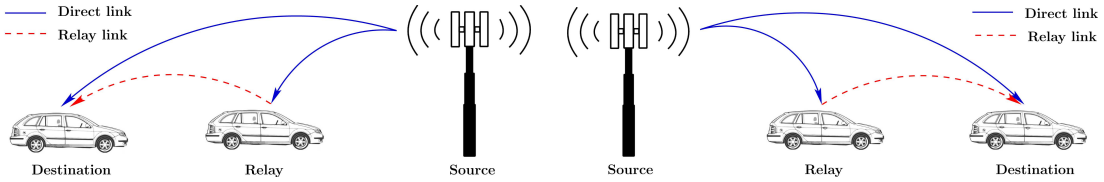

(a) Relay driving ahead destination. (b) Destination driving ahead relay.

Figure 3.22: Multi-hop measurement scenarios.

illustrated in Figure 3.4a. As RSU antenna we used the directional antenna 5, characteristics of which are summarized in Table 3.5. The source was constantly transmitting packets in broadcast mode with transmit parameters provided in Table 3.6. As relay, we used a prototype system developed by Kapsch TrafficCom for IEEE 802.11p-based V2V and V2I communications. The relay was placed inside the first test vehicle and connected to OBU antenna 4, characteristics of which can be found in Section 3.1.2. As destination node the CVIS platform was used. Similarly to the relay, the destination node was equipped with the OBU antenna 4.

In our measurements, we used a DF-based relaying scheme, i.e., the messages received by the relay node were first decoded and examined by the CRC. If the decoded packet passed the CRC, the unique packet identifier was extracted from the payload and stored to a log-file at the relay. Afterwards, the unmodified packet was re-transmitted. The destination node recorded all packets received via the direct link and via the relay hop. The difference between the direct and relay link is schematically illustrated in Figure 3.22. To separate these two links, we split the initially recorded data stream in the post-processing stage in to two streams based on the medium access control (MAC) addresses of the source and the relay nodes, contained in the header of each decoded packet. Thus, the first data stream contains only the packets transmitted by the RSU, while all packets transmitted from the relay are ignored. For the second data stream, the packets transmitted by the RSU are ignored, which allows us to obtain the data stream of the relay link. We note that the direct link and the relay link are decoded independently, and thus the destination benefits from a packet received via the relay hop, if and only if this packet was not received directly from the RSU.

For multi-hop measurements we considered the following two scenarios:

- *Relay ahead*: In this case, the relay drives ahead of the destination, as shown in Figure 3.22a. This implies that the relay enters and exits the communication range of the RSU before the destination. This scenario allows us to extend the coverage to distances where the destination did not yet enter the communication range of the RSU.

- *Destination ahead*: Here, the relay drives behind the destination (cf. Figure 3.22b). In this case, the relay enters the communication range of the RSU after the destination and remains in the coverage after the destination has left it already. Therefore, this scenario allows us to extend the communication range to distances where the destination has already left the communication range of the RSU.

Table 3.15: Throughput increase achievable by using additional packets received via relay link.

	Mean additional packets	**Maximum additional packets**	**Mean relative to direct link**	**Maximum relative to direct link**
Before RSU	300	396	9.5 %	12 %
Within RSU	393	654	13 %	28 %
After RSU	286	435	9 %	11 %

Since the position of the relay and the destination relative to each other was constant during one measurement run, it was only possible to extend the communication range in either negative or positive direction.

Since the emphasis of our work is on benchmarking the potential improvements from vehicular relaying, rather than the separate evaluation of the V2V and V2I links, we compare the performance of the direct link to what we call the combined-source link. To obtain the combined-source data stream from the direct and the relay streams, we proceed as follows. First, we use the data received via the direct link. Next, we search for the packets which were received via the relay link, but are missing in the direct link data stream. These additional packets can be divided into three groups. The first group contains the packets received from the relay before the destination entered the communication range of the RSU (relay ahead scenario). The second group contains the packets received from the relay after the destination left the communication range of the RSU (destination ahead scenario). And the third group contains the packets that were transmitted when destination was within the RSU communication range. Thus, the packets of the latter group increase the packet reception probability within the RSU range, while the packets of the first two groups extend the communication range of the RSU.

Table 3.15 summarizes the statistics of the additional packets received via the relay link based on 14 independent measurement runs (7 measurements for each scenario). The first two columns show the mean and maximum number of the packets received before, within, and after the RSU communication range. The third and the forth column show the same information expressed as a percentage of the total number of packets received via direct link. We observe that combining information received via the direct and rthe elay link allows us to increase the throughput within the RSU communication range by 13 % on average. Moreover, the destination was on average able to receive 9 % more packets outside the RSU communication range. In total this yields an average throughput enhancement of more than 20 % (recall that a communication range extension is only possible in one direction, depending on the measurement scenario).

Figure 3.23a shows PDR curves for combinations of two particular measurements as a function of the distance. The direct link performance is indicated by the red line and the combined-source link is shown by the green line. Within the communication range of the

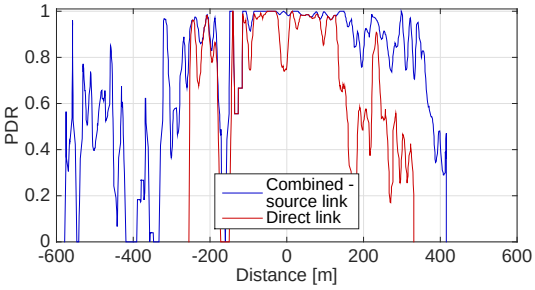

(a) PDR as a function of the relative distance for direct (red) and combined-source (blue) link.

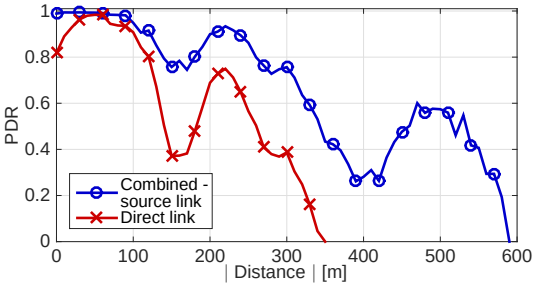

(b) PDR as a function of the absolute distance for direct (red) and combined-source (blue) link.

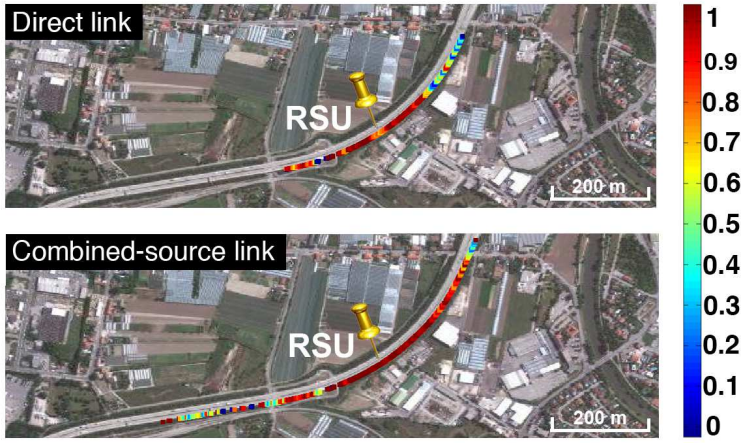

(c) PDR plotted on a satellite map. Colorbar indicates the mapping of PDR values into the colormap. The upper plot shows the PDR performance for direct link and the lower plot for combined-source link.

Figure 3.23: PDR performance of direct and combined-source link.

RSU, i.e., distances d such that $d^- \approx -280\,\text{m}$ to $d^+ \approx 330\,\text{m}$, we observe that the PDR curve based on the combined-source link is close to 1 and is strictly above the PDR of the direct link. This is particularly noticeable at $d = 0\,\text{m}$, where the destination is passing directly under the RSU. Due to the fact that the signal strength directly below the gantry is rather weak, we observe a drop of the PDR at $d = 0\,\text{m}$ for direct link, which is compensated by using the additional information provided by the relay.

We note that the combined-source PDR performance shown in Figure 3.23a represents a synthesis of two measurements with different scenarios. The part of the curve within the communication range of the RSU and at positive distances outside the RSU communication range, was obtained while the destination was driving ahead of the relay. The part of the combined-source PDR curve at the negative distances before entering the RSU communication range was obtained during the measurement in which the relay was driving ahead of the destination.

Based on these observations we conclude that the use of a relay does not only increase the packet reception probability within the RSU communication range, but also significantly extends the communication range. In particular, if a relay selection scheme is applied, the destination could first choose a relay that is driving ahead and thus extends the communication range into negative distances relative to the RSU. After passing the RSU, the destination could switch to a relay that is driving behind to further expand the communication range into positive distances.

Table 3.16: RCR and UCR for direct and combined-source link.

	Direct link	**Combined-source link**	**Mean increase in coverage**
Mean RCR	160 m	205 m	70 %
Mean UCR	310 m	410 m	30 %

To further visualize the effects of the communication range extension and increased packet reception probability in Figure 3.23c we show PDR on a satellite map. Here, the PDR values close to 1 are shown by dark red color, and the dark blue corresponds to PDR values close to 0. The PDR curve of the direct link is shown in the upper plot, while the second plot represents the PDR curve of the combined-source link. By simple visual comparison of these plots, we conclude that the communication range can be almost doubled by using a simple DF-based relaying scheme.

To summarize the obtained results we present the PDR as a function of the absolute distance in Figure 3.23b for direct and combined-source link. These curves constitute an average over 14 measurements for the direct link and the combined-source link. The RCR and UCR calculated on the basis of these PDR vs. distance plots are given in Table 3.16. In particular, the RCR is increased by 30 % and the UCR is increased by 70 % when using additional information from the relay.

Based on evaluations of real-world vehicular multi-hop measurements we conclude that the throughput and the communication range of V2I systems can be significantly increased by using a simple two-hop DF mechanism. It has been shown that the throughput within the communication range of the RSU can be increased by 13 %. Depending on the relative position of relay and destination it was possible to further enhance the total throughput and achieve up to 30 % increase in RCR. These results can be further improved by using more sophisticated relaying algorithms on the physical and network layers.

3.8 Discussion

In this chapter, we provide a comprehensive set of guidelines for deployment of future V2I systems. All design and deployment suggestions are based on extensive V2I experiments. These experiments address the effects of transmit parameters, the RSU and OBU antennas, and evaluate the impact of specific highway environments, such as tunnels, grass covered embarkments and noise protection walls. Our considerations go even one step ahead of conventional V2I communications and we evaluate, the performance of a two-hop DF relay link.

With respect to the transmit parameters we have analyzed the effects of packet length and data rate. We have shown that both, higher data rates and longer packets lead to performance degradation in terms of reliability and coverage. However, the performance of

V2I systems with higher data rates is more sensitive to the change of the driving lane. In particular the range within which reliable communication is guarantied was nearly halved and the throughput was reduced by more than 20 %. To maintain reliable connectivity in the context of V2I communications we therefore suggest to use lower data rates and increase the packet length if higher throughput is required.

In the context of the RSU antennas we have evaluated the system performance with various antenna types, gains, and mounting positions. Our results reveal the importance of deliberate RSU antenna mounting. To achieve homogeneous coverage and avoid undesirable performance degradation for one of the driving directions, we recommend to mount the RSU antennas in the middle of the highway. We have further shown that omni-directional RSU antennas perform inferior to directional RSU antennas. Moreover, we have shown that high-gain directional antennas yield a significant performance improvements. Increasing antenna gain by 4 dBi we achieved five times greater communication range and by 125 % more throughput.

Not only the RSU antennas play a significant role in the performance of V2I systems, but also the OBU antenna design should not be neglected. We have analyzed the performance achieved with three differently manufactured omni-directional OBU antennas with antenna gains between 4 dBi and 6 dBi. We have obtained RCR improvement of up to a factor of three and up to 30 % more throughput when using a better suited OBU antenna.

With respect to vehicle traffic-induced fading we have shown that the instantaneous traffic situation inside a tunnel severely impacts the signal propagation. However, in contrast to our expectations not the traffic density alone, but also the position and the size of the moving objects between OBU and RSU are strongly influencing the communication quality.

To circumvent the negative impact of LOS obstruction induced by realistic vehicular traffic and to increase the reliability of V2I communications, we suggested to use a two-hop DF relaying scheme. We have evaluated the suggested approach using real-world experiments. The results have shown that a simple cooperative network is capable of significantly improving the PDR. The throughout was increased by 30 % and the RCR was increased by 70 %. We therefore strongly support the cooperative communication approach in the context of dependable vehicular communications.

4

Vehicle-to-Infrastructure Performance Models

In this chapter we introduce a simple and yet accurate approach for modeling realistic distance-dependent packet-error performance. We suggest a quantization-based algorithm for reduction of the model complexity. The proposed algorithm does not only reduce the number of model parameters, by taking into account inherent correlations between them, but also localizes realistic environmental impairments. We further extend this model, initially designed for modeling the packet-error performance only, to a model capable of reproducing realistic signal-to-noise ratio (SNR) behavior. This hidden Markov model (HMM)-based approach can be successfully applied for modeling the packet-error and SNR performance of any distance-dependent wireless communication system. As a proof of concept we parametrize the model based on the results of extensive vehicle-to-infrastructure (V2I) field measurements, performed in urban environment. Finally, we show that the resulting model is capable of predicting the performance of V2I communication systems in various urban scenario with known topological characteristics.

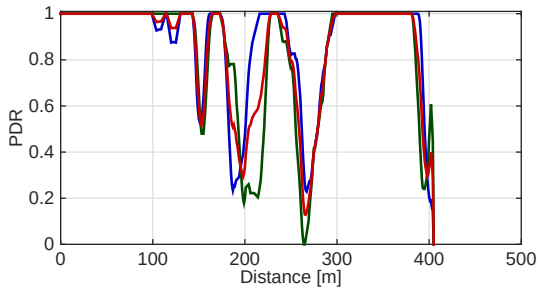

Figure 4.1: Example of measured PDR vs. distance performance. Different colors represent repetitions of the same measurement at different times.

4.1 Packet-Error Model

Based on the results of extensive field measurements (cf. Chapter 3) we have evaluated verious aspects of V2I communication systems. We presented a multitude of realistic packet-error traces in the form of packet delivery ratio (PDR) vs. distance curves. The measurement results show that realistic performance of V2I communication systems cannot be closely reproduced by simplified propagation models. Such simplifications often include omni-directionality of both, the receive and the transmit antennas, probability of packet reception decreasing exponentially with the distance, or packet loss probability of 0 % within certain range around the transmitter. Nevertheless, such simplistic propagation models are frequently used for upper layer simulations, for the development of important system components, e.g., synchronization, scheduling and fault tolerance mechanisms. In is necessary to ensure that these important parts of the system are developed and tested in simulation environments, physical layer (PHY) of which resembles real-world measurements as close as possible. Therefore in this section we suggest a computationally inexpensive and accurate way of reproducing measured V2I patterns.

An example of measured PDR performance is shown in Figure 4.1. Different colors represent repetitions of the same measurement taken with a time lag of several minutes. This means that all system elements remain the same, except for the moving scatterers induced by the realistic traffic and pedestrians. The three exemplary measurements shown here have much in common: PDR at distances d such that $0\,\mathrm{m} \leq d \leq 100\,\mathrm{m}$ equals 1, for $d \geq 400\,\mathrm{m}$ no signal reception is possible, at distances $d = 150\,\mathrm{m}$ and $d = 280\,\mathrm{m}$ all three measurement repetitions experience nearly the same drop of PDR performance. Such repetitive behavior is caused by transmit parameters, transceiver equipment and measurement environment. However, there are subtle differences between the three measurements. For instance, the green PDR curve equals 1 at distances $100\,\mathrm{m} \leq d \leq 150\,\mathrm{m}$, while the blue and the red curves experience slight performance degradation in this range. Also the deep notch of the PDR that appears at distances $180\,\mathrm{m} \leq d \leq 230\,\mathrm{m}$ has different shape in all three measurements. These unique effects, expressed in terms of distinct PDR values are most likely due to the instantaneous traffic situation in each measurement. We therefore seek a model that carefully

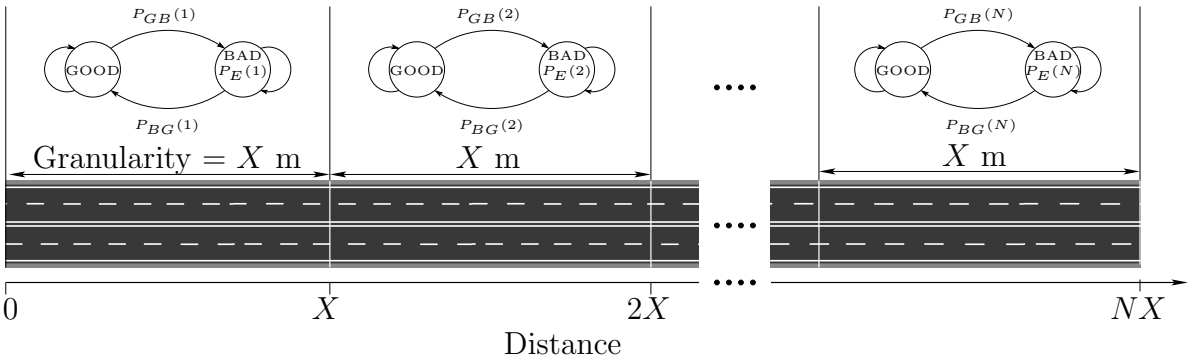

Figure 4.2: Schematic illustration of the proposed range-dependent modified Gilbert model.

reproduces repeatable aspects of real-world V2I measurements and yet allow for some random deviations, to represent the effect of moving scatterers.

In this context we propose to use Gilbert's model introduced in Section 2.3.2. However, since the performance of vehicular communication links strongly depends on the distance between the transmitter and the receiver, such a two-state model with fixed parameters should not be used, to avoid the loss of important channel effects. To maintain an accurate representation of the propagation effects, we suggest to divide each measurement into N parts corresponding to N disjoint distance intervals of the same length, referred to as *granularity* hereafter. The transition probabilities (P_{BG}, P_{GB}) and the emission probability (P_E) are then estimated separately for each interval using the Baum-Welch algorithm (cf. Section 2.3.3). Once the model parameters for all N intervals are estimated, we can combine them as shown in Figure 4.2, to form a range-dependent modified Gilbert model. However, the model retains all properties of the original Gilbert's model, except that the model parameters (P_{BG}, P_{GB}, P_E) change as soon as the vehicle leaves the current interval. For the first distance interval the initial model state π_1 is chosen at random, whereas for all subsequent intervals, the initial state is equal to the final state in the previous interval. We refer to this model as *range-dependent modified Gilbert model* in what follows.

Clearly, the choice of the granularity is essential for the accuracy of the range-dependent modified Gilbert model. On the one hand, the granularity should not be small, because dividing the measured error pattern into very short intervals will destroy the statistics of the data. On the other hand, estimating the model parameters for large intervals, inevitably averages out the local behavior of the communication link. Therefore, a crucial question for the design of our range-dependent modified Gilbert model is how to select the granularity. To answer this question we first estimate the model parameters with granularities between 1 m and 300 m. For model parameter estimation we adopt a principle closely related to a statistical resampling technique called jackknife [94]. Particularly, if we have M measurement repetitions in total, we leave out one of them and perform iterative parameter estimation based on the remaining $M - 1$ measurement data samples. When the parameter set Θ is estimated we generate L packet-error patterns using the range-dependent modified Gilbert

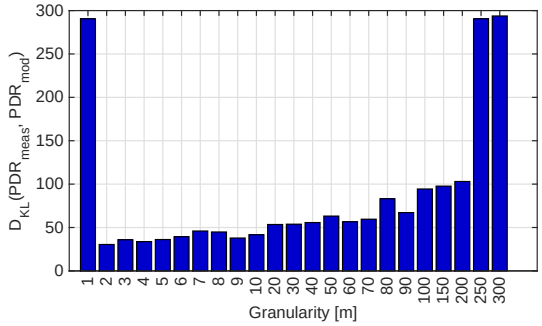

(a) KLD between measured and model-generated PDR vs. distance curves.

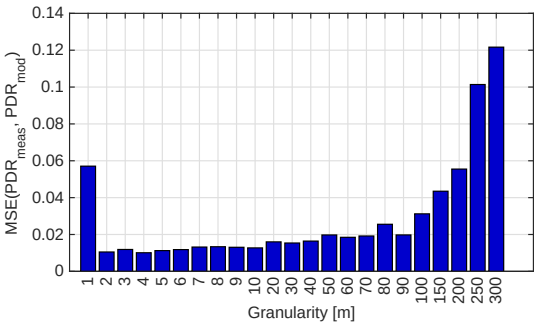

(b) MSE between measured and model-generated PDR vs. distance curves.

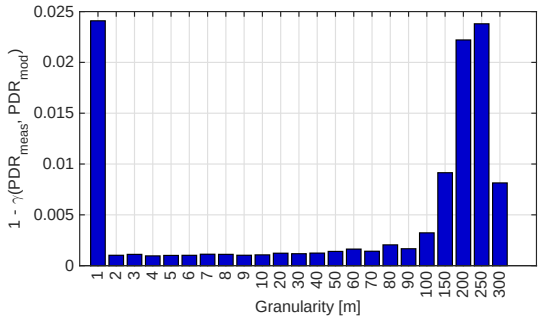

(c) Complementary collinearity between measured and model-generated PDR vs. distance curves.

Figure 4.3: Influence of granularity on the performance of the range-dependent modified Gilbert model in terms of KLD, MSE, and collinearity. All results are calculated based on the comparison of $M = 10$ measured and $L = 10^4$ model-generated curves.

model. Next, we convert the model-generated packet-error patterns into PDR sequences, as described in Section 3.2. Finally, we compare them one by one to the PDR sequence of the measurement that was left out for parameter estimation. To assess the similarity of the measured and model-generated PDR sequences we use a set of similarity criteria consisting of Kullback-Leibler divergence (KLD), mean squared error (MSE) and collinearity (cf. Section 2.3.4). We thus have as many sets of similarity criteria, as model-generated packet-error patterns. Finally, we take the median of all these values to obtain a single set of similarity criteria for each measurement repetition. The same procedure is repeated for all M measurements and the median is taken, to constitute performance of the model. This model performance evaluation procedure will be deployed in the remainder of this chapter.

The set of similarity criteria obtained in this manner based on $M = 10$ measured and $L = 10^4$ modeled packet-error traces is shown in Figure 4.3. We note that Figure 4.3c shows the complementary collinearity $1 - \gamma$. All three similarity criteria presented in Figure 4.3 follow the same trend, which verifies the validity of the approach, chosen for model accuracy assessment. From the results presented here we conclude that the granularity should not be less than 2 m, to ensure stable model performance. Poor performance of the model with granularity 1 m is due to insufficient data for parameter estimation, on the one hand and due to broken down statistical dependencies, on the other hand. Similarly, the granularities

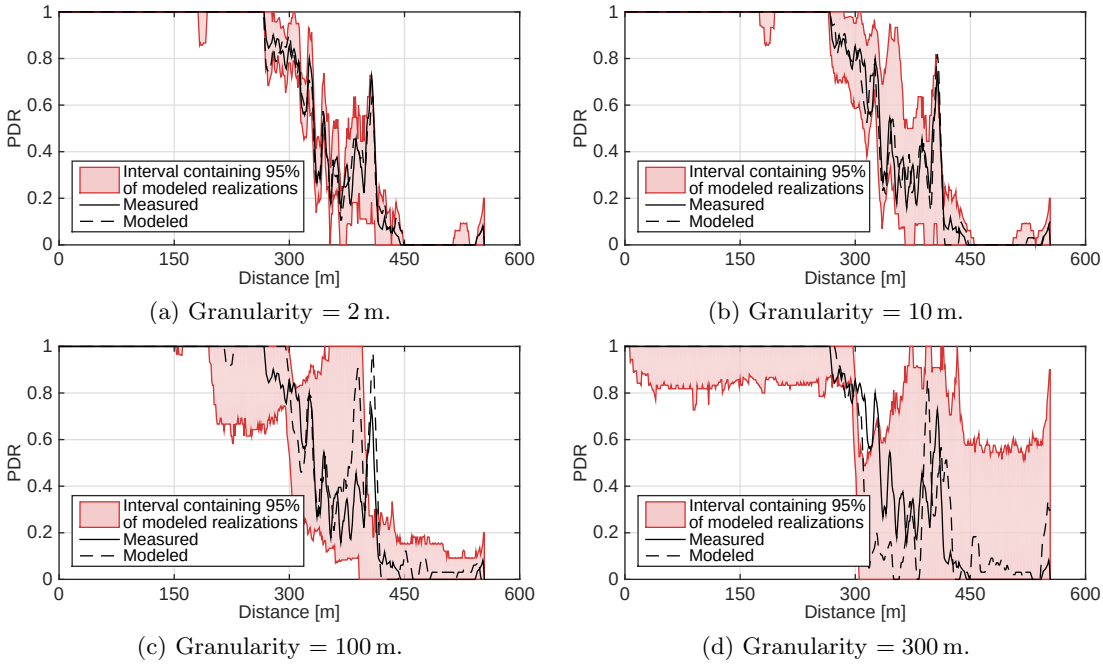

(a) Granularity = 2 m. (b) Granularity = 10 m.

(c) Granularity = 100 m. (d) Granularity = 300 m.

Figure 4.4: PDR as a function of distance. Solid lines represent a measured sample and dashed lines represent a randomly selected model-generated sample. The colored bands contain 95 % of all model-generated results for a given granularity.

> 100 m are not recommended, since they average out important distance dependencies. Otherwise, the general trend of all three similarity criteria suggests that estimation of the model parameters with smaller granularities, leads to a better approximation of the measurement. However, granularities smaller than 10 m do not yield significant improvements of model accuracy, while considerably increasing the computational overhead of the range-dependent modified Gilbert model.

To visualize the effect of granularity on the performance of the range-dependent modified Gilbert model, we compare measured and model-generated PDR sequences in Figure 4.4. Here, the model granularity is 2 m, 10 m, 150 m, and 300 m. The measured sample is shown using a black solid line and a model-generated performance curve is shown with a black dashed line. The red colored bands represent the interval in which 95 % of all 10^4 model realizations lie. When comparing the measured and the modeled samples, we clearly see that the model with small granularities (cf. Figure 4.4a and 4.4b) reproduces the measurement almost indistinguishably close. For larger granularities the realistic distance dependencies inherit to the measured PDR curves are not reflected by the model (cf. Figure 4.4c and 4.4d). Furthermore, we note that for the model with small granularity, the 95 % intervals are very tight, i.e.,almost all realizations approximate the measurement result very well. In contrast, the 95 % intervals for the model with granularity 150 m or 300 m are significantly wider, meaning that the deviations from the measurement can be substantial. The colored bands also mark the borders between consecutive intervals of the range-dependent modified Gilbert model, which are particularly well pronounced for granularities of 150 m and 300 m.

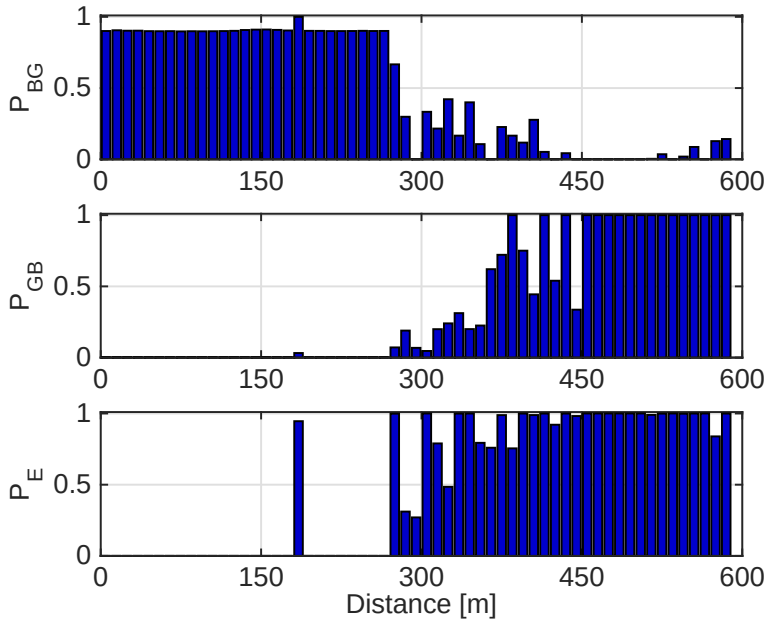

Figure 4.5: An example parameters of our range-dependent modified Gilbert model with a granularity of 10 m.

We conclude that the granularity of our range-dependent modified Gilbert model is a trade-off between accuracy of the model and its complexity. Thus, to ensure high reproducibility of the measured results and keep the computational overhead of the model within manageable limits we suggest to use a granularity of 10 m.

An example for the parameters of the range-dependent modified Gilbert model with a granularity of 10 m is shown in Figure 4.5. In the close vicinity of the roadside unit (RSU), for distances d with $0 \leq d \leq 280$ m, the model is predominantly in the good state. In this case, the probability of leaving the good state P_{GB} is fairly low and the probability of leaving the bad state P_{BG} is above 0.9. Moreover the model in this range is nearly error-free due to the very low error probability P_E. The probabilities change drastically around 450 m. Here, the bad state is dominating and the error probability is close to 1. We thus note, that the model states in the beginning and on the edge of the communication range are persistent. In the intermediate range $280 < d < 450$, neither of the two states is persistent and the model parameters change significantly between the consecutive intervals.

4.2 Quantization Algorithm for Model Dimension Reduction

In Section 4.1 we have shown that the granularity of the range-dependent modified Gilbert model, hereafter called the original model, constitutes a trade-off between the accuracy of the model and its complexity. However, small granularities lead to a considerable increase of the number of intervals, thereby increasing the computational overhead of the model. In order to ensure high accuracy of the model while keeping the number of parameters low, we

suggest to use vector quantization (VQ). The main reason for using VQ instead of scalar quantization (SQ) is that the model parameters P_{BG}, P_{GB} and P_E are not independent of each other. Hence, the joint quantization will improve the overall quality of the quantized representation. Furthermore, VQ is frequently used for classification purposes in speech or image recognition. Hence, it can be applied to localize and subsequently parametrize certain environmental and propagational aspects. Finally, jointly quantizing all three model parameters reduces the number of possible parameter combinations by a factor of K^2 as compared to SQ, where K is the number of quantization levels.

In the following, we introduce the VQ design and subsequently find an optimal number of quantization levels. First, we parametrize the original model with granularity 10 m based on the selected set of measurements. Next, we combine the model parameters for the nth interval into a vector $\boldsymbol{x}_n = (P_{BG,n}, P_{GB,n}, P_{E,n})$, with $n = 1, \ldots, N$. In the following $\boldsymbol{X}_N = \{\boldsymbol{x}_n\}_{n=1}^{N}$ denotes the set of all model parameters. Using the LBG algorithm [69], we now aim to find a set of representative vectors $\boldsymbol{Q}_K = \{\boldsymbol{q}_k\}_{k=1}^{K}$ with $K < N$, such that the average distortion $\mathcal{D}$, defined in (4.3), is minimized. The VQ design consists of the following steps:

1. **Initialization**: The iteration count i is set to 0. The initial set of representative vectors $\boldsymbol{Q}_K^{(0)} = \left\{\boldsymbol{q}_k^{(0)}\right\}_{k=1}^{K}$ is chosen randomly, and we set $\mathcal{D}^{(-1)} = \infty$.

2. **Assignment:** Each vector of model parameters $\boldsymbol{x}_n$ is allocated to its nearest-neighbor representative vector $\boldsymbol{q}_{k^\star}^{(i)}$ according to the smallest Euclidean distance, i.e.,

$$\boldsymbol{q}_{k^\star}^{(i)} = \underset{k \in \{1,\ldots,K\}}{\arg\min} \left\| \boldsymbol{x}_n - \boldsymbol{q}_k^{(i)} \right\|. \tag{4.1}$$

3. **Computation of average distortion:** All model parameter vectors $\boldsymbol{x}_n$, which have the representative vector $\boldsymbol{q}_{k^\star}^{(i)}$ as their nearest neighbor are grouped into a cluster

$$\mathcal{C}_{k^\star}^{(i)} = \left\{ \boldsymbol{x}_n \in \boldsymbol{X}_N : \boldsymbol{q}_{k^\star}^{(i)} = \underset{k}{\arg\min} \left\| \boldsymbol{x}_n - \boldsymbol{q}_k^{(i)} \right\| \right\}. \tag{4.2}$$

   The average distortion $\mathcal{D}^{(i)}$ of the current set of representative vectors is then given by

$$\mathcal{D}^{(i)} = \frac{1}{N} \sum_{k^\star=0}^{K} \sum_{\boldsymbol{x}_n \in \mathcal{C}_{k^\star}^{(i)}} \left\| \boldsymbol{x}_n - \boldsymbol{q}_k^{(i)} \right\|. \tag{4.3}$$

4. **Update:** If $\mathcal{D}^{(i)} < \mathcal{D}^{(i-1)}$, we update the set of representative vectors $\boldsymbol{Q}_K^{(i+1)} = \left\{\boldsymbol{q}_k^{(i+1)}\right\}_{k=1}^{K}$ by computing the component-wise arithmetic mean of all model parameter vectors in a cluster. Next, the iteration count i is incremented by one and the algorithm continues with the assignment step.

5. **Termination:** The algorithm terminates if $\mathcal{D}^{(i)} = \mathcal{D}^{(i-1)}$, or if the maximum number of iterations is reached.

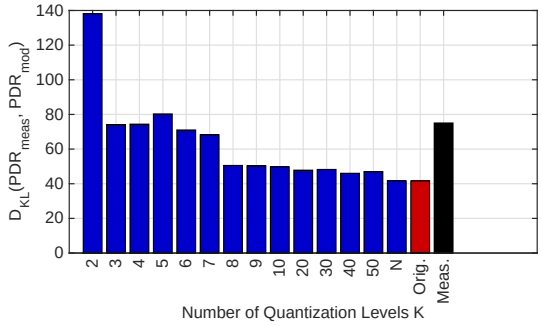

(a) KLD between measured and model-generated PDR vs. distance curves.

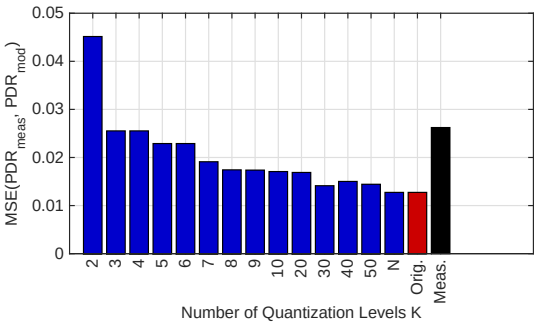

(b) MSE between measured and model-generated PDR vs. distance curves.

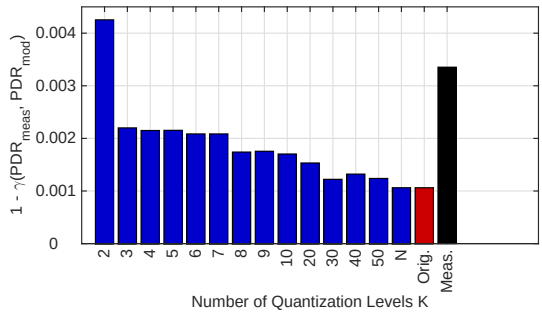

(c) Complementary collinearity between measured and model-generated PDR vs. distance curves.

Figure 4.6: Influence of the number of quantization levels K on the performance of the quantized range-dependent modified Gilbert model in terms of KLD, MSE, and complementary collinearity. All results are calculated based on the comparison of $M = 10$ measured and $L = 10^4$ model-generated curves. The red bar indicates the performance of the range-dependent modified Gilbert model with unquantized parameters. The black bar shows the measured reference.

The main disadvantage of the LBG algorithm is that it finds only the nearest local minimum and is dependent on the selection of the initial parameters $\boldsymbol{Q}_K^{(0)} = \{\boldsymbol{q}_k^{(0)}\}_{k=1}^K$. In order to alleviate problems associated with the initialization of the LBG algorithm, we repeat the VQ procedure 10^5 times and take the set of representative vectors leading to the smallest distortion.

The number of quantization levels K, defines how many details of the initial model parameters should be omitted. For instance by setting $K = N$ we do not omit any details. Thus, the representative values are equal to the initial parameters, the average distortion is zero and the performance will be the same as for the original model. However, this is not what we are looking for in our attempt to reduce the number of model parameters. We are particularly interested in $K \ll N$. To find the optimal number of quantization levels we quantize parameters of the original model with K quantization levels ranging between 2 and 50. Next, we use the quantized model parameters to generate packet-error patterns with the range-dependent modified Gilbert model and compare them to their measured counterparts. The result of this model performance assessment is shown in Figure 4.6 in terms of KLD,

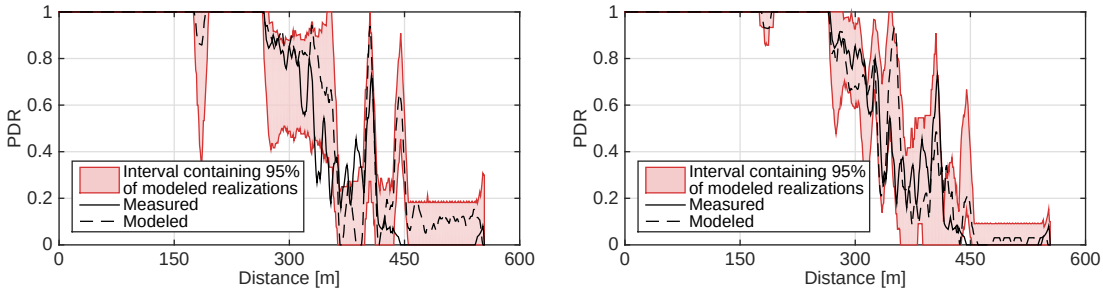

(a) Number of quantization levels $K = 3$.

(b) Number of quantization levels $K = 8$.

Figure 4.7: PDR as a function of distance. Solid lines represent a measured sample and dashed lines represent a randomly selected model-generated sample. The colored bands contain 95 % of all model-generated results for a given number of quantization levels.

MSE, and complementary collinearity . All three similarity criteria presented here follow the same trend and we clearly see that the larger values of K lead to higher model accuracy. By setting $K = N$ the performance of the model with quantized parameters indeed equals that of the original model, indicated by the red bar in Figure 4.6.

The most pronounced difference in the model performance is achieved when using 3 quantization levels instead of 2. For $3 \leq K \leq 7$ the model performance is nearly the same and the next noticeable accuracy improvement is attained for $K = 8$. We also note that further increase of K results in barely perceptible accuracy enhancements. Hence, we conclude that quantizing the model parameters with $K > 8$, only leads to an unnecessary increase of the model overhead. To find out whether the level of accuracy achievable with $K = 8$ is sufficient, we compare it to measured reference. Therefor we calculate KLD, MSE, and collinearity between all M repetitions of the same measurement and take the median of the resulting $\frac{M!}{M-1}$ values. The measured reference values obtained in this way are indicated by the black bars in Figure 4.6. We notice that for all three similarity criteria the black bars are significantly higher than the blue bar for $K = 8$. This implies that the measured packet-error patterns are more similar to the model-generated patterns than to each other.This is due to the fact that the model parameters were estimated based on all measurement repetitions and therefore, represent an average measured performance. We conclude that the model accuracy for $K = 8$ is sufficient, but not necessary. In fact, the necessary model accuracy is achieved already with $K = 3$ quantization levels.

To get a better perceptible picture of the accuracy loss introduced by the model parameter quantization, we compare measured and model-generated PDR sequences in Figure 4.7, where the model parameters were quantized with $K = 3$ and $K = 8$ levels. Here, measured sample is shown using black solid line and the model-generated performance is shown with a black dashed line. The red bands represent the interval in which 95 % of all model realizations lie. Comparing these results to the performance of the original model with granularity 10 m (cf. Figure 4.4b), we note that the performance difference between the original model and the model with quantized parameters is negligibly small, for both values of K. However, the 95 %

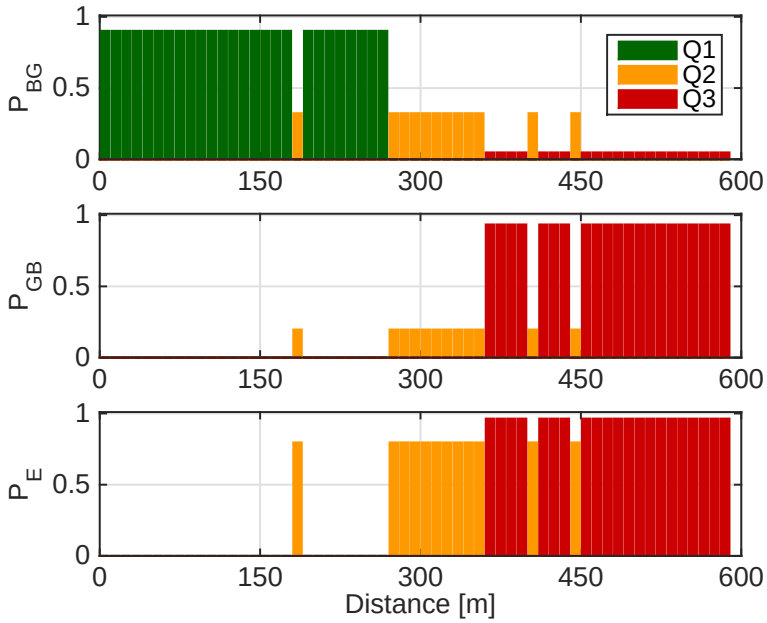

Figure 4.8: An example of the parameters of our range-dependent modified Gilbert model with 10 m granularity and $K = 3$ quantization levels. The unquantized counterpart is shown in Figure 4.5.

intervals for the model, parameters of which are quantized with $K = 3$, are slightly broader. Nevertheless, the agreement between the measured and the model-generated PDR samples is high, for both numbers of quantization levels. Therefore, we suggest to quantize the model parameters with $K = 3$ levels.

An example of the quantized parameters of our range-dependent modified Gilbert model with $K = 3$ quantization levels is shown in Figure 4.8. Here, different colors represent parameters corresponding to different quantization levels, which we associate with certain (communication) quality levels denoted by $Q_1, \ldots, Q_K$. The quality levels are arranged in descending order. Hence, the best communication quality is reproduced by the model with parameters of level Q_1 is and the worst with Q_K. To this end, we compute the average error probability $\bar{p}_e^{(k)}$ for each quantization level as follows:

$$\bar{p}_{e,k} = \frac{P_{GB,k}}{P_{GB,k} + P_{BG,k}} P_{E,k}, \qquad k = 1, \ldots, K, \tag{4.4}$$

where $P_{GB,k}, P_{BG,k}, P_{E,k}$ are the quantized model parameters corresponding to the kth quality level Q_k. The quantization levels are then enumerated such that $\bar{p}_{e,1} < \cdots < \bar{p}_{e,K}$.

A big benefit of the model parameters' quantization is the fact that it is no longer necessary to provide the set of model parameters $\boldsymbol{x}_n$ for each interval separately. It is sufficient to state the quality level for each of the N intervals. Then the respective parameters can be obtained from a lookup table, which only has $3K$ entries. Figure 4.9a shows an example of the quality levels for our range-dependent modified Gilbert model. The corresponding quantized

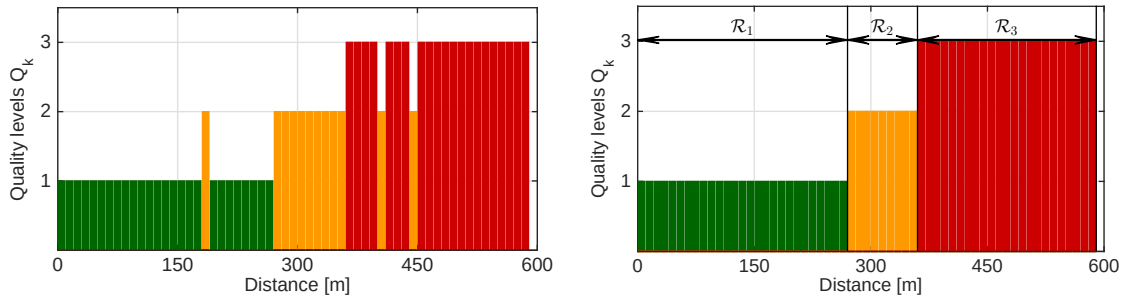

(a) Quality levels corresponding to the quantized model parameters presented in Figure 4.8.

(b) Quality levels after applying DP algorithm.

Figure 4.9: Quality levels: quantized and simplified-quantized representation.

parameters are depicted in Figure 4.8. The parameters corresponding to the best quality level Q_1 are located in the vicinity of the transmitter and the parameters corresponding to the poorest communication quality Q_3 are found on the edge of the coverage range. We also note that this representation of the model parameters allows us to set clear boundaries between different communication quality levels. Therefore, the whole communication range can be divided into three non-overlapping quality regions, each of which is determined by a single set of model parameters.

To optimally divide the communication range into respective quality regions we suggest to use a dynamic programming (DP) approach distantly related to the one presented in [67] and [117]. Assume that a vector $\boldsymbol{L} = [l_1, l_2, \ldots, l_N]$ contains the quality levels for N intervals of the range-dependent modified Gilbert model with quantized parameters, similar to the ones illustrated in Figure 4.9a. In this case, elements of the vector $\boldsymbol{L}$ take values $l_n \in \{1, \ldots, K\}$, where $n \in \{1, \ldots, N\}$ is the interval index. We aim at dividing the N intervals into K disjoint regions $\mathcal{R}_k$, such that the quality levels for all intervals combined into one region are the same, i.e.,$\forall\ n \in \mathcal{R}_k \Rightarrow\ l_n = k$. Each region $\mathcal{R}_k$ consists of adjacent interval indices, i.e.,$\mathcal{R}_1 = [1, 2, \ldots, r_1]$, $\mathcal{R}_2 = [r_1 + 1, \ldots, r_2]$, up to $\mathcal{R}_K = [r_{K-1} + 1, \ldots, N]$. We further note that each region $\mathcal{R}_k$ must have at least one element. Under this conditions it is sufficient to find the set of boundaries $r_1, r_2, \ldots r_{K-1}$. Algorithm 4.1 explains the DP approach consisting of three phases. First, the algorithm computes the squared errors

$$d_k^i = (l_i - k)^2, \qquad i = 1, \ldots, N, \quad k = 1, \ldots, K. \tag{4.5}$$

Based on the squared errors the partial distortions c_k^n (cf. Algorithm 4.1) for the first $K - 1$ regions are found. Next, the algorithm calculates the total distortion c_K and recursively finds the set of boundaries $r_1, r_2, \ldots r_{K-1}$ minimizing c_K. Example 1 illustrates the basic operation of this DP algorithm by means of a sequence $\boldsymbol{L}$ with $N = 5$ and $K = 3$.

Algorithm 4.1 *DP algorithm for finding optimal boundaries of quality regions.*

Input:

N - number of intervals

K - number of quality levels (regions)

$\boldsymbol{L} \leftarrow [l_1, l_2, \ldots, l_N]$ - quality levels for N intervals

Phase 1 - Compute partial distortion

for $k = 1$ to $K - 1$ **do**
  for $n = k$ to $N - (K - k)$ **do**
    if $k = 1$ **then**
      $c_1^n \leftarrow \frac{1}{n} \sum_{i=k}^{n} d_1^i$
    else
      for $j = 1$ to $n - 1$ **do**
        $\widetilde{c}_j \leftarrow \frac{1}{j} \sum_{i=n-j+1}^{n} d_k^i + c_{k-1}^{n-j}$
      end for
      $c_k^n \leftarrow \min(\widetilde{c}_1, \ldots, \widetilde{c}_{n-1})$
      $i_k^n \leftarrow \underset{j=1,\ldots,n-1}{\arg\min}\ \widetilde{c}_j$
    end if
  end for
end for

Phase 2 - Compute total distortion

for $j = K$ to N **do**
  $\widetilde{c}_j \leftarrow \frac{1}{N-j+1} \sum_{i=j}^{N} d_K^i + c_{K-1}^{j-1}$
end for
$c_K \leftarrow \min(\widetilde{c}_K, \ldots, \widetilde{c}_N)$
$i_K \leftarrow \underset{j=K,\ldots,N}{\arg\min}\ \widetilde{c}_j$

Phase 3 - Recursively find indicies $[r_1, r_2, \ldots, r_{K-1}]$ **corresponding to** c_K

$r_{K-1} \leftarrow i_K$
for $k = K - 2$ to 1 **do**
  $r_k \leftarrow i_{k+1}^{r_{k+1}}$
end for$r_{K-1} \leftarrow r_{K-1} - 1$

Output: Boundaries of the quality regions $[r_1, r_2, \ldots, r_{K-1}]$

Example 1. Assume that the range-dependent modified Gilbert model consists of $N = 5$ intervals. The corresponding parameters are quantized with $K = 3$ levels. The resulting vector of quality levels is $\boldsymbol{L} = [1, 1, 2, 3, 3]$. The optimal solution in this example can be inferred directly from $\boldsymbol{L}$. However, this is no longer the case for realistic data (cf. Figure 4.9a). We are interested to find the set boundaries $[r_1, r_2]$ that correspond to the optimal quality region assignment. According to Algorithm 4.1, we proceed as follows:

1. Set $k = 1$, hence $n = 1 : 3$ and calculate partial distortion for the first region
   $c_1^1 = d_1^1 = 0$
   $c_1^2 = \frac{1}{2}(d_1^1 + d_1^2) = 0$
   $c_1^3 = \frac{1}{3}(d_1^1 + d_1^2 + d_1^3) = \frac{1}{3}$

2. Set $k = 2$, hence $n = 2 : 4$ and calculate partial distortion for the second region
   n = 2: $\widetilde{c}_1 = d_2^2 + c_1^1 = 1$
   $c_2^2 = \widetilde{c}_1 = 1, \quad i_2^2 = 1$
   n = 3: $\widetilde{c}_1 = d_2^3 + c_1^2 = 0, \quad \widetilde{c}_2 = \frac{1}{2}(d_2^2 + d_2^3) + c_1^1 = \frac{1}{2}$
   $c_2^3 = \widetilde{c}_1 = 0, \quad i_2^3 = 1$
   n = 4: $\widetilde{c}_1 = d_2^4 + c_1^3 = \frac{4}{3}, \quad \widetilde{c}_2 = \frac{1}{2}(d_2^3 + d_2^4) + c_1^2 = \frac{1}{2}, \quad \widetilde{c}_3 = \frac{1}{3}(d_2^2 + d_2^3 + d_2^4) + c_1^1 = \frac{2}{3}$
   $c_2^4 = \widetilde{c}_2 = \frac{1}{2}, \quad i_2^4 = 2$

3. Set $k = 3$, hence $n = 3 : 5$ and calculate total distortion
   $\widetilde{c}_1 = \frac{1}{3}(d_3^3 + d_3^4 + d_3^5) + c_2^2 = \frac{4}{3}, \quad \widetilde{c}_2 = \frac{1}{2}(d_3^4 + d_3^5) + c_2^3 = 0, \quad \widetilde{c}_3 = d_3^5 + c_2^4 = \frac{1}{2}$
   $c_3 = \widetilde{c}_4 = 0, \quad i_3 = 4$

4. Perform traceback operation
   $r_2 = i_3 = 4$
   $r_1 = i_2^4 = 2$
   $r_2 = 4 - 1 = 3.$

Thus, the set of boundaries is given as $[r_1 = 2, r_2 = 3]$ and the corresponding quality regions are $\mathcal{R}_1 = [1, 2]$, $\mathcal{R}_2 = [3]$, $\mathcal{R}_3 = [4, 5]$.

Similar to the Viterbi algorithm, this recursion can be visualized using trellis diagram. Illustration of such diagram. Figure 4.10 depicts the trellis corresponding to the considered example. The red arrows indicate the optimal path. Here, we show all partial distortions c_k^n and the total distortion c_K. However, for conciseness and clarity we only point out $\widetilde{c}_1$ and $\widetilde{c}_2$ required for calculation of c_2^3, as an example.

Applying this DP approach to the quality level vector shown in Figure 4.9a we obtain the result presented in Figure 4.9b. The high quality communication region $\mathcal{R}_1$ includes the first 280 m between the transmitter and the receiver. It is followed by the intermediate quality region $\mathcal{R}_2$ that covers the subsequent 90 m of range. The range between 370 m and 600 m is characterized as unreliable quality region $\mathcal{R}_3$.

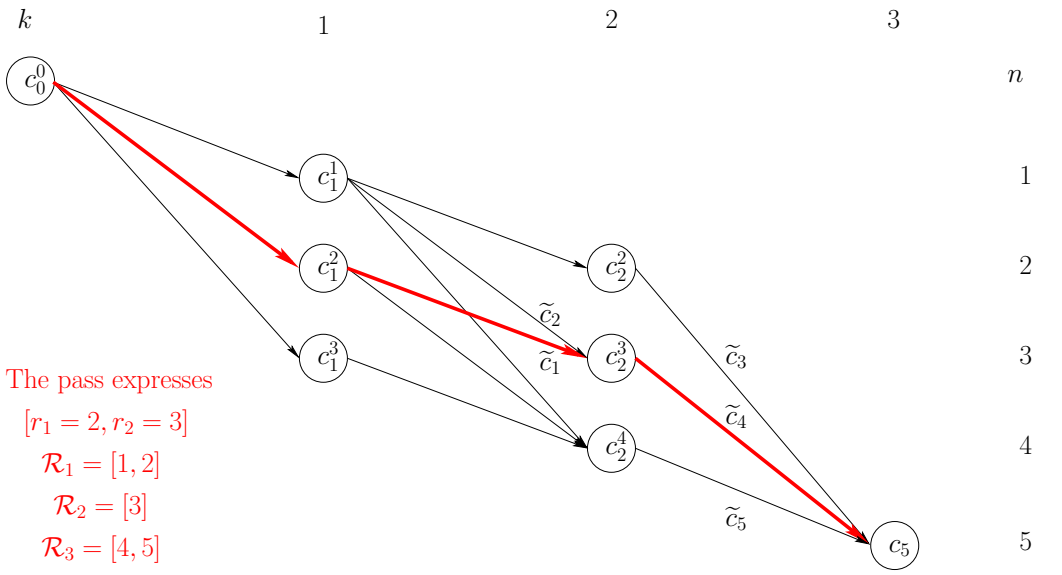

Figure 4.10: Trellis-type illustration showing the relations in DP algorithm for finding the optimal boundaries between the quality regions for $N = 5$ and $K = 3$.

Finally, we note that the discontinuities of the quality regions in Figure 4.9a at distances 185 m, 405 m and 445 m, where parameters change from Q_1 and Q_3 to Q_2 for the duration of one interval, are called forth by street intersections. We therefore conclude that the proposed VQ algorithm does not only reduce the complexity of the range-dependent modified Gilbert model, but also enables localization, and successive characterization of realistic environmental impairments in terms of model parameters. The aspects of such environment-aware modeling will be discussed in more detail in Section 4.4.

4.3 Signal-to-Noise Ratio Model

In this section, we introduce an extension of the range-dependent modified Gilbert model. With this extension the model can produce SNR patterns correlated with the packet-error patterns. To enable thiss extension, we need to know how likely certain SNR values are in either state of the model. Although this information is hidden initially, we can infer it from the measurement data. To this end, the most likely sequence of states is recursively determined using the Viterbi algorithm, once the model parameters are known. This reveals the connection between the model states and the detection events. Therefore, we can associate each measured SNR value with one of the states. Figure 4.11 shows an example for the mapping between the measured SNRs and the states for each quality level. Here individual measured SNR values are indicated by cross markers and the solid lines show the median SNR trend, computed based on the SNR values within one interval.

The advantage of our state-dependent SNR modeling becomes obvious when comparing SNR in the good state (cf. Figure 4.11a) and in the bad state (cf. Figure 4.11b). The median

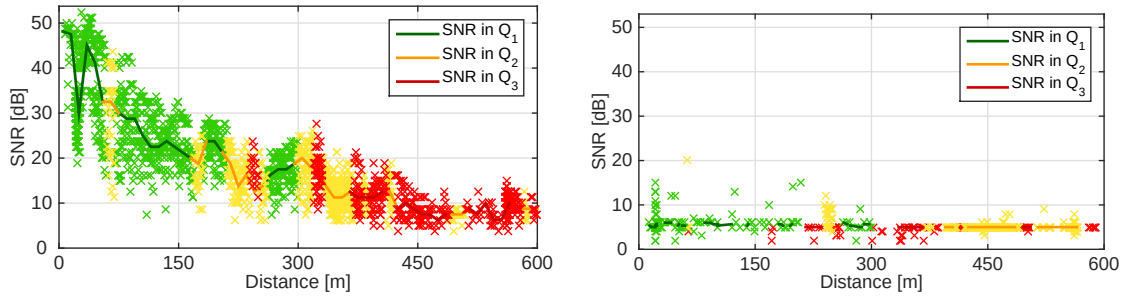

(a) SNR in good state.

(b) SNR in bad state.

Figure 4.11: Measured SNR values in good and bad states vs. distance. The solid lines show the median SNRs. Colors represent different link quality levels.

SNR in the bad state is almost constant over the considered distances and the dependence on the quality level is negligible. However, in the good state the SNR varies significantly over the distance and its dependence on the quality level is well pronounced. The largest SNR is achieved in quality level $Q1$ and the SNR of quality level Q_3 is significantly smaller than in the other two levels.

To model the variations of the SNR as a function of the transmitter-receiver distance, a combination of path loss, shadowing, and small scale fading is frequently used. Path loss results from dissipation of the power radiated by the transmitter, as well as the propagation channel effects. Shadowing is caused by obstacles between the transmitter and receiver, which attenuates signal power through absorption, reflection, scattering, and diffraction. The variations due to combination of path loss and shadowing are also known as large scale fading (as they occur over large distances, relative to the wavelength). The median SNR in Figure 4.11 can therefore be interpreted as large scale fading. The deviation of the measured SNR values from the median can be viewed as small scale fading. The small scale fading occurs due to constructive and destructive superposition of multipath signal components. The relation between large and small scale fading is schematically shown in Figure 4.12. We suggest to adopt this approach based on combination of large and small scale fading to reproduce the measured SNR performance with the range-dependent modified Gilbert model.

The measured SNR is defined as follows:

$$\mathrm{SNR} = P_{TX} - P_N - L_P - L_S, \tag{4.6}$$

where P_{TX} is the transmit power, L_P is the propagation loss, and L_S is the system loss. All quantities in (4.6) are on a logarithmic scale. The system loss incorporates the cable losses, the gain of transmit and receive antennas, as well as any losses due to imperfections of the receiver hardware implementation. Due to limited knowledge about the detailed receiver processing, a precise derivation of the system loss is hardly possible for most of performance measurements. But since we develop a model that incorporates the effects of both, the channel and the standard compliant transceiver chain, we do not require precise knowledge

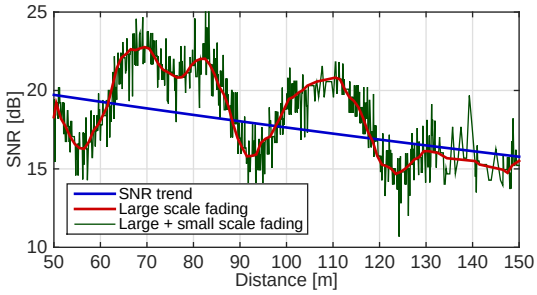

Figure 4.12: Visualization of the individual contributions to the SNR model: SNR trend, large scale fading, and small scale fading.

of the system loss. Instead, we focus on reproducing the joint effect of the propagation and the system losses, which we refer to as *transceiver chain loss* hereafter. By subtracting the transceiver chain loss and the noise from the transmit power, we obtain the distance-dependent SNR trend (without the effects of shadowing and small scale fading). The SNR trend is depicted by the blue line in Figure 4.12.

To model the SNR trend, we fit the measured SNR values of the kth link quality level to an exponential function of the form

$$\overline{\mathsf{SNR}}_k = \alpha_k \cdot e^{\beta_k \cdot d}, \quad k = 1, 2, \ldots, K, \tag{4.7}$$

where d is the transmitter-receiver distance in meters and SNR is in dB. The fit is performed separately for both states. Regardless of the measurement parameters and environment, the SNR trend in the bad state is constant over the distance for all quality levels and amounts to approximately 5 dB. Therefore, in the bad state $\alpha_k = 5$ and $\beta_k = 0,\ k = 1, 2, \ldots, K$. For the good state, the SNR trend depends on the quality level.

To complete the large scale fading model, we next suggest a way of reproducing the shadowing effects. On the linear scale the shadowing is commonly modeled by a log-normal distribution of the received signal power. This corresponds to a normally distributed random variable on the logarithmic scale. In order to create a correlated Gaussian random process, we use a general autoregressive (AR) modeling approach. The correlation is essentially introduced by shaping the spectrum of a white input process with a linear filter. The advantage of using the AR approach is twofold, it exhibits excellent correlation matching and is computationally inexpensive.

An AR process of order p can be generated via the following difference equation:

$$y_k[n] = -\sum_{i=1}^{p} \gamma_{i,k} y[n-i] + w[n]. \tag{4.8}$$

Here, $w[n] \sim \mathcal{N}(0, \sigma_k^2)$ is the uncorrelated filter input signal and $y[n]$ is the signal obtained at the output of the filter. The AR model for the kth quality level consists of the set of filter coefficients $\{\gamma_{i,k}\}_{i=1}^{p}$ and the variance σ_k^2.

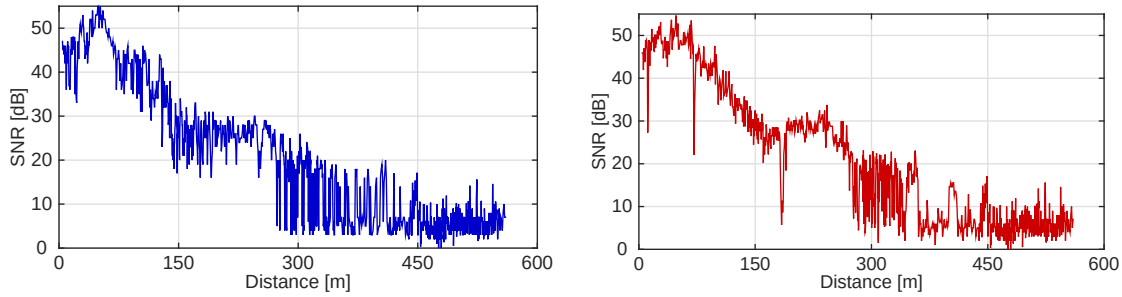

(a) Measured SNR sample.

(b) Model-generated SNR sample

Figure 4.13: Measured SNR values in good and bad states vs. distance. The solid lines show the median SNRs. Colors represent different link quality levels.

In order to estimate the AR filter coefficients for each of the N intervals, we first subtract the general SNR trend from the median SNR. Next, the autocorrelation function of the resulting deviations from the general SNR trend is computed. Finally, the AR filter coefficients are determined by solving the set of p Yule-Walker equations. These equations are guaranteed to have a unique solution and can be solved efficiently by the Burg algorithm [23]. Comparing the performance achievable for $1 \leq p \leq 10$, we found out that the AR filter of order 1 (denoted as AR(1)) should be used, since larger filter orders did not yield significant improvements.

Thus, to model the large scale fading component ($\mathrm{LSF}^{Q_k}_{\mathrm{STATE}}$) we proceed as follows:

- generate normally distributed random variables with the specified variance σ_k^2,
- introduce correlation by shaping the spectrum of these random variables by the AR(1) filter with parameter $\gamma_{1,k}$,
- add the resulting correlated process to the general SNR trend.

An example of the large scale fading generated in this way is depicted by the red curve in Figure 4.12.

We note, that the deviations from the SNR trend in the bad state for all quality levels is negligible (cf. Figure 4.11b). Therefore, the shadowing effects are only modeled in the good state and the large scale fading in the bad state is given as $\mathrm{LSF}^{Q_k}_{\mathrm{BAD}} = \mathrm{LSF}^{Q}_{\mathrm{BAD}} = 5\,\mathrm{dB}$, $k = 1, 2, \ldots, K$.

To model the small scale fading, we compute the deviation of measured SNR from the median SNR for each interval. The distribution of this deviation is closely approximated by a clipped Laplace distribution. Thus, the probability density function of the small scale fading value η is as follows:

$$p(\eta) = \frac{1}{2c\delta} e^{-|\eta|/\delta}, \quad \eta \in \{-\eta_{\max}, \eta_{\max}\}, \tag{4.9}$$

here the normalization factor c is given by

$$c = \int_{-\eta_{\max}}^{\eta_{\max}} \frac{1}{2\delta} e^{-|\eta|/\delta} \mathrm{d}\eta, \tag{4.10}$$

and the values for $\eta_{\max}$ and δ are specified based on the measured SNR. The details of the proposed modeling approach are summarized in Algorithm 4.2.

Algorithm 4.2 *Generation of packet-error patterns with corresponding SNR sequences.*

Input:
N - number of intervals
K - number of quality levels
P - number of error pattern digits per interval

Phase 1 - Large scale fading generation

if STATE = BAD **then**
  $\mathrm{LSF}^{Q}_{\mathrm{BAD}}(1:N) \leftarrow 5\,\mathrm{dB}$
else
  for $k = 1$ to K **do**
    $\mathrm{LSF}^{Q_k}_{\mathrm{GOOD}}(1:N) \leftarrow \overline{\mathsf{SNR}}_k(1:N) + y_k(1:N)$
  end for
end if

Phase 2 - Error pattern and SNR generation

for $n = 1$ to N **do**
  find quality level Q_k of interval n
  generate length-P error pattern using parameters Q_k
  STATE $\leftarrow$ resulting sequence of states
  for $p = 1$ to P **do**
    $\eta \leftarrow$ generate small scale fading realization
    if STATE(p) = GOOD **then**
      $\mathrm{SNR}(p) \leftarrow \mathrm{LSF}^{Q_k}_{\mathrm{GOOD}}(n) + \eta$
    else
      $\mathrm{SNR}(p) \leftarrow \mathrm{LSF}^{Q}_{\mathrm{BAD}}(n) + \eta$
    end if
  end for
end for

Figure 4.13 illustrates the performance of the proposed modeling approach. In particular, Figure 4.13a shows a randomly selected measured SNR pattern. The SNR pattern shown in Figure 4.13b is model-generated. We obtain a very good agreement between both SNR curves, which validates the accuracy of the proposed modeling approach.

4.4 Environment-Aware Model

In this section, we suggest an algorithm for the generation of realistic packet-error and SNR patterns by taking into account effects of the environment on the radio propagation. To parameterize the model we use real-world measurements performed in the city of Bologna, Italy. The measurements are acquired in the framework of iTETRIS project are given in Section 3.1.3. For this measurement campaign, 22 RSU locations were carefully selected. We analyzed the surrounding area of all RSU locations using Google Earth [4]. The Google Earth road information is generated and validated by means of satellite imagery and GPS traces. The resulting maps are commonly regarded as the highest-quality road data publicly available

today. Based on our observations, the city center of Bologna is sufficiently well represented by the following four types of street surroundings, hereafter referred to as layouts. The layouts are as follows:

Layout 1 - street surrounded by buildings from both sides.

Layout 2 - street surrounded by buildings from one side and by vegetation from the other side.

Layout 3 - street surrounded by vegetation from both sides.

Layout 4 - open area street.

The street layouts are schematically illustrated in Figure 4.14. All identified layouts are applicable to both one-way and two-way streets, with two or three lanes in each direction.

Layout 1 is schematically represented in Figure 4.14a. The type and the exterior material of the surrounding buildings are not considered in our simple model. The only constraint is the height of the buildings, which is confined by the hight of the RSU antenna. Therefore, the buildings in the considered layout should be at least 6.5 m in height.

Layout 2 comprises two different settings. The first setting is very similar to the one shown in Figure 4.14a, however the buildings on one side of the street are replaced by vegetation. The second setting is schematically illustrated in Figure 4.14b. In this case, a two-way street is surrounded by the buildings from both sides and the driving directions are separated by a median stripe covered with vegetation. For the sake of simplicity, the density and the type of vegetation are not covered by our model. However, the sam height constraint as for layout 1, applies here as well. Therefore, the height of both the buildings and the vegetation should be ≥ 6.5 m.

Figure 4.14c shows a schematical representation of layout 3, in which the street is surrounded by vegetation from both sides. Similarly to the layout 2, vegetation on one of the street sides can alternatively be introduced by the median stripe. The density and type of vegetation is not considered and the height of the vegetation should be ≥ 6.5 m.

In contrast to the other layouts, layout 4 is less likely to occur in the city center and is frequently found in outlying suburbs. In this case, there are neither tall buildings, nor dense vegetation on the street sides. Instead, the street might be surrounded by agricultural field, lawn, parking area, playing grounds, industrial construction sites, etc. An example of this layout is schematically illustrated in Figure 4.14d. Street layout 4 is also applicable for settings with sparse vegetation and buildings, as well as noise barriers or construction walls of height < 6.5 m.

Parametrizing the range-dependent modified Gilbert model by measurements taken at locations with similar street layouts and successive parameter quantization with Algorithm presented in Section 4.2, yieldclosely related parameters. In contrast, the model parameters obtained from measurements performed in dissimilar layouts differ significantly. We conclude that for V2I measurements in urban environments, the performance is strongly influenced by the street layout.

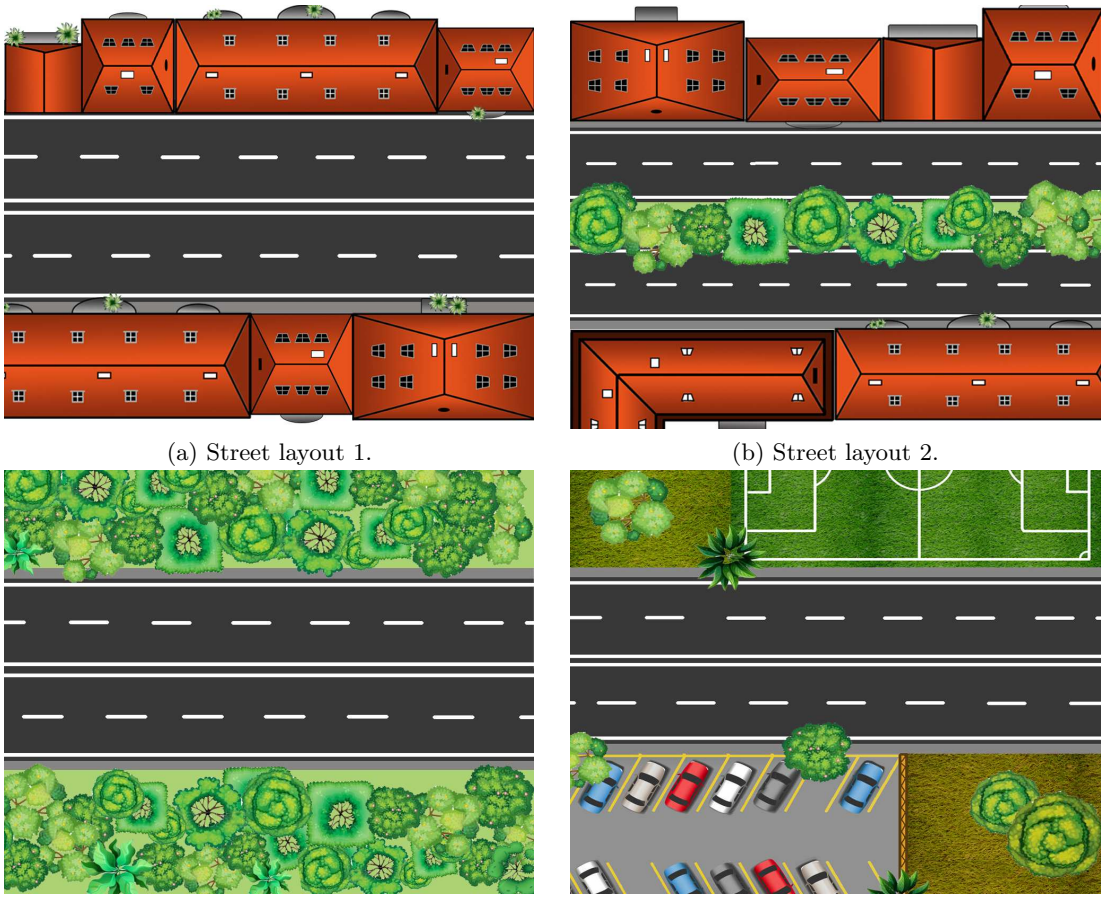

(a) Street layout 1.

(b) Street layout 2.

(c) Street layout 3.

(d) Street layout 4.

Figure 4.14: Schematic illustration of urban street layout types.

Analyzing the quantized model parameters for different measurement locations, we notice that certain street topology-related aspects have significant influence on the communication quality, regardless of the considered layout. Our extensive study of the model parameters, influenced by various street topologies shows that there are four main types of urban impairments that affect the communication quality. These impairments, schematically represented in Figure 4.15, include street intersections, interruptions in the median stripe, roundabouts, and road curvatures.

An example of a street intersection is shown in Figure 4.15a. This type of impairment occurs when two or more roads either meet, or cross each other. The influence of a street intersection on communication quality, depends on the distance relative to the RSU. For instance, an intersection in the close vicinity of the transmitter reduces the communication performance. Therefore the parameters within the quality region $\mathcal{R}_1$ are changed to level Q_2. However, if an intersection occurs within the region $\mathcal{R}_3$, the communication quality is improved and consequently the parameters are replaced by Q_2. The presence of a street intersection within the quality region $\mathcal{R}_2$ does not have an effect on the model parameters. The duration, for which the model parameters are interchanged is defined by the largest

dimension of the impairment in the driving direction. In most cases the parameters are changed for $3-5$ consecutive model intervals, which translates to $30-50\,\mathrm{m}$ wide intersection.

An interruption in the median strip, schematically shown in Figure 4.15b, has an effect on the communication quality that is similar to intersect. However, this type of impairment is only applicable to layout 2 and occurs most frequently in connection with an intersection or a u-turn. In this case, the model parameters of the level Q_2 are used within the quality regions $\mathcal{R}_1$ and $\mathcal{R}_3$ for the duration of the impairment. The parameters within the region $\mathcal{R}_2$ remain unchanged. The overall impact of an interruption in the median stripe is slightly less noticeable compared to a street intersection. This is due to shorter duration of this impairment, resulting in parameter change for $1-3$ consecutive model intervals only.

A further intersection-like impairment is a roundabout, illustrated in Figure 4.15c. This impairment usually yields a loss of line-of-sight (LOS) connection to the transmitter. Therefore, the quality of communication is significantly degraded while the vehicle is in the roundabout. The range-dependent modified Gilbert model accounts for this impairment by changing the parameters to quality level Q_3 within the high and intermediate quality regions $\mathcal{R}_1$ and $\mathcal{R}_2$. While the parameters within the region $\mathcal{R}_3$ are not affected by a roundabout. In most cases, this impairment results in a change of model parameters for $5-8$ consecutive intervals and therefore the impact of a roundabout on the V2I performance is fairly large.

For the aforementioned impairments, we assume that the vehicle continues driving in the same direction as before. In some cases however, the street topology is such, that the vehicle changes its heading without an intention to turn or leave the street. We refer to such street topology, in which the heading is changed by $\geq 20°$, as a curvature. The measurement results indicate that a curvature leads to significant deterioration of the communication quality and eventually to a connection breakdown about 100 m after it starts. To model this impairment, the model parameters are changed to Q_3 starting at the start of a curvature and the coverage range is terminated after additional 100 m. This impairment can also be used to model the case when the vehicle leaves the road on which the RSU is located.

To accurately reproduce the effect of urban impairments, the model parameters should be changed to the respective quality level 5 m ahead the start of the impairment and last 5 m after the impairment ends.

We next give an example in which the quality levels (Q_1, Q_2, Q_3) are used as building blocks to setup an environment-aware model. Let us assume that we model V2I communication along a street with layout 1 (cf. Figure 4.14a). First, we use the quality region parameters to get the coarse model shown in Figure 4.16a. Next, we refine the model to account for propagation impairments by adjusting the model parameters where necessary. In our example, there is a 30 m wide intersection starting 185 m away from the transmitter. Therefore, we change the parameters to Q_2 in the range $180-220\,\mathrm{m}$. Furthermore, a roundabout of 50 m diameter starts 295 m away from the transmitter. We thus change the parameters from Q_2 to Q_3 in the range $290-350\,\mathrm{m}$. Finally, the street along which the vehicle is driving is curved starting 420 m after the position of the RSU. Since the street curvature occurs in the unreli-

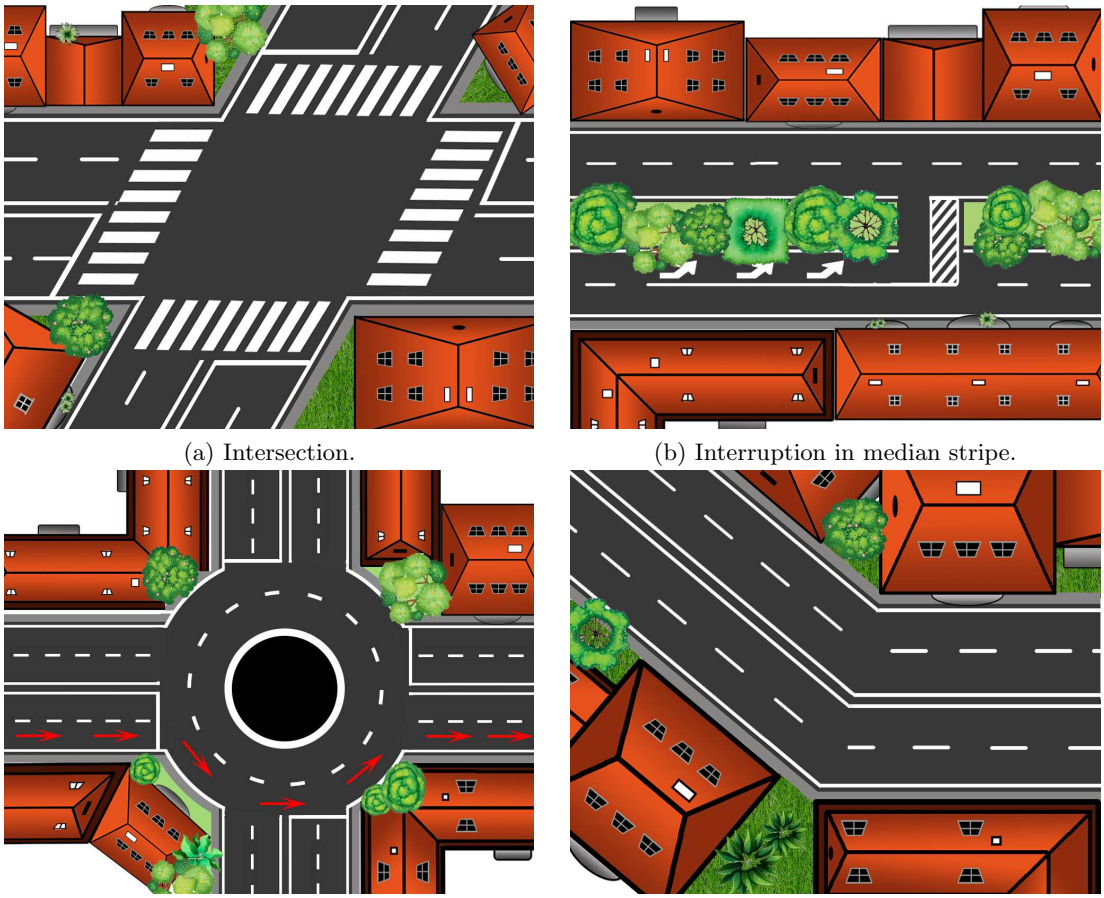

(a) Intersection.

(b) Interruption in median stripe.

(c) Roundabout.

(d) Curvature.

Figure 4.15: Schematic illustration of urban impairments.

able communication range, the parameters remain unchanged. However, the communication range is terminated within 100 m and thus the packet reception ends at 520 m. The resulting model parameters, taking into account the propagation impairments, are shown in Figure 4.16b. As soon as the model parameters capturing the street layout and impairments are fixed, packet-error and SNR patterns can be generated using the range-dependent modified Gilbert model.

4.5 Model Validation and Results

In this section we provide the model parameters for the identified urban street layouts and evaluate the performance of the proposed modeling approach. We start with the packet-error model and subsequently evaluate the performance of the SNR-enabled model.

The proposed model is clearly most useful if the set of parameters, extracted from a particular measurement, can be used to describe the link performance for other locations with similar street layouts. To show that this is indeed the case, we first introduce the notion of primary and secondary measurements. The primary measurement is used for the model

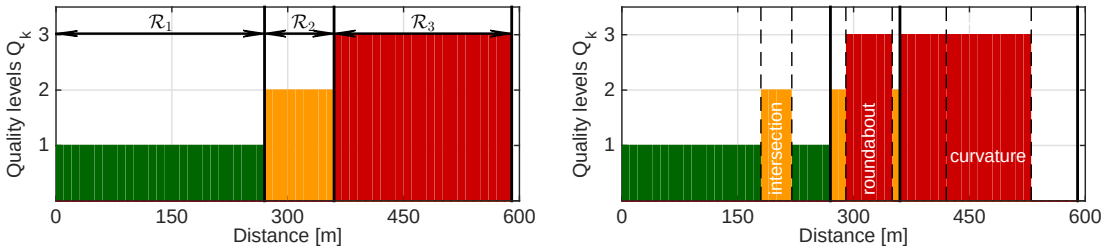

(a) Model parameters divided in non-overlapping quality ranges.

(b) Model parameters divided in quality ranges with realistic environmental impairments.

Figure 4.16: Parameters of simplified model with $K = 3$ quality ranges.

parameter estimation. The estimated parameters are then used to model the communication performance of the secondary measurement, carried out at a different site. By comparing the model output to the secondary measurement, we quantify how representative our model is for scenarios with similar street layouts. We note that the type and position of impairments do need not be the same for primary and secondary measurements.

For each of the four environments we have chosen two RSU locations, one as the primary and the other as the secondary measurement. The exact positions of the chosen RSUs are given in Table 3.7 and the corresponding environments are shown in Figure 3.6. We selected the measurement locations based on the following two criteria: (i) the street layout should remain the same within the coverage range of the RSU and (ii) sthe econdary measurements should the influence of all impairment types.

The parameters of the range-dependent modified Gilbert model with quantized parameters, hereafter referred to as the quantized model, are summarized in Table 4.1. From the model parameters it follows that the range of V2I communication in urban environments significantly depends on the street layout. In the street layouts 1 and 2, the communication terminates 480 m after the RSU. For the layouts 3 and 4, the communication can be sustained for additional 150 m. It is interesting to note that all three communication ranges are present only for layout 1. For the other layouts there are only two regions and the remaining quality level is only used to model impairments. As expected, parameters leading to the best performance correspond to layout 4, e.g., open area with less to none environment-induced propagation limiting factors. In this case, the best communication quality region $\mathcal{R}_1$ including the first 550 m between transmitter and receiver. The performance in the subsequent 80 m is resembled by the model with parameters Q_3. Slightly worse is the performance on streets with layout 3. Here, the parameters of quality level Q_1 are used in the region $0-400$ m and of the level Q_2 for the subsequent 230 m. The performance achievable on streets with the layout 1 and 2 is nearly the same, although the quality region $\mathcal{R}_1$ of the layout 2 is 60 m larger. This performance advance is however compensated by the absence of the quality region $\mathcal{R}_2$ and 30 m earlier start of the region $\mathcal{R}_3$.

We next evaluate the performance of the proposed packet-error modeling approach based on a set of similarity criteria. The similarity criteria include three distance-dependent mea-

Table 4.1: Parameters of the simplified range-dependent modified Gilbert model for urban environments.

Parameter \ Quality	Q_1	Q_2	Q_3
Street layout 1			
Quality region [m]	0 - 270	271 - 360	361 - 480
P_{BG}	0.89	0.40	0.07
P_{GB}	0.01	0.23	0.97
P_E	0.01	0.88	0.97
Street layout 2			
Quality region [m]	0 - 330	Impairments only	331 - 480
P_{BG}	0.88	0.88	0.16
P_{GB}	0.01	0.19	0.47
P_E	0.01	0.96	0.80
Street layout 3			
Quality region [m]	0 - 400	401-630	Impairments only
P_{BG}	0.92	0.88	0.05
P_{GB}	0.01	0.19	0.98
P_E	0.01	0.83	0.94
Street layout 4			
Quality region [m]	0 - 550	Impairments only	551 - 630
P_{BG}	0.90	0.86	0.07
P_{GB}	0.02	0.11	0.95
P_E	0.01	0.99	0.85

sures and one descriptive statistical measure. As distance-dependent measures KLD, MSE, and complementary collinearity are used. The percentage of erroneous packets is chosen as descriptive statistical measure. These measures are introduced and defined in Section 2.3.4. In what follows we evaluate the performance of three modeling approaches:

- The **original model** proposed in Section 4.1. In this case, we used the secondary measurement to parametrize the range-dependent modified Gilbert model with granularity 10 m.
- The **quantized model** discussed in Section 4.2. In this case, we used the parameters of the original model that were quantized with 3 quantization levels.
- The environment-aware modeling approach suggested in Section 4.4 that we will refer

to as **prediction**. We decide to call the results of the environment-aware model a prediction, since the model parametrization is based on the primary measurement and packet-error pattern generation for the secondary measurements is based solely on the layout and position of the impairments.

To evaluate the accuracy of the aforementioned modeling approaches we compute the measured reference based on M repetitions of the secondary measurement, as suggested in Section 4.2. The number of measurement repetition is $6 \leq M \leq 10$, which is sufficient to build a representative statistic of the measured performance. The reference values of the distance-dependent measures serve as an upper bound in our evaluation that should not be exceeded by an accurate model. Moreover, the deviation from the measured percentage of erroneous packets should be as small as possible. Table 4.2 summarizes the resulting reference values together with the model performance for the street layouts identified in Section 4.4.

From Table 4.2 it follows that all three modeling approaches satisfy the accuracy criteria, regardless of the street layout. The original model outperforms the quantized and the environment-aware models at the cost of larger model dimension. Surprisingly, the accuracy of the environment-aware model is almost as good as that of the quantized model, although it does not require measurements at the secondary location to model the communication performance. In the following, we state more precisely the relation between accuracy achieved by the model and the measured reference. We therefor take the reference values of the distance-dependent measures as 100 % of the allowed dissimilarity. The difference between the percentage of erroneous packets in measured and model-generated traces will be denoted as deviation from the reference.

In particular, for layout 1 the KLD, MSE and complementary collinearity of the original model are 13 %, 50 %, and 45 % of the measured reference, respectively. The KLD of the environment-aware model is more than doubled compared to the original model. Nevertheless, it is well below the upper bound and amounts to 30 % of the reference. The MSE and the complementary collinearity of the environment-aware model are 65 % and 80 % of the reference, respectively. The performance of the quantized model in terms of distance-dependent measures is only slightly better than that of the environment-aware model. However, the quantized model reproduces the percentage of erroneous packets the best, leading to deviation from the measured reference value by 0.5 %. The original model underestimates the percentage of erroneous packets by 1.3 % and the environment-aware model overestimates it by 1.2 %.

Similarly, for layout 2 the best performance is achieved with the original model. Particularly, the KLD is by 80 % below the upper bound, the MSE is nearly the half of the measured reference, and the complementary collinearity amounts to 74 % of the reference value. The KLD, MSE and complementary collinearity of the environment-aware model are 70 %, 96 %, and 83 % of the measured reference, respectively. The performance of the quantized model in terms of the distance-dependent measures is well in-between the other two approaches. In terms of the percentage of erroneous packets the best match is surprisingly achieved with the

Table 4.2: Performance evaluation of the range-dependent modified Gilbert model (original model), the range-dependent modified Gilbert model with quantized parameters (quantized model), and the environment-aware model (prediction).

Street layout 1				
	Measured reference	**Original model**	**Quantized model**	**Prediction**
$\mathbf{D}_{\mathrm{KL}}$	243.73	32.54	54.2	71.41
MSE	0.062	0.031	0.04	0.041
$\mathbf{1}-\gamma$	0.031	0.014	0.016	0.025
$\hat{\mathbf{P}}_{\mathbf{e}}$ [%]	12.7	11.4	13.2	13.9
Street layout 2				
$\mathbf{D}_{\mathrm{KL}}$	122.93	19.65	44.69	69.28
MSE	0.057	0.031	0.051	0.055
$\mathbf{1}-\gamma$	0.077	0.057	0.06	0.064
$\hat{\mathbf{P}}_{\mathbf{e}}$ [%]	19.4	17	18	19.9
Street layout 3				
$\mathbf{D}_{\mathrm{KL}}$	113.21	39.93	84.62	72.02
MSE	0.052	0.015	0.042	0.038
$\mathbf{1}-\gamma$	0.019	0.017	0.02	0.019
$\hat{\mathbf{P}}_{\mathbf{e}}$ [%]	24.4	24.8	22.5	23.6
Street layout 4				
$\mathbf{D}_{\mathrm{KL}}$	47.45	18.21	26.61	28.77
MSE	0.03	0.006	0.009	0.01
$\mathbf{1}-\gamma$	0.02	0.001	0.003	0.004
$\hat{\mathbf{P}}_{\mathbf{e}}$ [%]	43.3	43.8	43.5	39.1

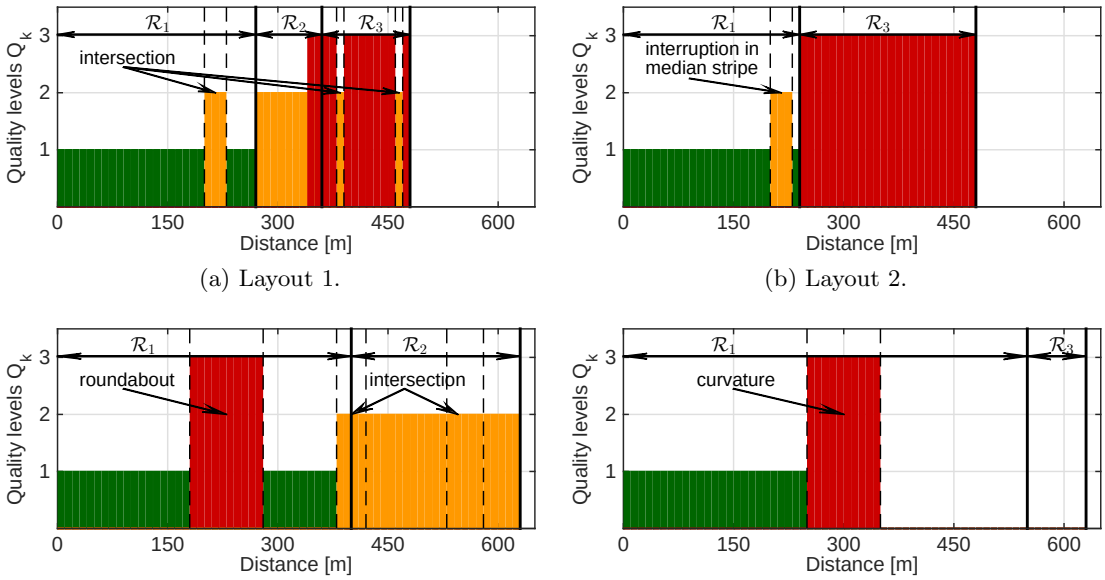

(a) Layout 1. (b) Layout 2.

(c) Layout 3. (d) Layout 4.

Figure 4.17: Parameters of the environment-aware model for the secondary measurements of different street layouts.

environment-aware model, for which the deviation from the measured reference is only 0.5 %. The original and the quantized models underestimate the percentage of erroneous packets by 2.4 % and 1.4 %, respectively.

Surprisingly, for layout 3 the environment-aware model outperforms the quantized model with respect to all similarity criteria. More specifically, the KLD is 65 % and 75 % related to the reference values for the environment-aware model and the quantized model, respectively. The same relationship is given in terms of the MSE, which is on average 70 % of the reference for the prediction and 80 % for the quantized model. The complementary collinearity of the environment-aware model is the same as the measured reference. The complementary collinearity of the quantized model exceeds the reference value by 5 %. The deviation of the percentage of erroneous packets is 1.2 % for the prediction and 1.9 % for the quantized model. The best performance is still achieved with the original model.

Finally, for street layout 4 the performance of the quantized model and the environment-aware model, in terms of the distance-dependent measures, is nearly the same. In particular the KLD, MSE, and complementary collinearity of this models amount to 60 %, 30 %, and 15 % of the measured reference, respectively. The performance of the original model in this respect is better. The KLD is 40 %, the MSE is 20 %, and the complementary collinearity is 5 % of the measured reference. With respect to the percentage of erroneous packets, the quantized model achieves the best performance with a deviation of only 0.2 %. A slightly larger deviation from the reference is achieved by the original model. The environment-aware model underestimates the percentage of erroneous packets by 4.2 %.

Comparing the measured reference value of $\hat{P}_e$ for different street layouts, we notice that the largest amount of packet-errors was obtained for street layout 4. This is in contrast to

our expectations based on the model parameters given in Table 4.1. As mentioned earlier, we expected to achieve the best communication performance for layout 4 and slightly worse performance for layout 3. The reason for this discrepancy is the non-uniform distribution of the impairments among the secondary measurements of different layouts, detailed in Figure 4.17. The parameters used to predict performance of the secondary measurements with layout 4, indicate the presence of a road curvature starting 250 m after the RSU (cf. Figure 4.17a). Therefore, the model parameters are changed to quality level Q_3 and communication is terminated after 100 m. This particularly implies that the total communication range is reduced by 280 m. Even more importantly, the high quality region $\mathcal{R}_1$ is shortened from 550 m to 250 m, as compared to the idealized settings without impairments (cf. Table 4.1). The parameters used to predict the performance of the secondary measurement with street layout 3 are shown in Figure 4.17c. They indicate two intersections, located within the quality region $\mathcal{R}_2$ and a roundabout located within the region $\mathcal{R}_1$. The intersections do not have any influence on the performance in this case. However, the roundabout leading to partial loss of the LOS considerably reduces the communication performance. In contrast, the secondary measurements of street layouts 1 (cf. Figure 4.17a) and 2 (cf. Figure 4.17b) comprise only intersections and interruption in the median stripe. These impairments have a less pronounced influence on the communication quality. This explains larger amount of lost packets in the secondary measurements of layouts 3 and 4, compared to layouts 1 and 2.

Figure 4.18 shows the performance of the proposed modeling approaches for different street layouts. A randomly chosen repetition of the secondary measurements is shown using a black solid line. The dashed lines indicate the performance of different models. For each layout the top plot illustrates the performance of the original model, the middle plot shows the performance of the quantized model, and the button plot depicts the environment-aware model's result. The red colored bands represent the empirical intervals containing 95 % of all 10^4 model realizations. Comparing the PDR curves with the model parameters illustrated in Figure 4.17, we can clearly spot the effects of particular impairments. We note that the PDR curves originating from the packet-error traces generated by the original model are almost identical to the measured counterparts. Moreover, the empirical confidence intervals in this case are fairly tight. The quantized model is only imperceptibly less accurate. In the case of the environment-aware model, the agreement between the model-generated result and the measurements is good as well. However, the 95 % bounds are wider, which points to a higher uncertainty of the result compared to the original model. Nevertheless, the prediction made by the environment-aware model on the basis of the street layout and impairments highly accurate.

Next, we evaluate the importance of the street layout for the accuracy of the environment-aware model. To this end, we compare the PDR performance of the environment-aware model with parameters estimated based on the primary measurements with the same (matching) street layout and with three different (mismatching) layouts. Recall that the parameters for all layouts are given in Table 4.1. Note that we use theoriginal assignment of the quality

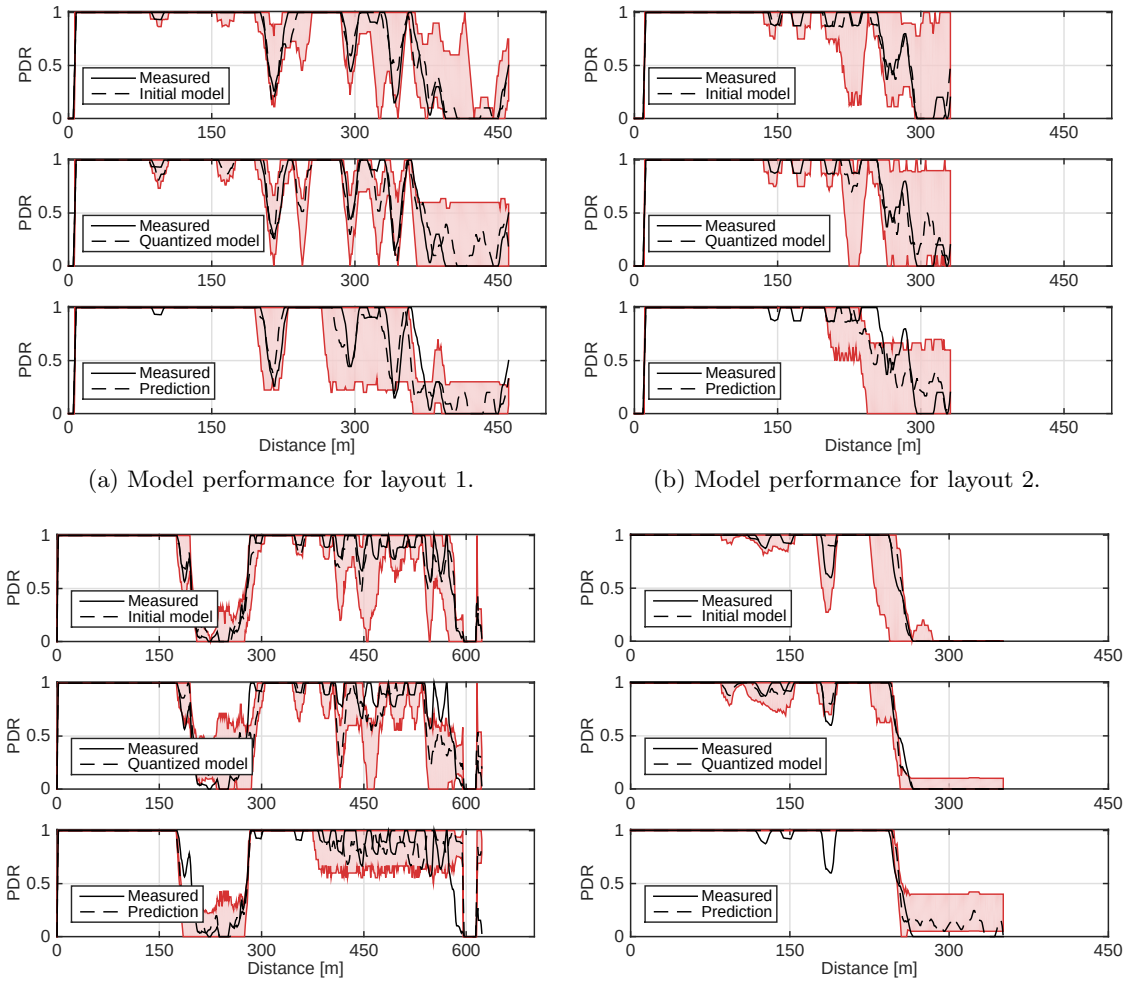

(a) Model performance for layout 1.

(b) Model performance for layout 2.

(c) Model performance for layout 3.

(d) Model performance for layout 4.

Figure 4.18: Performance comparison of different modeling approaches for the defined street layouts. The plots from top to bottom illustrates performance of the original, the quantized, and the environment-aware model, respectively. Solid black lines represent measurement repetition and dashed black lines show a realization of respective model, both chosen at random. Colored bands show empirical intervals containing 95 % of all model realizations.

ranges, as well as the position and type of the impairments. We only change the transition and emission probabilities (P_{BG}, P_{GB} and P_E). We denote the performance achieved by the environment-aware model with mismatching parameters as prediction for layout s, where $s \in \{1, 2, 3, 4\}$ denotes the street layout. The performance of the environment-aware model with parameters estimated based on the primary measurement with matching layout is denoted as prediction.

The performance achieved by the environment-aware model with matching and mismatching parameters is summarized in Table 4.5. All four measures indicate that the street layout has a significant influence on the communication performance and, consequently, on the model parameters. Regardless of the street layout, the agreement with the measurements is significantly higher when matching parameters are used. Moreover, when parameters of a

Table 4.3: Performance evaluation of the environment-aware model with parameters estimated for mismatched street layouts.

Street layout 1				
	Prediction	**Prediction for layout 2**	**Prediction for layout 3**	**Prediction for layout 4**
$\mathbf{D}_{\mathrm{KL}}$	71.41	88.41	88.11	93.39
MSE	0.041	0.044	0.058	0.042
$\mathbf{1-\gamma}$	0.025	0.029	0.028	0.029
$\hat{\mathbf{P}}_{\mathbf{e}}$ [%]	13.9	10.6	8.7	10.1
Street layout 2				
	Measured reference	**Prediction for layout 1**	**Prediction for layout 2**	**Prediction for layout 3**
$\mathbf{D}_{\mathrm{KL}}$	69.28	211.91	81.14	74.95
MSE	0.055	0.082	0.071	0.065
$\mathbf{1-\gamma}$	0.064	0.194	0.097	0.087
$\hat{\mathbf{P}}_{\mathbf{e}}$ [%]	19.9	30.8	25.3	23.8
Street layout 3				
	Measured reference	**Prediction for layout 1**	**Prediction for layout 2**	**Prediction for layout 4**
$\mathbf{D}_{\mathrm{KL}}$	72.02	171.35	110.35	82.45
MSE	0.038	0.119	0.042	0.044
$\mathbf{1-\gamma}$	0.019	0.089	0.076	0.025
$\hat{\mathbf{P}}_{\mathbf{e}}$ [%]	23.6	16.3	18.4	20.1
Street layout 4				
	Measured reference	**Prediction for layout 1**	**Prediction for layout 2**	**Prediction for layout 3**
$\mathbf{D}_{\mathrm{KL}}$	28.77	42.22	58.19	78.60
MSE	0.01	0.026	0.048	0.082
$\mathbf{1-\gamma}$	0.004	0.028	0.064	0.091
$\hat{\mathbf{P}}_{\mathbf{e}}$ [%]	39.1	34.2	30.5	25.9

mismatching layout are used, the distance-dependent measures exceed the upper bounds of dissimilarity (cf. measured reference values in Table 4.2) in most cases. The only exception is layout 1, in which the KLD, MSE and complementary collinearity are slightly below the measured reference when the parameters of the three mismatching layouts are used. However, mismatching parameters lead to a significantly larger deviation of the percentage of erroneous packets from the reference value. More precisely, the deviation amounts to 1.9 %, 4 %, and 2.6 % when using parameters of the layouts 2, 3, and 4, respectively. However, when the model parameters of the matching layout are used the deviation is 1.2 % only.

For street layout 2, the worst performance is achieved when using the parameters estimated on the basis of the layout 1. In this case, the KLD exceeds the measured reference value by 70 %, the MSE by 45 % and the complementary collinearity is 2.5 times larger than the reference. The deviation from the reference value of the percentage of erroneous packets is 11.4 %, which is significantly more than the 0.5 % achievable by the environment-aware model with parameters of matching layout. When parameters of street layouts 3 and 4 are used, the KLD does not exceed the upper bound. However, the MSE is above the reference value by 25 % and 14 % with the parameters of layouts 3 and 4, respectively. The same relation holds for the complementary collinearity.

Similarly, for street layout 3 poor performance of the environment-aware model is attained when using parameters of layout 1. The KLD, MSE and complementary collinearity exceed the upper bound by 50 %, 130 % ,and 370 %, respectively. When using parameters of layouts 2 and 4, the KLD and the MSE do not exceed the upper bounds. However, the complementary collinearity is 30 % and 300 % larger than the reference, for the layout 2 and 4 respectively. The average percentage of the erroneous packets deviates from the reference by 8.1 %, 6 %, and 4.3 %, when parameters of the layouts 1, 2, and 4 are used. In contrast, this deviation for the case of the environment-aware model with parameters of the matching layout amounts to only 1.2 %.

For layout 4, the incompatibility of the mismatching parameters is most notable with respect to the percentage of erroneous packets. In particular, $\hat{P}_e$ is underestimated by 9.1 %, 12.8 %, and 17.4 %, when using parameters of layouts 1, 2, and 3 respectively. The deviation from the reference value of $\hat{P}_e$ is only 4.2 % when parameters of the matching layout are used. The relation of the distance-dependent measures is similar as for the other three layouts. The exact values can be found in Table 4.5.

Figure 4.19 compares of the performance the environment-aware model that uses parameters of the matching and the mismatching street layouts. An example of the measured PDRs is shown using a black solid line. The performance of the environment-aware model with parameters of the matching layout is shown using a green dashed line. Finally, the performance of the model employed for a mismatching layout is represented with red dash-dotted line. Regardless of the considered layout, the PDRs generated by the environment-aware model with parameters of the matching layout (cf. green curves) are significantly closer to the measured curves than the PDRs generated by the same model with mismatching param-

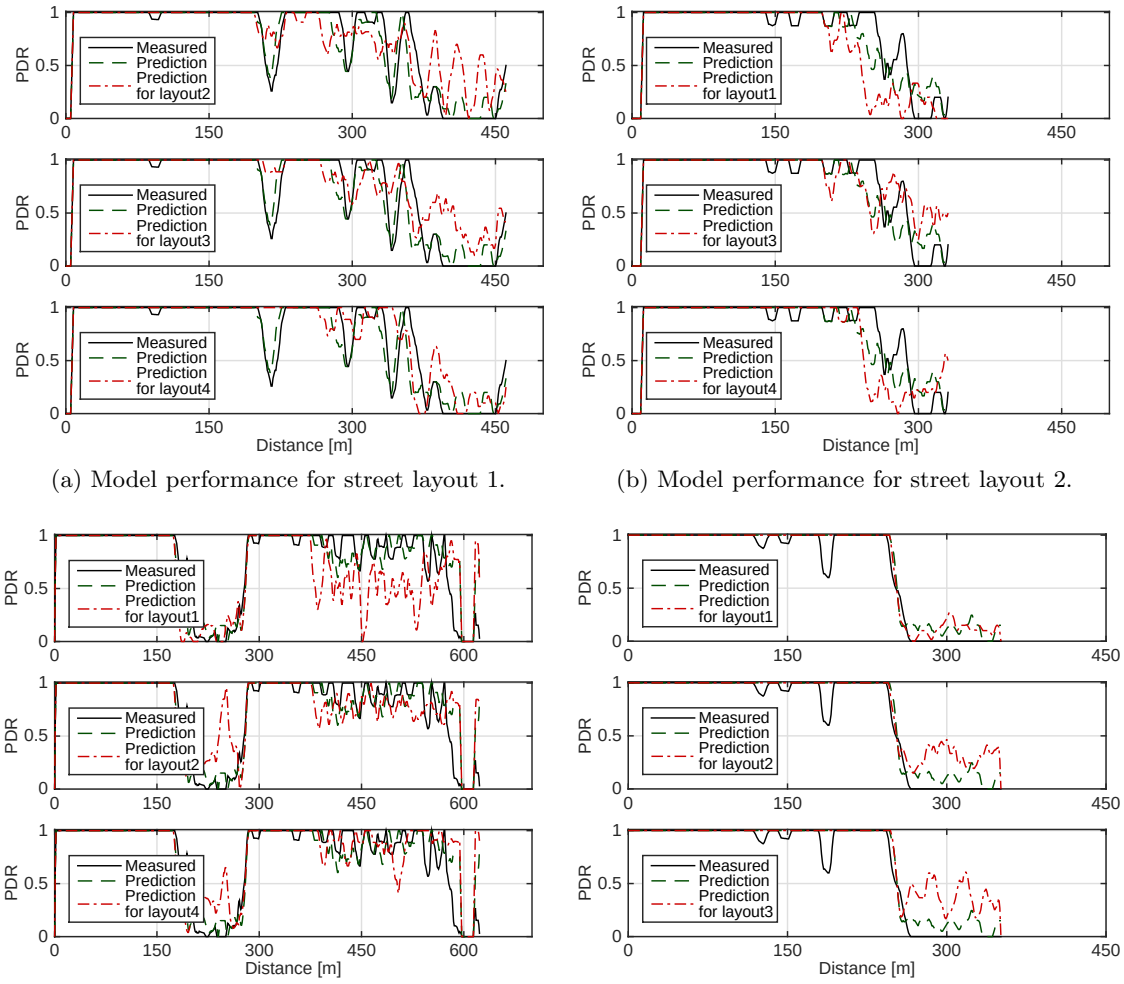

(a) Model performance for street layout 1.

(b) Model performance for street layout 2.

(c) Model performance for street layout 3.

(d) Model performance for street layout 4.

Figure 4.19: Performance of the environment-aware model with parameters estimated for different street layouts. The black solid lines indicate measured PDR curves, the green dashed lines show result of the environment-aware model with parameters of the same layout, and the red dash-dotted curves represent the performance of the same model employed for a different street layout.

eters (cf. red curves). This performance difference is particularly noticeable at the position of the impairments. The performance within the high quality communication region $\mathcal{R}_1$ can be reproduced comparably well, regardless of the layout. This is due to the fact that the parameters of quality level Q_1 are nearly the same for all street layouts, as can be seen from Table 4.1.

We therefore conclude that the packet-error performance of realistic V2I links can be modeled sufficiently well with the proposed environment-aware model. The key components for the reliability of the proposed model are a suitable model parametrization with respect to the street layout and an exact quality level assignment based on type and position of the impairments. Certainly, the accuracy achievable with the original model is higher than that of the environment-aware model, but the two approaches are designed for different purposes.

Table 4.4: SNR model parameters.

State	Quality level Q_k	SNR trend		Shadowing		Small scale fading	
		α_k	β_k	$\gamma_{1,k}$	σ_k^2	δ	$\eta_{\max}$
Street layout 1							
Good	$k=1$	43.43	−0.003	−0.087	2.484	2.12	5
	$k=2$	40.71	−0.002	−0.335	3.999		
	$k=3$	27.42	0	−0.018	1.610		
Bad	$k=1,2,3$	5	0	–			
Street layout 2							
Good	$k=1$	33.35	−0.003	−0.113	4.678	1.12	5
	$k=2$	30.53	−0.002	0.747	0.513		
	$k=3$	19.55	0	−0.075	1.603		
Bad	$k=1,2,3$	5	0	–			
Street layout 3							
Good	$k=1$	49.56	−0.003	−0.511	5.500	1.87	5
	$k=2$	29.01	−0.001	0.365	3.368		
	$k=3$	16.03	0	−0.091	0.606		
Bad	$k=1,2,3$	5	0	–			
Street layout 4							
Good	$k=1$	33.16	−0.002	−0.785	2.923	1.70	5
	$k=2$	30.38	−0.001	0.059	3.226		
	$k=3$	18.20	0	0.731	0.081		
Bad	$k=1,2,3$	5	0	–			

The original model should be applied to generate repetitions of an existing measurement, similarly to replay models discussed in Section 2.2.1. On the other hand the environment-aware model is intended to model wireless V2I transmissions at locations where no measurements were performed.

Next, we evaluate the performance of the environment-aware model with respect to the accuracy of the model-generated SNR patterns. To enable the model with SNR generation capabilities we have used the approach introduced in Section 4.3. The parameters of the model, estimated based on the primary measurement for each street layout, are given in

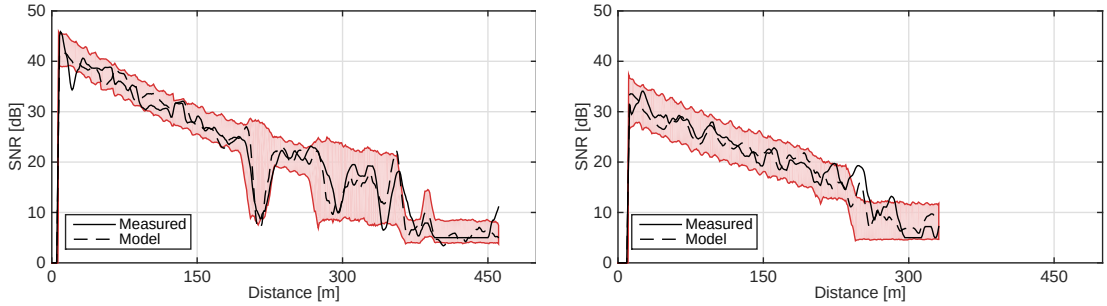

(a) Model performance for layout 1.

(b) Model performance for layout 2.

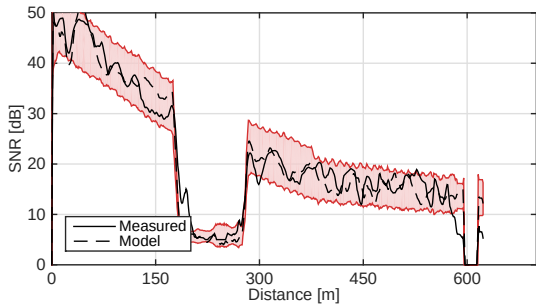

(c) Model performance for layout 3.

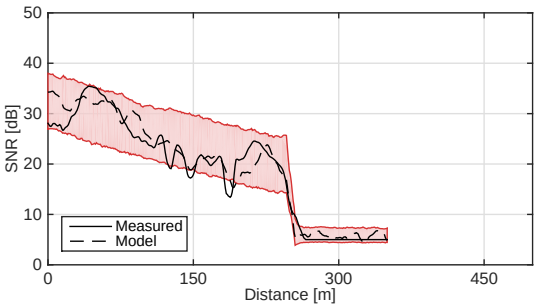

(d) Model performance for layout 4.

Figure 4.20: SNR vs. distance performance for the defined street layouts. Solid black lines represent a randomly chosen measurement repetition. Dashed black lines show a randomly chosen realization of the model. Colored bands show empirical intervals containing 95 % of all model realizations.

Table 4.4. Analyzing the model parameters we notice that in the good state the value β_3, i.e.,exponential decay of the SNR trend, equals to zero for all layouts. This implies that the SNR trend for quality level Q_3 is not distance dependent. The same holds for SNR trend in the bad state for all quality levels. We also note that the highest SNR can be achieved within the quality range $\mathcal{R}_1$ on urban streets with layout 3. At the same time, this layout is characterized by the lowest SNR achievable in quality level Q_3. Thus, for street layout 3 the quality levels have the strongest influence on the SNR. For layouts 2 and 4 the SNR trends are essentially equal. In both cases, the SNR in quality level Q_1 is slightly higher than in Q_2. However, the SNR trend in quality level Q_2 decays slower. The same is true for layout 1, with the only difference that the SNR values are on average 10 dB higher.

In Figure 4.20 we illustrate the results obtained using performance of the environment-aware model in terms of SNR for different street layouts. A randomly selected secondary measurement is shown using a black solid line. The dashed black lines demonstrate the SNR prediction generated by the environment-aware model and the red colored bands contain 95 % of all 10^4 model realizations. These results indicate an excellent agreement between the measured and the model-generated SNR patterns for all environments. The empirical confidence intervals clearly depend on the quality level. The tightest bounds are achieved for the quality level Q_3. Here the 95 % intervals are only 2 to 3 dB wide. For the other quality levels, the deviation from the measurement is $\leq$ 10 dB. We attribute this difference

Table 4.5: Performance evaluation of the environment-aware SNR model.

	MSE	$\mathbf{1-\gamma}$	**p-value**	$\mathbf{D_{KS}}$	$\mathbf{D_{PDR}}$
Street layout 1					
Measured	17.34	0.008	0.057	0.296	0.102
Modeled	14.90	0.003	0.079	0.104	0.224
Street layout 2					
Measured	23.46	0.026	0.093	0.341	0.108
Modeled	22.07	0.014	0.150	0.119	0.227
Street layout 3					
Measured	22.45	0.009	0.073	0.308	0.099
Modeled	19.25	0.008	0.309	0.133	0.255
Street layout 4					
Measured	15.57	0.003	0.084	0.256	0.156
Modeled	11.86	0.002	0.092	0.157	0.250

reflected by the empirical confidence bounds to the effects of large-scale fading, which are more pronounced in the high and intermediate quality levels Q_1 and Q_2.

To emphasize the high accuracy of the proposed SNR modeling approach, we compare the model-generated SNR sequences to the measured counterparts in terms of the MSE and the complementary collinearity. We note that the KLD does not lead to consistent and easily interpretable results, when comparing the SNR. We assume that this is due to stronger variations of the SNR, as compared to the PDR. The percentage of erroneous packets in the context of the SNR model evaluation is obviously inapplicable. As an alternative statistical measure we perform the two-sample Kolmogorov-Smirnov test introduced in Section 2.3.4. The model performance evaluation in terms of the distance-dependent measures and the Kolmogorov-Smirnov statistic are summarized in Table 4.5. The measured reference values of the Kolmogorov-Smirnov statistic are obtained by performing the hypothesis test between all measurement repetitions and taking the median of the resulting values. Similarly, for the model-generated results the hypothesis test was performed between each measurement repetition and 10^4 realizations of the model.

The SNR sequences generated by the environment-aware model conform to the accuracy requirements in terms of the distance-dependent measures, for all street layouts. In particular, the MSE is 15 % less than the measured reference for layouts 1 and 3. In the case of layouts 2 and 4, the MSE is 6 % and 23 % below the upper bound, respectively. The complementary collinearity for layouts 1 and 2 is roughly three and two times smaller than the measured

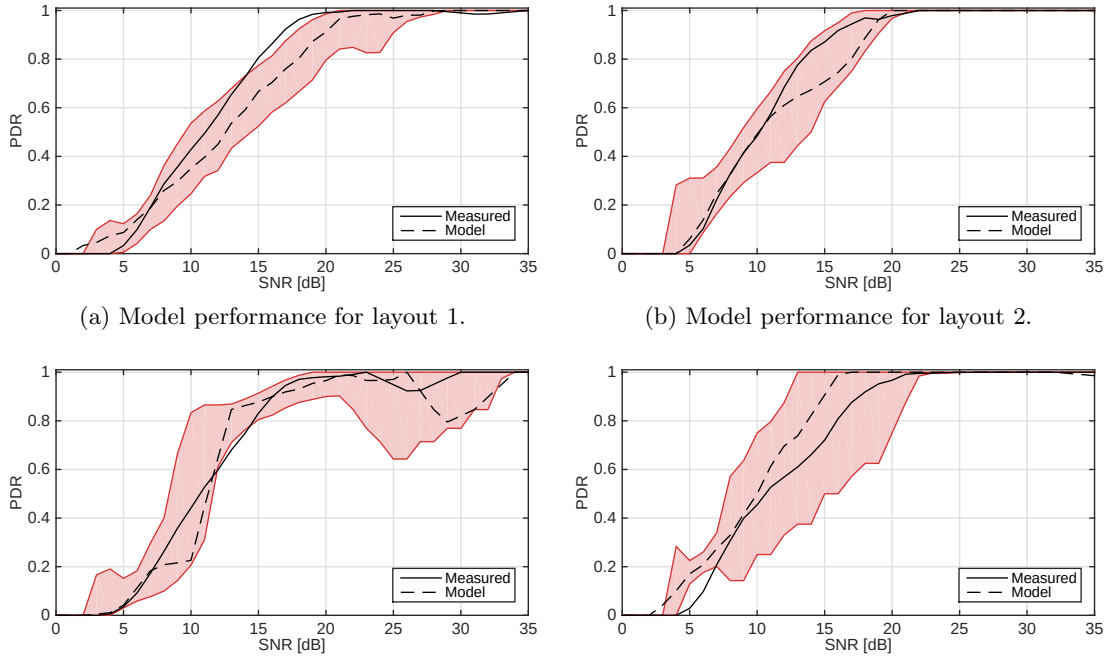

(a) Model performance for layout 1.

(b) Model performance for layout 2.

(c) Model performance for layout 3.

(d) Model performance for layout 4.

Figure 4.21: PDR vs. SNR performance for the defined street layouts. Solid black lines represent a randomly chosen measurement repetition. Dashed black lines show a randomly chosen realization of the model. Colored bands show empirical intervals containing 95 % of all model realizations.

reference. For layouts 3 and 4 the complementary collinearity amounts to 90 % and 67 % of the reference value, respectively.

With respect to D_{KS}, defined as the largest vertical distance between two empirical cumulative distribution functions (CDFs), we note that the distance between the CDFs of the measured SNR patterns is on average three times larger than the distance between the measured and the model-generated patterns, regardless of the street layout. To interpret the results regarding the p-value, we recall that the null hypothesis is rejected if the p-value is equal to or smaller than the significance level α, which in our case is 0.05. For all street layouts the p-values are > 0.05 for either the measured or the modeled SNR patterns. The p-values indicate the likelihood that the measured and the model-generated SNR samples.

Finally, in Figure 4.21 we show the PDR as a function of the SNR for different street layouts. The black solid lines represent a randomly selected secondary measurement. The dashed black lines show the performance originating from the environment-aware model and the colored bands contain 95 % of all model realizations. These plots indicate good agreement between the measured and the model-generated performance. To substantiate this statement, we calculate D_{PDR}, which is defined as the largest vertical distance between two PDR vs. SNR curves. The results summarized in Table 4.5 show that D_{PDR} is nearly the same for all street layouts and can be up to 0.25. This is nearly twice as large as the deviation between the measured PDR vs. SNR curves. Nevertheless, the empirical evaluation have proven high accuracy of our simple SNR model that only relies on the street layout and topology.

4.6 Application Examples

Both the range-dependent modified Gilbert model proposed in Section 4.1 and the environment-aware model introduced in Section 4.4 can be broadly utilized in a variety of simulation tools. These models are of particular interest in the process of developing and testing upper layer protocols and mechanisms. Such mechanisms include, but are not limited to, congestion control, message dissemination, delay tolerant networking, floating car data, and geocasting. The proof of concept and evaluation of new network layer algorithms is often done in ns-2 or ns-3 simulation environments. These packet-level discrete-event simulators use a centric event scheduler to handle events such as transmission, forwarding, and reception of packets. The wireless channel in these simulation environments is most frequently represented by the Nakagami-m model [80]. However, such kind of PHY obstruction may lead to unrealistic results and misleading conclusions. In this section, we list a few research proposals that focus on protocol design in the context of vehicular communications and could use the proposed model to improve the reliability and sustainability of their results.

Quite a few research groups have studied the effect of beacon congestions and suggested solutions to reliably minimize the impact of such congestions on the performance of safety-related vehicular applications. In the context of intelligent transportation system (ITS), beacon messages are regularly broadcasted by each vehicle to notify the neighbors of its presence and status. Moreover, there exist event-driven warning messages that are emitted when an on-board unit (OBU) or RSU detects a safety critical situation. These messages carry time-critical information of high importance and need to be transmitted reliably. To ensure that the event-driven messages are not lost due to simultaneous transmission with a beacon message, it is necessary to develop algorithms that reduce the beacon load and reserve resources for higher-priority messages. To avoid beacon congestions one of the following two approaches is usually applied: (i) beacon rate control and (ii) beacon transmit power control. An example of a rate-adaptive collision control algorithm is given in [33]. The devised algorithm maintains the beacon load under a given threshold by dynamically adapting the nodes' beacon rate. Each node controls the aggregated beacon load by monitoring the wireless channel and estimating the number of neighbors. The nodes then adjust their beacon rate such that the aggregated beacon load is kept below a given threshold. Power-adaptive collision control algorithms were suggested by the authors of [24] and [114]. The algorithm presented in [24] adjusts the transmit power as a function of the estimated number of neighbors. If the number of neighbors is below the predefined threshold, a node increases its transmit power. Otherwise the transmit power is decreased. In [114], each node acquires the status of the neighboring nodes within the carrier-sense range and uses this information to determine the maximum common transmit power, such that the aggregated beacon load is below a specified threshold. This information is then broadcast to other nodes in the carrier-sense range that collectively choose the transmit power value to ensure fairness. A statistical approach based on transmit power adaptation for beaconing congestion control is suggested

in [35]. In this case, each vehicle locally computes the power needed to comply with a given maximum beacon load. This load is estimated based on channel parameters, vehicle density, and beaconing rate. The authors of [68] analyze the performance of the beacon congestion control algorithms based on adjusting the transmit rate, transmit power, or a combination of both. All these studies were performed by conducting ns-2 simulations for various scenarios and vehicle densities. The authors claim to achieve realistic packet-error rates by using the IEEE 802.11 PHY extension that implements a Nakagami model for the radio propagation.

Along with congestion control applications, distributed control applications are frequently considered in the research community. While time-triggered messages are the foundation of most distributed control applications, some vehicular scenarios require dissemination of event-driven messages as well. The state-of-the-art for disseminating such event-driven messages is to let all nodes repeat the received messages, which consequently leads to broadcast storms. Different ways of mitigating broadcast storms have been evaluated in [116]. Here, several broadcast algorithms are compared from an application perspective using simulations. In [88] information dissemination protocols for vehicular ad-hoc networks (VANETs) are evaluated in general. The authors of [21] are particularly focusing on information dissemination in a platooning environment. Similarly, the authors of [56] propose a message dissemination scheme based on relay selection for platooning applications. The proposed algorithm minimizes the probability of error of unicast and broadcast transmission, without degrading the performance of the co-existing time-triggered messages. The performance of the proposed message dissemination schemes is evaluated by means of simulations, where the wireless propagation in which is modeled by path loss and a distance-dependent parameter m of the Nakagami-m distribution.

Information dissemination is further considered in the context of delay tolerant networks [37]. Delay tolerant networks deal with communication in impaired networks with long latencies, high packet loss rates, and frequent disconnectivity. Pioneering work that reveals fundamental issues of such networks, including optimal choice of data rate when driving through connectivity islands is presented in [48]. The authors of [91] analyze intermittent connectivity observed in a VANETs and propose a disruption tolerant network service. The authors consider a mesh network of RSUs in which vehicles open communication dialogs using the IEEE 802.11p protocol when entering the range of an RSU. However, these dialogs may be interrupted, for instance when the vehicle leaves the communication range or when packet losses occur. With the help of the proposed disruption tolerant network service the authors claim to achieve seamless and efficient message dissemination over several RSUs, with non-overlapping coverage ranges. This work is of particular interest since the authors use real-world V2I transmission patterns to evaluate their mechanism. However, the number of measurement repetitions used for the evaluation is rather small. This issue could be easily solved with the help of the range-dependent modified Gilbert model, which constitutes a computationally inexpensive way to generate realistic performance traces based on a small number of available measurement.

Another type of upper layer application, where our model may be beneficial, is the so-called floating car data collection. It is a commonly used method for collecting traffic related information such as vehicle speed an ambient temperature directly from the vehicles on the road. The relevant information is collected by a vehicle from its sensors and delivered to an RSU by means of IEEE 802.11p-based wireless communication. This approach enables data collection from numerous vehicles. In this context, the authors of [92] presented a solution for targeting data collection to specific road areas, time periods and sensor types. Evaluation of the proposed solution is performed with the help of an ns-3 simulation environment with special simulator extensions that incorporate the effects of propagation delay and packet losses.

Likewise, the development of geocasting protocols is largely based on simulations with ns-2 or ns-3. Geocasting protocols enable vehicle-to-vehicle (V2V) and V2I communication based on the IEEE 802.11 technology, ad-hoc principles, and wireless multi-hop techniques, using geographical positions. An extensive overview of the existing geocast routing protocols for VANETs is given in [14]. The authors of [81] suggest a communication scheme for VANETs that accounts for highly dynamic topology, road-constrained vehicle movement, and presence of obstacles. To evaluate the proposed scheme simulations were performed in which the two-ray model was used to represent a LOS transmission between the vehicle and the RSU. A geocast routing protocol based on flooding in defined forwarding zones is introduced in [45]. The position-based routing is analyzed in highway and urban scenarios, however the aspects of PHY are entirely disregarded. The design of a security solution for geocasting is proposed in [39]. This scheme is based on cryptographic protection, secure neighbor discovery, mobility-related checks, trustworthy neighborhood assessment, and rate limitation. For simulation-based assessment, the authors utilized the network simulator ns-2 with the Nakagami propagation model. The transmission power was configured to obtain a communication range of 10^4 m under deterministic propagation. However, our results in Chapter 3 indicate that such assumptions are fundamentally misleading.

this overview shows that the development of upper layer applications and protocols is to a large extent based on simulations with rather simplistic PHY layer assumptions. Therefore, there is a risk that in real-world conditions the proposed techniques might perform significantly worse, thereby compromising the reliability of safety-related vehicular applications and postponing the roll-out of this highly demanded technology. Our model allows to carry out plausibility checks of the aforementioned protocols and mechanisms under realistic propagation conditions, increasing the overall reliability of the attained results.

4.7 Discussion

In this chapter, we have introduced two modeling approaches that allow us to generate of realistic distance-dependent packet-error and SNR traces. Although both models are parametrized based on real-world performance measurements and use an HMM-based ap-

proach for data generation, their fields of application are fundamentally different. The range-dependent modified Gilbert model should be used if a set of measurements at the location of interest is available, even if their number is not sufficient to draw generalized conclusions. On the other hand, the environment-aware model is intended for use in situations where no prior knowledge about the communication quality at the location of interest is available. The model will predict the performance based on the topological characteristics of the environment.

To parametrize the range-dependent modified Gilbert model, the available measurements are divided into equally large non-overlapping intervals and the statistical properties of the underlying stochastic process are analyzed for each interval separately. Our investigations suggest that the optimal length of such interval is 10 m. By using a two-state HMM with distance dependent parameters we are able to generate synthetic measurement repetitions. By comparing the model-generated results to the measured counterpart, we have shown that the packet-error traces generated in this way reproduce the measurements with high accuracy. We measured the accuracy in terms of distance-dependent measures and quantitative statistical measures. The excellent accuracy of the range-dependent modified Gilbert model suggest the use of ur model to increase the reliability of results which are based on a limited number of measurements.

To obtain the environment-aware model we have started from the range-dependent modified Gilbert model with quantized parameters. Through a set of extensive evaluations we have shown that the optimal number of quantization levels for V2I settings is 3, regardless of the environment. The quantization of the model parameters with the optimal number of quantization levels allows us to precisely localize environmental impairments. To find the boundaries of the communication quality regions we have suggested a dynamic programming algorithm that finds the set of boundaries which minimizes the MSE. Each quality region is governed by a single set of model parameters, regardless of its length. However, in realistic settings the quality regions are often interrupted or shortened due to the presence of environmental impairments. Thus, the parameters representing different communication qualities can be used as a building blocks to model the communication performance in the presence of realistic propagation impairments.

To showcase the efficiency this environment-aware modeling approach, we used real-world V2I measurements conducted at 22 different urban locations. Based on an extensive analysis of various environmental aspects such as street layout and topology, as well as type and position of the impairments, we have shown that the V2I communication performance in urban environments is largely determind by the street layout. We have identified four types of street layouts, representative for most urban environments and provided model parameters for each of them. According to our results, the best performance can be achieved in open areas, frequently found in suburbs. Our investigations have further suggested intersections, interruptions in the median stripe, roundabouts and road curvatures have most significant influence on the communication performance in urban settings. To demonstrate the accuracy of the environment-aware approach, we have predicted the V2I communication performance

at four different urban locations, chosen according to our definition of the street layouts. We estimate parameters of the model based on measurements at other locations, with the same street layouts but with a different type and different distribution of the impairments. The evaluations in terms of distance-dependent and quantitative statistical measures underpin the accuracy of the suggested modeling approach. When using model parameters of the matching street layout, the distance dependent measures are well below the upper bound and the deviation from the reference value of the quantitative measure is $\leq 10\,\%$. We thus conclude that out model is well suited for the generation of realistic V2I communication patterns for certain urban locations.

We further note that both, the range-dependent modified Gilbert model and the environment-aware model, are restricted to neither urban scenarios, nor to the V2I settings. The environment-aware model can easily be adapted to highway or rural settings by redefining the set of street layouts and impairments. The models can be successfully applied to reproduce or predict the performance of any distance-dependent communication system. We note, however, that the assumptions on the optimal granularity size and number of quantization levels derived in this thesis are only valid for V2I-type communications and may need to be revised for other communication systems.

5

Conclusions and Outlook

In this thesis, we evaluated the performance of vehicle-to-infrastructure (V2I) communication systems based on extensive real-world measurement campaigns carried out on Austrian highways. Generally, these systems are a subclass of intelligent transportation systems (ITSs) that also include vehicle-to-vehicle (V2V) communications. By the end of this decade vehicles will be equipped with the required communication units. As long as such communication-enabled smart vehicles do not sufficiently proliferate, the main stakeholders focus on the deployment of smart roads. This ensures that the early adopters benefit from the technology from the start. While there is much ongoing work in this direction, the roll-out of the first real smart road is intended for the beginning of 2016. This ambitious smart road project is called the Cooperative ITS Corridor [99] and it will connect the cities of Rotterdam and Vienna through Frankfurt and Munich. The chain of highways equipped with ITS infrastructure units will guide the vehicles through the boarders of three countries without interruption in the basic service. To enable seamless operation of the Cooperative ITS Corridor and ITS in general, well-conceived deployment of roadside units (RSUs) is required. A major contribution of this thesis is to lay down recommendations for optimal deployment of future communication infrastructure-enabled vehicular systems.

In particular, we have evaluated system performance with various RSU and on-board unit (OBU) antenna types, antenna gains, and mounting positions. We suggest to utilize directional RSU antennas instead of omni-directional antennas, because they allow to achieve up to three times larger reliable communication range and up to 30 % higher throughput. Furthermore, we have shown that directional RSU antennas with higher gain yield significant improvements. Specifically the communication range is extended by a factor of five and the throughput is increased by 125 % when deploying directional RSU antennas with 4 dB higher gain. However, the performance growth is not strictly proportional to the antenna gain, since with increasing antenna gain the sensitivity to imprecise antenna mounting is increasing as

well. With respect to antenna positioning we recommend to mount RSU antennas above the middle of the highway, rather than on the outer side closer to the highway shoulder, to guarantee homogeneous coverage and avoid undesirable performance degradation for one of the driving directions. The OBU antennas have a strong impact on the overall performance of V2I communication systems. Comparing the performance of three differently manufactured omni-directional OBU with nearly the same antenna gain, we have shown that up to three times greater communication range and up to 30 % more throughput is achievable through careful design of vehicular antennas.

Irrespective of the hardware components, we recommend to transmit shorter packets at lower data rates to guarantee reliable information dissemination. This is because both, higher data rates and longer packets lead to performance degradation in terms of reliability and coverage. However, if higher throughput is required under a constant transmit power constraint, we recommend to transmit longer orthogonal frequency-division multiplexing (OFDM) frames rather than using higher order modulation and coding schemes. In case that the attained throughput is not sufficient, we recommend to use cooperative communication approaches and relay the packets over several hops. This recommendation was verified by a series of real-world experiments carried out with a single infrastructure unit used as message source and two vehicles serving as relay and destination. Even in such simple settings the throughput was increased by 30 % and the packet delivery reliability was improved significantly. Moreover, we were able to achieve an increase of the reliable communication range of up to 30 %. We therefore strongly support the cooperative communication approach in the context of dependable vehicular communications, to mitigate the negative impact of LOS obstruction and to improve the overall system performance.

For our simple two-hop extension of the fundamental V2I communication system we have adopted time-division multiplexing schemes. That is, the transmission initiated by the RSU and the one of the relay take place at different time instances. By doing so, we ensured that there was only one transmitter active at any time and no interference occurred at the destination node. In the evaluated setting we just used a single relay and therefore the resulting delay was low. In general, it would be interesting to investigate the trade-off between the reliability increase and the relevance loss, resulting from multi-hop communication in the ITS domain. On the other hand, it is worthwhile to evaluate the performance of vehicular ad-hoc networks, in which several nodes are active simultaneously. Interference-prone vehicular communication has been rarely investigated through real-world measurements, mainly due to high costs. Simulation-based investigations suggest that packet losses due to simultaneous transmissions by several nodes are unavoidable. At this time several alternatives to the standardized carrier sense multiple access with collision avoidance algorithm have been proposed. However, a measurement-based verification of these algorithms under real-world conditions is currently lacking.

Another approach to handle the disadvantages and improve the reliability of IEEE 802.11p systems is to combine it with other network access technologies. Currently, the 4G Long-

Term Evolution (LTE) communication standard is under intensive investigation as a key radio access network alternative/supplement. Such a hybrid approach that exploits the merits of both, ITS G5 and cellular technologies, has the potential to increase spectrum efficiency and improve reliability of time-critical vehicular communications. However, the coexistence of the two technologies and the resulting benefits need yet to be carefully analyzed through real-world measurements and we thus suggest to address these issues in the near future.

To model the performance of V2I communications, we proposed an approach to reliably reproduce the measured performance. Our hidden Markov model-based approach is capable of emulating distance-dependent measured packet-error and signal-to-noise ratio patterns with high accuracy. The probabilistic assumptions of our model ensure that on the one hand the statistical properties of the measured data are maintained and on the other hand the resulting patterns are not deterministic. Each model realization can be seen as a measurement repetition. We refer to this modeling approach as distance-dependent modified Gilbert model. To provide access to the measurement data presented in this thesis, we have estimated the model parameters for 12 different setups and released them under a noncommercial academic use license [7]. With the help of the accompanying MATLAB software, realistic V2I communication performance in highway environments with different transmit parameters, RSU antenna types, antenna gains, and RSU positions are easily generated. This model and the resulting know-how transfer in domain of V2I measurements constitutes another major contribution of this thesis to the scientific community.

We have further extended the range-dependent modified Gilbert model such that the communication performance can be modeled for locations, at which measurements have not been conducted. To obtain this model, we have jointly quantized the parameters of the original model and found empirically the optimum number of quantization levels. Thorough investigations have shown that the model parameters obtained in this manner allow us to precisely localize the propagation impairments. We have parametrized our model based on V2I measurements performed at 22 different urban locations. It turned out that the resulting model parameters are influenced by the street layout and the propagation impairments such as roundabouts and intersections. Based on these considerations we identified types of street layouts and impairments that are representative for urban environments, and characterized them in the form of model parameters. The model parameters provided in this thesis can be used as a building blocks for our environment-aware model, which predicts the communication performance based on the street layout and the topology. We have demonstrated the accuracy of this environment-aware model by predicting the V2I communication performance at four different urban locations. The model accuracy was evaluated in terms of distance-dependent and quantitative statistical measures and the resulting values underpin the extraordinarily high precision of the proposed performance modeling technique. Thus, the final contribution of this thesis is a computationally inexpensive environment-aware model for V2I performance valid for urban locations.

The proposed modeling approaches are not restricted to urban environments or to V2I communication. Both models reproduce and predict the performance of any distance-dependent communication system. The environment-aware model is adaptable to highway or rural environments, by redefining the set of street layouts and impairments.

As directions for future research in the context of performance modeling we suggest to generalize the environment-aware model with respect to transmit parameters, such as data rate, packet length, and transmit power. It is furthermore worthwhile to incorporate the influence of the RSU antenna height and its mounting position. Moreover, the proposed models offer a solid basis for the investigation of hybrid and cooperative communication aspects in more detail. The integration of our models in the process of performance evaluation has an important advantage of saving time, cost, and complexity compared to measurements. For instance, to analyze the benefits achievable through multi-hop communications it is sufficient to have suitable models of V2I and V2V links. Finally, the model development can be extended beyond the results presented in this thesis by taking interference into account. Since real-life measurements with vehicles in interference-prone scenarios are complex and costly, a software defined radio-based channel emulator can be used as a substitute to repeated road trails.

List of Abbreviations

AF amplify-and-forward

AR autoregressive

CALM communications access for land mobiles

CDF cumulative distribution function

CIR channel impulse response

CRC cyclic redundancy check

CVIS cooperative vehicle-infrastructure systems

DF decode-and-forward

DP dynamic programming

DSRC dedicated short-range communications

DTMC discrete-time Markov chain

EIRP equivalent isotropically radiated power

ETSI European Telecommunications Standards Institute

GPS global positioning system

HMM hidden Markov model

IoT Internet of Things

ITS intelligent transportation system

KLD Kullback-Leibler divergence

KPI key performance indicator

LAN local area network

LOS line-of-sight

LTE Long-Term Evolution

MAC medium access control

MIMO multiple-input multiple-output

MSE mean squared error

NLOS non-line-of-sight

OBU on-board unit

OFDM orthogonal frequency-division multiplexing

PC personal computer

PDR packet delivery ratio

PER packet error rate

PHY physical layer

RCR reliable communication range

RF radio frequency

RSSI received signal strength indicator

RSU roadside unit

SINR signal to interference plus noise ratio

SISO single-input single-output

SNR signal-to-noise ratio

SQ scalar quantization

UCR unreliable communication range

V2I vehicle-to-infrastructure

V2V vehicle-to-vehicle

VANET vehicular ad-hoc network

VQ vector quantization

WAVE wireless access in vehicular environments

WLAN wireless local area network

WSU wireless safety unit

Bibliography

[1] *Cooperative vehicle-infrastructure systems (CVIS) project.* Available online: http://www.cvisproject.org/.

[2] *European FP7 ICT project iTETRIS.* Available online: http://ict-itetris.eu/.

[3] *Field traces from IEEE 802.11p vehicle-to-infrastructure measurement campaign.* Available online: http://www.uwicore.umh.es/V2I-measurement-campaign/.

[4] *Google Earth project.* Available online: http://www.google.com/earth/.

[5] *Number of passenger cars and commercial vehicles in use worldwide from 2006 to 2013 (in millions).* Available online: http://www.statista.com/statistics/281134/number-of-vehicles-in-use-worldwide/.

[6] *Project "Robust And Distributed Safety-Improved Traffic Telematics" (ROADSAFE).* Available online: https://portal.ftw.at/projects/roadsafe/.

[7] *Range-dependent modified Gilbert model packet-error generator.* Available online: https://www.nt.tuwien.ac.at/downloads/featured-downloads/.

[8] *Global status report on road safety 2013: Supporting a decade of action*, tech. rep., World Health Organization, 2013.

[9] T. Abbas, L. Bernado, A. Thiel, C. Mecklenbrauker, and F. Tufvesson, *Radio channel properties for vehicular communication: Merging lanes versus urban intersections*, IEEE Vehicular Technology Magazine, 8 (2013), pp. 27–34.

[10] T. Abbas, J. Karedal, and F. Tufvesson, *Measurement-based analysis: The effect of complementary antennas and diversity on vehicle-to-vehicle communication*, IEEE Letters on Antennas and Wireless Propagation, 12 (2013), pp. 309–312.

[11] F. Abrate, A. Vesco, and R. Scopigno, *An analytical packet error rate model for WAVE receivers*, in Proc. 74th IEEE Vehicular Technology Conference (VTC Fall), Sept. 2011.

[12] G. Acosta and M. Ingram, *Model development for the wideband expressway vehicle-to-vehicle 2.4 GHz channel*, in Proc. IEEE Wireless Communications and Networking Conference (WCNC), vol. 3, Apr. 2006, pp. 1283–1288.

[13] G. Acosta-Marum and M. Ingram, *Six time- and frequency- selective empirical channel models for vehicular wireless LANs*, IEEE Vehicular Technology Magazine, 2 (2007), pp. 4–11.

[14] S. Allal and S. Boudjit, *Geocast routing protocols for VANETs: Survey and guidelines*, in Proc. 6th International Conference on Innovative Mobile and Internet Services in Ubiquitous Computing (IMIS), July 2012, pp. 323–328.

[15] ASTM International, *Specification for telecommunications and information exchange between roadside and vehicle systems – 5 GHz band dedicated short range communications (DSRC) medium access control (MAC) and physical layer (PHY) specifications*. ASTM E2213, 2010.

[16] L. E. Baum, T. Petrie, G. Soules, and N. Weiss, *A maximization technique occurring in the statistical analysis of probabilistic functions of Markov chains*, The Annals of Mathematical Statistics, 41 (1970), pp. 164–171.

[17] C. Bergenhem, R. Johansson, and E. Coelingh, *Measurements on V2V communication quality in a vehicle platooning application*, in Multiple Access Communications, M. Jonsson, A. Vinel, B. Bellalta, and E. Belyaev, eds., vol. 8715 of Lecture Notes in Computer Science, Springer International Publishing, 2014, pp. 35–48.

[18] L. Bernado, A. Roma, A. Paier, T. Zemen, N. Czink, J. Karedal, A. Thiel, F. Tufvesson, A. Molisch, and C. Mecklenbräuker, *In-tunnel vehicular radio channel characterization*, in Proc. 73rd IEEE Vehicular Technology Conference (VTC Spring), May 2011.

[19] L. Bernado, T. Zemen, F. Tufvesson, A. Molisch, and C. Mecklenbrauker, *Delay and doppler spreads of nonstationary vehicular channels for safety-relevant scenarios*, IEEE Transactions on Vehicular Technology, 63 (2014), pp. 82–93.

[20] M. Boban, T. Vinhoza, M. Ferreira, J. Barros, and O. Tonguz, *Impact of vehicles as obstacles in vehicular ad hoc networks*, IEEE Journal on Selected Areas in Communications, 29 (2011), pp. 15–28.

[21] A. Böhm, M. Jonsson, and E. Uhlemann, *Co-existing periodic beaconing and hazard warnings in IEEE 802.11p-based platooning applications*, in Proc. 10th ACM International Workshop on Vehicular Internetworking, Systems, and Applications, VANET '13, ACM, 2013, pp. 99–102.

[22] A. Böhm, K. Lidström, M. Jonsson, and T. Larsson, *Evaluating cALM M5-based vehicle-to-vehicle communication in various road settings through field trials*, in Proc. 35th IEEE Conference on Local Computer Networks (LCN), Oct. 2010, pp. 613–620.

[23] J. Burg, *Maximum entropy spectral analysis*, in Proc. 37th Meeting of the Society of Exploration Geophysicists, 1967.

[24] G. Caizzone, P. Giacomazzi, L. Musumeci, and G. Verticale, *A power control algorithm with high channel availability for vehicular ad hoc networks*, in Proc. IEEE International Conference on Communications (ICC), vol. 5, May 2005, pp. 3171–3176.

[25] L. Cheng, B. Henty, D. Stancil, F. Bai, and P. Mudalige, *Mobile vehicle-to-vehicle narrow-band channel measurement and characterization of the 5.9 GHz dedicated short range communication (DSRC) frequency band*, IEEE Journal on Selected Areas in Communications, 25 (2007), pp. 1501–1516.

[26] X. Cheng, C.-X. Wang, D. Laurenson, S. Salous, and A. Vasilakos, *An adaptive geometry-based stochastic model for non-isotropic MIMO mobile-to-mobile channels*, IEEE Transactions on Wireless Communications, 8 (2009), pp. 4824–4835.

[27] G. Ching, K. Tsuda, and Y. Kishiki, *Analysis of path gain inside tunnels based on FDTD and ray tracing methods*, in Proc. International Symposium on Electromagnetic Theory (EMTS), May 2013, pp. 644–647.

[28] J. Davis and J. Linnartz, *Vehicle to vehicle RF propagation measurements*, in Proc. 28th Asilomar Conference on Signals, Systems and Computers, vol. 1, Oct. 1994, pp. 470–474.

[29] S. Demmel, A. Lambert, D. Gruyer, G. S. Larue, and A. Rakotonirainy, *IEEE 802.11p empirical performance model from evaluations on test tracks*, Journal of Networks, 9 (2014), pp. 1485–1495.

[30] S. Demmel, A. Lambert, D. Gruyer, A. Rakotonirainy, and E. Monacelli, *Empirical IEEE 802.11p performance evaluation on test tracks*, in Proc. 4th IEEE Intelligent Vehicles Symposium, June 2012, pp. 837–842.

[31] S. Dickey, C.-L. Huang, and X. Guan, *Field measurements of vehicle to roadside communication performance*, in Proc. 66th IEEE Vehicular Technology Conference (VTC Fall), Sept. 2007, pp. 2179–2183.

[32] O. Dousse, M. Franceschetti, N. Macris, R. Meester, and P. Thiran, *Percolation in the signal to interference ratio graph*, Journal of Applied Probability, 43 (2006), pp. 552–562.

[33] M. Drigo, W. Zhang, R. Baldessari, L. Le, A. Festag, and M. Zorzi, *Distributed rate control algorithm for VANETs (DRCV)*, in Proc. 6th ACM International Workshop on Vehicular Internetworking, Systems, and Applications, VANET '09, ACM, 2009, pp. 119–120.

[34] D. Eckhoff, C. Sommer, and F. Dressler, *On the necessity of accurate IEEE 802.11p models for IVC protocol simulation*, in Proc. 75th IEEE Vehicular Technology Conference (VTC Spring), May 2012.

[35] E. Egea-Lopez, J. Alcaraz, J. Vales-Alonso, A. Festag, and J. Garcia-Haro, *Statistical beaconing congestion control for vehicular networks*, IEEE Transactions on Vehicular Technology, 62 (2013), pp. 4162–4181.

[36] ETSI, *Intelligent transport systems (ITS); radiocommunications equipment operating in the 5.855 MHz to 5.925 MHz frequency band; harmonized EN covering essential requirements of article 3.2 of the R&TTE directive.* Draft ETSI EN 302 571 V0.0.2, Dec. 2007.

[37] K. Fall, *A delay-tolerant network architecture for challenged internets*, in Proc. ACM Conference on Applications, Technologies, Architectures, and Protocols for Computer Communications, SIGCOMM '03, New York, NY, USA, 2003, ACM, pp. 27–34.

[38] P. Fazio, M. Tropea, and F. De Rango, *A novel PER degradation model for VANETs*, IEEE Communications Letters, PP (2015).

[39] A. Festag, P. Papadimitratos, and T. Tielert, *Design and performance of secure geocast for vehicular communication*, IEEE Transactions on Vehicular Technology, 59 (2010), pp. 2456–2471.

[40] M. Fisz, *Probability Theory and Mathematical Statistics*, Krieger, 3 ed., 1963.

[41] H. Friis, *A note on a simple transmission formula*, Proceedings of the IRE, 34 (1946), pp. 254–256.

[42] M. Gan, F. Mani, F. Kaltenberger, C. Oestges, and T. Zemen, *A ray tracing algorithm using the discrete prolate spheroidal subspace*, in Proc. IEEE International Conference on Communications (ICC), June 2013, pp. 5710–5714.

[43] M. Gan, Z. Xu, V. Shivaldova, A. Paier, F. Tufvesson, and T. Zemen, *A ray tracing algorithm for intelligent transport systems in tunnels*, in Proc. 6th IEEE International Symposium on Wireless Vehicular Communications (WiVeC), Sept. 2014.

[44] T. Gaugel and H. Hartenstein, *Appropriate selection of urban vehicle-to-vehicle radio propagation models*, in Proc. 21st IEEE Symposium on Communications and Vehicular Technology (SCVT), Nov. 2014.

[45] H. Ghafoor and K. Aziz, *Position-based and geocast routing protocols in VANETs*, in Proc. 7th International Conference on Emerging Technologies (ICET), Sept. 2011.

[46] E. N. Gilbert, *Capacity of a burst-noise channel*, Bell System Technical Journal, 39 (1960), pp. 1253–1265.

[47] E. Giordano, R. Frank, G. Pau, and M. Gerla, *CORNER: a realistic urban propagation model for VANET*, in Proc. 7th International Conference on Wireless On-demand Network Systems and Services (WONS), Feb. 2010, pp. 57–60.

[48] D. Goodman, J. Borras, N. B. Mandayam, and R. Yates, *INFOSTATIONS: a new system model for data and messaging services*, in Proc. 47th IEEE Vehicular Technology Conference (VTC Spring), vol. 2, May 1997, pp. 969–973.

[49] J. Gozalvez, M. Sepulcre, and R. Bauza, *IEEE 802.11p vehicle to infrastructure communications in urban environments*, IEEE Communications Magazine, 50 (2012), pp. 176–183.

[50] J. Gozalvez, M. Sepulcre, and R. Bauza, *Impact of the radio channel modelling on the performance of communication VANET protocols*, Telecommunication Systems, 50 (2012), pp. 149–167.

[51] G. Grau, D. Pusceddu, S. Rea, O. Brickley, M. Koubek, and D. Pesch, *Vehicle-2-vehicle communication channel evaluation using the CVIS platform*, in Proc. 7th International Symposium on Communication Systems Networks and Digital Signal Processing (CSNDSP), July 2010, pp. 449–453.

[52] M. Haenggi, J. Andrews, F. Baccelli, O. Dousse, and M. Franceschetti, *Stochastic geometry and random graphs for the analysis and design of wireless networks*, IEEE Journal on Selected Areas in Communications, 27 (2009), pp. 1029–1046.

[53] O. Häggström and R. Meester, *Nearest neighbor and hard sphere models in continuum percolation*, Random Structures & Algorithms, 9 (1996), pp. 295–315.

[54] R. He, A. Molisch, F. Tufvesson, Z. Zhong, B. Ai, and T. Zhang, *Vehicle-to-vehicle propagation models with large vehicle obstructions*, IEEE Transactions on Intelligent Transportation Systems, 15 (2014), pp. 2237–2248.

[55] M. Herdin, N. Czink, H. Ozcelik, and E. Bonek, *Correlation matrix distance, a meaningful measure for evaluation of non-stationary MIMO channels*, in Proc. 61st IEEE Vehicular Technology Conference (VTC Spring), vol. 1, May 2005, pp. 136–140.

[56] L. Hoang, E. Uhlemann, and M. Jonsson, *An efficient message dissemination technique in platooning applications*, IEEE Communications Letters, PP (2015), pp. 1–1.

[57] IEEE Computer Society, *IEEE standard for information technology– local and metropolitan area networks– specific requirements– part 11: Wireless LAN medium access control (MAC) and physical layer (PHY) specifications amendment 6: Wireless access in vehicular environments*, July 2010. Available online: http://ieeexplore.ieee.org/servlet/opac?punumber=5514473.

[58] IEEE Vehicular Technology Society, *IEEE trial-use standard for wireless access in vehicular environments (WAVE) - resource manager*, Oct. 2006. Available online: http://ieeexplore.ieee.org/stamp/stamp.jsp?tp=&arnumber=1715701.

[59] ——, *IEEE standard for wireless access in vehicular environments (WAVE) - networking services*, Dec. 2010. Available online: http://ieeexplore.ieee.org/stamp/stamp.jsp?tp=&arnumber=6044681.

[60] ——, *IEEE standard for wireless access in vehicular environments - security services for applications and management messages*, Apr. 2013. Available online: http://ieeexplore.ieee.org/stamp/stamp.jsp?tp=&arnumber=6509896.

[61] M. Jakobsen, T. Pedersen, and B. Fleury, *Analysis of stochastic radio channels with temporal birth-death dynamics: A marked spatial point process perspective*, IEEE Transactions on Antennas and Propagation, 62 (2014), pp. 3761–3775.

[62] J. Karedal, F. Tufvesson, T. Abbas, O. Klemp, A. Paier, L. Bernado, and A. Molisch, *Radio channel measurements at street intersections for vehicle-to-vehicle safety applications*, in Proc. 71st IEEE Vehicular Technology Conference (VTC Spring), May 2010.

[63] J. Karedal, F. Tufvesson, N. Czink, A. Paier, C. Dumard, T. Zemen, C. Mecklenbräuker, and A. Molisch, *A geometry-based stochastic MIMO model for vehicle-to-vehicle communications*, IEEE Transactions on Wireless Communications, 8 (2009), pp. 3646–3657.

[64] S. Kaul, K. Ramachandran, P. Shankar, S. Oh, M. Gruteser, I. Seskar, and T. Nadeem, *Effect of antenna placement and diversity on vehicular network communications*, in Proc. 4th Annual IEEE Communications Society Conference on Sensor, Mesh and Ad Hoc Communications and Networks (SECON), June 2007, pp. 112–121.

[65] M. Killat and H. Hartenstein, *An empirical model for probability of packet reception in vehicular ad hoc networks*, EURASIP Journal on Wireless Communications and Networking, 2009 (2009).

[66] A. N. Kolmogorov, *Sulla determinazione empirica di una legge di distribuzione*, Giornale dell'Istituto Italiano degli Attuari, 4 (1933), pp. 83–91.

[67] B. Kurkoski and H. Yagi, *Concatenation of a discrete memoryless channel and a quantizer*, in Proc. IEEE Information Theory Workshop (ITW), Jan. 2010.

[68] L. Le, R. Baldessari, P. Salvador, A. Festag, and W. Zhang, *Performance evaluation of beacon congestion control algorithms for VANETs*, in Proc. IEEE Global Telecommunications Conference (GLOBECOM), Dec. 2011.

[69] Y. Linde, A. Buzo, and R. Gray, *An algorithm for vector quantizer design*, IEEE Transactions on Communications, 28 (1980), pp. 84–95.

[70] K. Mahler, P. Paschalidis, A. Kortke, M. Peter, and W. Keusgen, *Realistic IEEE 802.11p transmission simulations based on channel sounder measurement data*, in Proc. 78th IEEE Vehicular Technology Conference (VTC Fall), Sept. 2013.

[71] K. Mahler, P. Paschalidis, M. Wisotzki, A. Kortke, and W. Keusgen, *Evaluation of vehicular communication performance at street intersections*, in Proc. 80th IEEE Vehicular Technology Conference (VTC Fall), Sept. 2014.

[72] T. Mangel, O. Klemp, and H. Hartenstein, *A validated 5.9 GHz non-line-of-sight path-loss and fading model for inter-vehicle communication*, in Proc. 11th International Conference on ITS Telecommunications (ITST), Aug. 2011, pp. 75–80.

[73] T. Mangel, M. Michl, O. Klemp, and H. Hartenstein, *Real-world measurements of non-line-of-sight reception quality for 5.9 GHz IEEE 802.11p at intersections*, in Communication Technologies for Vehicles, T. Strang, A. Festag, A. Vinel, R. Mehmood, C. Rico Garcia, and M. Röckl, eds., vol. 6596 of Lecture Notes in Computer Science, Springer Berlin Heidelberg, 2011, pp. 189–202.

[74] F. Martelli, M. Renda, and P. Santi, *Measuring IEEE 802.11p performance for active safety applications in cooperative vehicular systems*, in Proc. 73rd IEEE Vehicular Technology Conference (VTC Spring), May 2011.

[75] D. Matolak, I. Sen, W. Xiong, and N. Yaskoff, *5 GHz wireless channel characterization for vehicle to vehicle communications*, in Proc. IEEE Military Communications Conference (MILCOM), vol. 5, Oct. 2005, pp. 3016–3022.

[76] J. Maurer, T. Fügen, T. Schafer, and W. Wiesbeck, *A new inter-vehicle communications (IVC) channel model*, in Proc. 60th IEEE Vehicular Technology Conference (VTC Fall), vol. 1, Sept. 2004, pp. 9–13.

[77] J. Maurer, T. Fugen, and W. Wiesbeck, *Narrow-band measurement and analysis of the inter-vehicle transmission channel at 5.2 GHz*, in Proc. 55th IEEE Vehicular Technology Conference (VTC Spring), vol. 3, 2002, pp. 1274–1278.

[78] J. Maurer, T. Fügen, and W. Wiesbeck, *Physical layer simulations of IEEE802.11a for vehicle-to-vehicle communications*, in Proc. 62nd IEEE Vehicular Technology Conference (VTC Fall), vol. 3, Sept. 2005, pp. 1849–1853.

[79] R. Meireles, M. Boban, P. Steenkiste, O. Tonguz, and J. Barros, *Experimental study on the impact of vehicular obstructions in VANETs*, in Proc. IEEE Vehicular Networking Conference (VNC), Dec. 2010, pp. 338–345.

[80] M. Nakagami, *The m-distribution-a general formula of intensity distribution of rapid fading*, Statistical Method of Radio Propagation, (1960).

[81] M. Nekoui and H. Pishro-Nik, *A universal geocast scheme for vehicular ad hoc networks*, in Proc. 7th IEEE Consumer Communications and Networking Conference (CCNC), Jan. 2010.

[82] J. Nuckelt, M. Schack, and T. Kürner, *Deterministic and stochastic channel models implemented in a physical layer simulator for Car-to-X communications*, Advances in Radio Science, 9 (2011), pp. 165–171.

[83] A. Paier, *The Vehicular Radio Channel in the 5 GHz Band*, PhD thesis, Vienna University of Technology, Austria, 2010.

[84] A. Paier, L. Bernado, J. Karedal, O. Klemp, and A. Kwoczek, *Overview of vehicle-to-vehicle radio channel measurements for collision avoidance applications*, in Proc. 71st Vehicular Technology Conference (VTC Spring), May 2010.

[85] A. Paier, D. Faetani, and C. Mecklenbräuker, *Performance evaluation of IEEE 802.11p physical layer infrastructure-to-vehicle real-world measurements*, in Proc. 3rd International Symposium on Applied Sciences in Biomedical and Communication Technologies (ISABEL), Nov. 2010.

[86] A. Paier, J. Karedal, N. Czink, C. Dumard, T. Zemen, F. Tufvesson, A. F. Molisch, and C. F. Mecklenbräuker, *Characterization of vehicle-to-vehicle radio channels from measurements at 5.2 GHz*, Wireless Personal Communications (WPC), 50 (2009), pp. 19–32.

[87] A. Paier, R. Tresch, A. Alonso, D. Smely, P. Meckel, Y. Zhou, and N. Czink, *Average downstream performance of measured IEEE 802.11p infrastructure-to-vehicle links*, in Proc. IEEE International Conference on Communications (ICC), May 2010.

[88] S. Panichpapiboon and W. Pattara-Atikom, *A review of information dissemination protocols for vehicular ad hoc networks*, IEEE Communications Surveys Tutorials, 14 (2012), pp. 784–798.

[89] P. Paschalidis, K. Mahler, A. Kortke, M. Wisotzki, M. Peter, and W. Keusgen, *2 x 2 MIMO measurements of the wideband car-to-car channel at 5.7 GHz on urban street intersections*, in Proc. 74th IEEE Vehicular Technology Conference (VTC Fall), Sept. 2011.

[90] P. Paschalidis, M. Wisotzki, A. Kortke, W. Keusgen, and M. Peter, *A wideband channel sounder for car-to-car radio channel measurements at 5.7 GHz and results for an urban scenario*, in Proc. 68th IEEE Vehicular Technology Conference (VTC Fall), Sept. 2008.

[91] T. Paulin and S. Bessler, *A disruption tolerant connectivity service for ITS applications using IEEE 802.11p*, in Proc. 11th European Wireless Conference 2011 - Sustainable Wireless Technologies, Apr. 2011.

[92] ——, *Controlled probing - a system for targeted floating car data collection*, in Proc. IEEE Conference on Intelligent Transportation Systems (ITSC), Oct. 2013.

[93] T. Pedersen, G. Steinbock, and B. Fleury, *Modeling of reverberant radio channels using propagation graphs*, IEEE Transactions on Antennas and Propagation, 60 (2012), pp. 5978–5988.

[94] M. H. Quenouille, *Problems in plane sampling*, Ann. Math. Statist., 20 (1949), pp. 355–375.

[95] L. Reichardt, T. Schipper, and T. Zwick, *"Virtual Drive" physical layer simulations for vehicle-to-vehicle communication*, in Proc. International Symposium on Electromagnetic Theory (EMTS), Aug. 2010, pp. 883–886.

[96] O. Renaudin, V. Kolmonen, P. Vainikainen, and C. Oestges, *Wideband MIMO car-to-car radio channel measurements at 5.3 GHz*, in Proc. 68th IEEE Vehicular Technology Conference (VTC Fall), Sept. 2008.

[97] ——, *Car-to-car channel models based on wideband MIMO measurements at 5.3 GHz*, in Proc. 3rd European Conference on Antennas and Propagation (EuCAP), Mar. 2009, pp. 635–639.

[98] ——, *Wideband measurement-based modeling of inter-vehicle channels in the 5 GHz band*, in Proc. 5th European Conference on Antennas and Propagation (EUCAP), Apr. 2011, pp. 2881–2885.

[99] P. Ross, *Thus spoke the autobahn*, IEEE Spectrum, 52 (2015), pp. 52–55.

[100] H. Schumacher and H. Tchouankem, *Highway propagation modeling in VANETS and its impact on performance evaluation*, in Proc. 10th Annual Conference on Wireless On-demand Network Systems and Services (WONS), Mar. 2013, pp. 178–185.

[101] H. Schumacher, H. Tchouankem, J. Nuckelt, T. Kürner, T. Zinchenko, A. Leschke, and L. Wolf, *Vehicle-to-vehicle IEEE 802.11p performance measurements at urban intersections*, in Proc. IEEE International Conference on Communications (ICC), June 2012, pp. 7131–7135.

[102] I. Sen and D. Matolak, *Vehicle channel models for the 5-GHz band*, IEEE Transactions on Intelligent Transportation Systems, 9 (2008), pp. 235–245.

[103] V. Shivaldova, G. Maier, D. Smely, N. Czink, A. Alonso, A. Winkelbauer, A. Paier, and C. Mecklenbräuker, *Performance evaluation of IEEE 802.11p infrastructure-to-vehicle tunnel measurements*, in Proc. 7th International Wireless Communications and Mobile Computing Conference (IWCMC), July 2011, pp. 848–852.

[104] V. Shivaldova and C. Mecklenbräuker, *Real-world measurements-based evaluation of IEEE 802.11p system performance*, in Proc. 5th IEEE International Symposium on Wireless Vehicular Communications (WiVeC), June 2013.

[105] V. Shivaldova, A. Paier, D. Smely, and C. Mecklenbrauker, *On roadside unit antenna measurements for vehicle-to-infrastructure communications*, in Proc. 3rd IEEE International Symposium on Personal Indoor and Mobile Radio Communications (PIMRC), Sept. 2012, pp. 1295–1299.

[106] V. Shivaldova, T. Paulin, A. Paier, and C. Mecklenbräuker, *Performance measurements of multi-hop communications in vehicular ad hoc networks*, in Proc. IEEE International Conference on Communications (ICC), June 2012, pp. 7162–7166.

[107] J. Singh, N. Bambos, B. Srinivasan, and D. Clawin, *Wireless lan performance under varied stress conditions in vehicular traffic scenarios*, in Proc. 56th IEEE Vehicular Technology Conference (VTC Fall), vol. 2, Sept. 2002, pp. 743–747.

[108] C. Sommer and F. Dressler, *Using the right two-ray model? a measurement based evaluation of PHY models in VANETs*, in Proc. 17th ACM International Conference on Mobile Computing and Networking (MobiCom), ACM, Sept. 2011.

[109] C. Sommer, D. Eckhoff, R. German, and F. Dressler, *A computationally inexpensive empirical model of ieee 802.11p radio shadowing in urban environments*, in Proc. 8th International Conference on Wireless On-Demand Network Systems and Services (WONS), Jan. 2011, pp. 84–90.

[110] T. Sukuvaara, *Field measurements of IEEE 802.11p based vehicular networking entity*, in Proc. 4th International Conference on Ubiquitous and Future Networks (ICUFN), July 2012, pp. 135–139.

[111] I. Tan, W. Tang, K. Laberteaux, and A. Bahai, *Measurement and analysis of wireless channel impairments in DSRC vehicular communications*, in Proc. IEEE International Conference on Communications (ICC), May 2008, pp. 4882–4888.

[112] H. Tchouankem, T. Zinchenko, H. Schumacher, and L. Wolf, *Effects of vegetation on vehicle-to-vehicle communication performance at intersections*, in Proc. 78th IEEE Vehicular Technology Conference (VTC Fall), Sept. 2013.

[113] The Commission of the European Communities, *Commision decision on the harmonised use of radio spectrum in the 5875-5905 MHz frequency band for safety-related applications of intelligent transport systems (ITS).* 008/671/EC, Aug. 2008.

[114] M. Torrent-Moreno, P. Santi, and H. Hartenstein, *Distributed fair transmit power adjustment for vehicular ad hoc networks*, in Proc. 3rd IEEE Communications Society Conference on Sensor and Ad Hoc Communications and Networks (SECON), vol. 2, Sept. 2006, pp. 479–488.

[115] Y. Wang, B. Kong, H. Leung, H. Jiang, and S. Chen, *An experimental vehicular wireless system and link performance analysis*, IEEE/ASME Transactions on Mechatronics, 17 (2012), pp. 508–518.

[116] N. Wisitpongphan, O. Tonguz, J. Parikh, P. Mudalige, F. Bai, and V. Sadekar, *Broadcast storm mitigation techniques in vehicular ad hoc networks*, IEEE Wireless Communications Magazine, 14 (2007), pp. 84–94.

[117] H. Yagi and B. Kurkoski, *Channel quantizers that maximize random coding exponents for binary-input memoryless channels*, in Proc. IEEE International Conference on Communications (ICC), June 2012, pp. 2228–2232.

[118] L.-T. Yang, H. Jiang, C.-C. Guo, Y.-H. Wang, J. Wu, and L.-J. Chen, *A four-state markov model based on measurements for evaluating the packet-level performance of VANET*, in Proc. 68th IEEE Vehicular Technology Conference (VTC Fall), Sept. 2008.

[119] A. Zajic, G. Stuber, T. Pratt, and S. Nguyen, *Wideband MIMO mobile-to-mobile channels: Geometry-based statistical modeling with experimental verification*, IEEE Transactions on Vehicular Technology, 58 (2009), pp. 517–534.

[120] Y. Zang, L. Stibor, G. Orfanos, S. Guo, and H.-J. Reumerman, *An error model for inter-vehicle communications in highway scenarios at 5.9GHz*, in Proc. 2nd International Workshop on Performance Evaluation of Wireless Ad Hoc, Sensor, and Ubiquitous Networks, Oct. 2005, pp. 49–56.

[121] C. Zhou, J. Waynert, T. Plass, and R. Jacksha, *Modeling RF propagation in tunnels*, in Proc. IEEE Antennas and Propagation Society International Symposium (APSURSI), July 2013, pp. 1916–1917.

[122] T. Zinchenko, H. Tchouankem, L. Wolf, and A. Leschke, *Reliability analysis of vehicle-to-vehicle applications based on real world measurements*, in Proc. 10th International Workshop on Vehicular Inter-networking, Systems, and Applications (ACM), ACM, June 2013, pp. 11–20.

[123] T. Zwick, C. Fischer, and W. Wiesbeck, *A stochastic multipath channel model including path directions for indoor environments*, IEEE Journal on Selected Areas in Communications, 20 (2002), pp. 1178–1192.